Astronomy & Astrophysics manuscript no. arti˙vfinal
July 28, 2006

A spectroscopic atlas of post-AGB stars and planetary nebulae selected from the IRAS Point Source Catalogue ⋆

O. Suárez[1], P. García-Lario[2], A. Manchado[3,4], M. Manteiga[5], A. Ulla[6], and S.R. Pottasch[7]

[1] Laboratorio de Astrofísica Espacial y Física Fundamental, INTA, Apartado de Correos 50727, E-28080 Madrid, Spain
[2] Research and Scientific Support Department of ESA, European Space Astronomy Centre, Villafranca del Castillo, Apartado de Correos 50727. E-28080 Madrid, Spain
[3] Instituto de Astrofísica de Canarias, c/Via Lactea, s/n, E-38200 La Laguna, Tenerife, Spain
[4] Consejo Superior de Investigaciones Científicas (CSIC), Spain
[5] Departamento de Ciencias de la Navegación y de la Tierra, E.T.S. de Náutica y Máquinas, Universidade da Coruña, E-15011 A Coruña, Spain
[6] Departamento de Física Aplicada, Facultade de Ciencias do Mar, Campus Marcosende-Lagoas, Universidade de Vigo, E-36310 Vigo, Pontevedra, Spain
[7] Kapteyn Astronomical Institute, Postbus 800 NL-9700 AV Groningen, The Netherlands

Received ¡date¿/Acepted ¡date¿

ABSTRACT

Aims. We study the optical spectral properties of a sample of stars showing far infrared colours similar to those of well-known planetary nebulae. The large majority of them were unidentified sources or poorly known in the literature at the time when this spectroscopic survey started, some 15 years ago.
Methods. We present low-resolution optical spectroscopy, finding charts and improved astrometric coordinates of a sample of 253 IRAS sources.
Results. We have identified 103 sources as post-AGB stars, 21 as "transition sources", and 36 as planetary nebulae, some of them strongly reddened. Among the rest of sources in the sample, we were also able to identify 38 young stellar objects, 5 peculiar stars, and 2 Seyfert galaxies. Up to 49 sources in our spectroscopic sample do not show any optical counterpart, and most of them are suggested to be heavily obscured post-AGB stars, rapidly evolving on their way to becoming planetary nebulae.
Conclusions. An analysis of the galactic distribution of the sources identified as evolved stars in the sample is presented together with a study of the distribution of these stars in the IRAS two-colour diagram. Finally, the spectral type distribution and other properties of the sources identified as post-AGB in this spectroscopic survey are discussed in the framework of stellar evolution.

Key words. Planetary nebulae – stars: AGB and Post-AGB – infrared radiation – stars: mass loss

1. Introduction

Post-Asymptotic Giant Branch (post-AGB, hereafter) stars are rapidly evolving low- and intermediate-mass stars (1−8 $M_\odot$) in the transition phase from the AGB to the Planetary Nebula (PNe, hereafter) stage (Kwok 1993; Habing 1996; van Winckel 2003). Their precursors, the AGB, stars are pulsating stars, very bright in the infrared, which can become heavily obscured in the optical by thick circumstellar envelopes formed as a consequence of their strong mass loss (up to $10^{-4}M_\odot$/yr). When the mass loss stops, the AGB star enters the so-called *post-AGB* stage, which is also accompanied by the cessation of the stellar pulsations. This is followed by a decrease in the optical depth of the circumstellar envelope as a consequence of the expansion, which implies that the central star can be seen again in the optical range if it were ever obscured at the end of the AGB. During this process, the effective temperature of the central star increases. This leads to a rapid change in the spectral type, which migrates from late- to early-type in very short timescales of just a few thousand years (Vassiliadis & Wood 1994).

The terminology used to define the various stages preceding the formation of a PN is sometimes confusing. In this work the term 'post-AGB star' will be applied to those sources that have already left the strong mass-losing AGB phase. When the temperature of the central star is

Send offprint requests to: O. Suárez. e-mail: olga@laeff.inta.es

⋆ Based mainly on observations collected at the European Southern Observatory (La Silla, Chile) and at the Observatorio del Roque de los Muchachos (La Palma, Spain)

hot enough (T≥20 000K), the ionization of the envelope starts, and we consider that the star has entered the PN stage. We will adopt the term 'transition source' for those stars in an intermediate stage between the post-AGB and PN stages, whose spectra are characterised by the simultaneous detection of a prominent stellar continuum and shock-excited emission lines.

The initial goal of the observations presented here was the discovery of new PNe among the 1084 sources included in the so-called 'GLMP catalogue' (García-Lario 1992). This was a colour-selected sample of IRAS sources showing the characteristic far-infrared colours of well known PNe. The strategy was based on the fact that PNe are located in a well-defined region of the IRAS two-colour diagram [12]−[25] *vs*. [25]−[60] almost exclusively populated by PNe and their immediate precursors, the post-AGB stars. In this region, only a small overlap exists with some young stellar objects and a few Seyfert galaxies, while normal stars and galaxies show completely different far-infrared colours (Pottasch et al. 1988). Not unexpectedly, as a byproduct of our search for new PNe, we found that many of the observed stars were actually post-AGB stars and transition sources, as well as peculiar very young PNe, rather than genuine, classical PNe.

Indeed, the use of IRAS data proved to be a highly successful method to identify new candidate sources in the transition from the AGB to the PN stage. Their strong infrared excess makes them very bright in the infrared and easily detectable at these wavelengths. Based on their characteristic colours, several lists with potential candidates were compiled in the past by Preite-Martinez (1988), Pottasch et al. (1988), van der Veen et al. (1989), Ratag et al. (1990), Hu et al. (1993), and other authors reported in the Strasbourg-ESO Catalogue of Galactic PNe (Acker et al. 1992). More specific searches for PNe based on other observational criteria were also made by van de Steene & Pottasch (1993) and Jacoby & van de Steene (2004). Other searches for post-AGB stars were based on the detection of infrared excesses around stars with optically bright counterparts, like those performed by (Oudmaijer et al. 1992; Oudmaijer 1996) in the last decade. Unfortunately, in many cases no spectroscopic confirmation was ever provided in the literature about the nature of the newly discovered sources. One of the main reasons for this is the poor astrometric accuracy of the IRAS data (∼15-30 arcsec), which makes the identification of the optical counterparts of the selected IRAS sources very difficult, especially in crowded fields close to the galactic plane and/or in the direction of the Galactic Centre.

In this paper we present, for the first time, the whole optical spectroscopic database of stars resulting from the survey carried out by our group in the optical from 1988 to 2003, concentrated on the stars in the GLMP sample for which indications of the presence of an optical counterpart were available. At the time when the observations were performed, priority was given to those sources suspected to be evolved stars. The results are presented in the form of an atlas including the largest set of spectroscopic data on post-AGB stars and transition sources published before that time. The atlas also contains improved astrometric coordinates and finding charts for all the sources observed. The spectral energy distributions (SEDs) from 1 to 100 μm of the objects observed were also studied, but they will be presented elsewhere, together with a more detailed analysis of some of the new sources found. Several papers dealing with other individual sources of strong interest found during the survey have already been published (e.g.,Manchado et al. (1989b); García Lario et al. (1991); Bobrowsky et al. (1998); García-Lario et al. (1999a))

In Sect. 2 we explain the selection criteria applied to include an IRAS source in our sample. In Sect. 3 we present the observations performed and the data reduction process. Section 4 describes the identification of the sources in the sample and the way the classification of the optical spectra was performed. The main properties of the sources identified as evolved stars are discussed in Sect. 5. Finally, in Sect. 6 we present our conclusions. Spectra and finding charts for individual sources are provided in Appendices A, B, C, D, E, and F (only available in electronic format).

2. Selection criteria

The selection criteria applied in this work are essentially the same as those adopted by Pottasch et al. (1988), with some modifications:

(i) The source must be well detected at 12, 25, and 60 μm in the IRAS Point Source Catalogue (see Beichman et al. 1988). The flux quality for each band must be:

$$FQUAL\ (12\ \mu\mathrm{m})\ \geq\ 2;$$

$$FQUAL\ (25\ \mu\mathrm{m})\ =\ 3;$$

$$FQUAL\ (60\ \mu\mathrm{m})\ =\ 3.$$

(ii) The ratios between the IRAS photometric fluxes must satisfy the following conditions:

$$\frac{F_\nu\ (12\ \mu\mathrm{m})}{F_\nu\ (25\ \mu\mathrm{m})} \leq 0.50;$$

$$\frac{F_\nu\ (25\ \mu\mathrm{m})}{F_\nu\ (60\ \mu\mathrm{m})} \geq 0.35.$$

(iii) When data at 100 μm are of good quality (FQUAL(100 μm) = 3), we further impose:

$$\frac{F_\nu\ (60\ \mu\mathrm{m})}{F_\nu\ (100\ \mu\mathrm{m})} \geq 0.60.$$

(iv) Sources must show a low IRAS variability index:

$$VAR \leq\ 60\ \%$$

The choice of criteria (i) and (ii) was mainly a direct consequence of the range of dust temperatures (T_d) expected in the circumstellar shells of post-AGB stars. If we assume a typical luminosity for a post-AGB star of

L=$10^4 L_\odot$, the dust temperature in the shell, following Scoville & Kwan (1976), would be:

$$T_{\rm d} = 1.658\, f^{-1/5} r^{2/5} L_*^{1/5}, \quad (1)$$

where f is the value of the emissivity of the dust grains at 50μm, r is the radius of the shell in pc, and L_* is the luminosity of the central star in solar units.

Using $f(50\,\mu{\rm m}) = 0.004$ (Draine & Lee 1984), we find a $T_{\rm d}$ between 200 K and 80 K for r between 0.01 pc and 0.1 pc, respectively (the expected range of radii of the expanding circumstellar envelope).

Criterium (iii) was added to avoid the potential contamination by young stellar objects, ultra-compact H II regions, and Seyfert galaxies, which can sometimes show very similar colours up to 60 μm.

Finally, the low IRAS variability was imposed to exclude AGB stars from the sample, since they are known to be strongly variable stars.

All the sources in the original GLMP sample satisfy criteria (i), (ii), and (iii), but not necessarily the last one, concerning the variability. Moreover, in the original GLMP catalogue, about half of the entries were associated with objects that were well identified in the literature, most of them PNe, and they were excluded from the atlas presented in this paper. There was also a significant number of known young stellar objects (∼20%) and a few Seyfert galaxies (∼5%), which were not considered either.

A slight, more recent modification of the selection criteria allowed the inclusion of about 100 additional sources in an extended version of the GLMP catalogue (García-Lario, private communication). This extension also contains those IRAS sources not detected in the 12 μm IRAS band (FQUAL (12 μm) = 1), but satisfying the rest of conditions mentioned above. Some of these sources were also included in our spectroscopic survey in the latest years and, as such, they are also considered in the following analysis.

The sample presented in this paper is thus comprised by a subset of sources taken from the two GLMP samples described above for which no identification was available (or was poorly established) at the time when these two catalogues were created, and for which optical spectroscopy was obtained.

A total of 253 different IRAS fields were searched, resulting in the successful identification of 205 optical counterparts.

With these selection criteria, our sample of post-AGB stars with optical counterparts is expected to be essentially complete, limited only by the IRAS sensitivity. Only a few C-rich post-AGB stars showing prominent solid state features attributed to SiC at 11.3 μm, and thus located in region VII of the IRAS colour-colour diagram, as defined by van der Veen & Habing (1988), may have escaped our identification. In addition, some post-AGB stars in the vicinity of the Galactic Centre could have also been missed due to the IRAS confusion in that region.

3. Observations and data reduction

The spectroscopic observations were conducted during several runs spanning 15 years from March 1988 to June 2003. The observations from the Southern Hemisphere were carried out in most cases at the European Southern Observatory (ESO, La Silla, Chile) with the 1.5 m ESO telescope, equipped with a Boller & Chivens spectrograph. The first and last runs of observations were carried out at the 3.6 m ESO telescope, located at the same site, using the ESO Faint Object Spectrograph and Camera EFOSC1 in the first run and EFOSC2 in the last one. The observations from the Northern Hemisphere were carried out at the 2.5m Isaac Newton Telescope at the Observatorio del Roque de los Muchachos (La Palma, Spain), using the IDS spectrograph, and at the 2.2 m telescope at the Observatorio Hispano-Alemán (Calar Alto, Spain), also equipped with a Boller & Chivens spectrograph.

The full log of the spectroscopic observations is shown in Table 1, where we list the telescopes and dates of the observations, together with the instrumentation used in each run, as well as the spectral resolution and the spectral range covered in each case. Exposure times were in the range from 10 to 60 min. depending on the brightness of the source observed, with mean exposure times of 20–30 min.

The optical spectra were reduced using IRAF, following standard techniques. After subtracting the bias, the two-dimensional CCD spectra were divided by the normalised flat-field of the corresponding night. Then, the cosmic ray events were identified and removed.

The sky contribution was determined by averaging two narrow regions of the CCD located at both sides of the object and then the mean sky was subtracted. For the wavelength calibration, several Cu-Ne or Cu-Ar lamp exposures were taken.

Several photometric standards were observed during each observing night and were used for flux calibration. The spectra of the target stars were flux calibrated and corrected for atmospheric extinction using these standards. We estimate typical errors in the absolute fluxes of ∼ 20%. These errors depend mainly on the stability of the seeing conditions for each night of observation.

In parallel with these spectroscopic observations, we also carried out a near infrared photometric survey (Manchado et al. 1989a; García-Lario et al. 1990, 1997). The data obtained in the near infrared helped in many cases to identify the right optical counterpart of the IRAS source, or to confirm the lack of it, in the case of the most obscured sources.

The counterpart identification strategy was the following: in many cases, before the observations took place, a single optical counterpart, close to the IRAS position, was identified in the Digitized Sky Survey (DSS) plates as the most plausible one. When no other information was available, this was the source observed at the telescope.

Sometimes, however, several faint sources with similar brightness were found located within the elliptical IRAS

Table 1. Log of the spectroscopic observations.

Run	Telescope	Instrumentation	Dates	Dispersion (Å/pix)	Spectral range (Å)	Number of obs. objects
#1	3.6 m ESO La Silla	EFOSC1	19-21 March 1988	3.79	3406-6975	12
#2	1.5 m ESO La Silla	Boller & Chivens	2-4 January 1989	2.47	4272-6812	24
#3	1.5 m ESO La Silla	Boller & Chivens	23-25 February 1990	2.80	4046-6920	41
#4	1.5 m ESO La Silla	Boller & Chivens	25-29 June 1990	3.47	4050-6925	34
#5	2.5 m INT La Palma	IDS	23-25 May 1991	2.81	3570-5226 / 5538-7240	4
#6	2.2 m Calar Alto	Boller & Chivens	November 1991	2.50	3830-6736	27
#7	1.5 m ESO La Silla	Boller & Chivens	19-25 August 1992	2.83	3590-9425	34
#8	1.5 m ESO La Silla	Boller & Chivens	10-13 March 1993	3.74	3321-11015	32
#9	2.5 m INT La Palma	IDS	1-4 July 1993	1.48	5376-7269	8
#10	1.5 m ESO La Silla	Boller & Chivens	13-17 March 1994	3.74	3285-10980	38
#11	2.5 m INT La Palma	IDS	18-24 August 1994	1.57	3779-5401 / 5570-7195	32
#12	1.5 m ESO La Silla	Boller & Chivens	11-15 February 1995	3.79	3532-11190	21
#13	2.5 m INT La Palma	IDS	13-16 June 1995	1.57	3700-5455 / 5488-7255	9
#14	2.5 m INT La Palma	IDS	9-10 April 2001	3.30	3702-7401	4
#15	3.6 m ESO La Silla	EFOSC2	23-25 June 2003	5.30	3600-9200	45

error box. In this case, we usually tried to observe the field in the near-infrared, where we identified the tentative counterpart on the basis of its peculiar near infrared colours (usually the brightest source or the most heavily reddened in the near infrared) first. If no near infrared information was available at the time of the spectroscopic observations, we usually took spectra of all the optical sources located in the field within the elliptical IRAS error box, starting from the closest one to the nominal IRAS position and/or the redder one.

In some cases the identification of the optical counterpart was clear (e.g., when a PN or a source displaying Hα emission was found). Sometimes, however, no special features were detected in the spectra of any of the stars tried, and it was more difficult to determine which of them (if any) was the star physically associated with the IRAS source. It might also be the case that none of the observed stars is the optical counterpart of the IRAS source, since stars on their way to becoming new PNe can become so heavily obscured by the material expelled during the previous AGB phase that they may not be detectable in the optical range. We will further discuss these uncertainties in Sect. 4.1.

The full list of the 253 IRAS fields observed is shown in Table 3 (only available in electronic format), where we also give: the entry number of the object in the GLMP catalogue, the IRAS name, the improved astrometric coordinates taken from the 2MASS Point Source Catalogue (Cutri et al. 2003) for which the estimated errors are of the order of $\sim 0.2''$ corresponding to the source identified as the right counterpart, and the far infrared IRAS colours [12]−[25] and [25]−[60], defined in the classical way as:

$$[12]-[25] = -2.5\ \log \frac{F_{12\mu\mathrm{m}}}{F_{25\mu\mathrm{m}}} \quad (2)$$

$$[25]-[60] = -2.5\ \log \frac{F_{25\mu\mathrm{m}}}{F_{60\mu\mathrm{m}}}. \quad (3)$$

In the last columns of this table, we also provide the classification assigned to each source and, in the case of the non-evolved objects, the spectral class or type, and we identify the spectroscopic observing run when every source was observed, according to the code given in Table 1.

In addition to the spectroscopic observations, CCD images of selected fields were also obtained through various standard broad and narrow filters covering the whole optical range and using several telescopes listed in Table 2. These images were bias and flat-field corrected and cleaned for cosmic rays using standard IRAF routines. No flux calibration was performed in this case.

In Appendices A, B, C, D, E, and F (only in electronic format) we show the spectrum and the finding chart for all the targets in the survey for which an optical counterpart was identified and a spectrum was taken. In most cases the finding charts are taken from the DSS. However, when extended emission was detected in our images, we used them for the atlas.

We prefer showing the images obtained through red filters (usually the R-band) if available, because in most cases the optical counterparts of the IRAS sources in our sample are expected to be brighter at longer wavelengths since on many occasions they are strongly reddened by their circumstellar envelopes. If convenient, we have also used our Hα images, in some cases, to better illustrate the morphology of those sources showing extended ionised emission.

4. Results

4.1. Classification of the sources in the sample

To classify the objects in the sample as a function of their nature and evolutionary stage, we have studied their optical spectra and the complementary information coming from the near infrared measurements made by García-

Table 2. Log of the direct imaging observations.

Run	Telescope	Instrumentation	Dates
#a	3.6m ESO (La Silla)	EFOSC1	June 1990
#b	JKT (La Palma)	CCD	July 1990
#c	0.90m Dutch (La Palma)	CCD	March 1994
#d	2.5m NOT (La Palma)	ALFOSC	June 2000
#e	2.5m NOT (La Palma)	ALFOSC	May 2001
#f	3.6m ESO (La Silla)	EFOSC2	June 2003

Lario et al. (1997) and from other sources in the literature. The assigned classifications are shown in Table 3[1].

The determination of the evolutionary stage of an object can lead to some uncertainties, especially when trying to discriminate between post-AGB stars and young stellar objects. If the source is located within the boundaries or close to a known star-forming region, we have assumed it is most probably young. The luminosity obtained in the spectral classification can also give us some hints about its evolutionary stage, since the young stars are expected to show spectra corresponding to a low luminosity class (usually V), while post-AGB stars show extended atmospheres and low gravities usually corresponding to the high luminosity classes I and III.

To take these uncertainties into account, we have introduced a two-letter code in Tables[1] 4, 5, and 6. The letters rang from A to D and rate our confidence in the data presented, with A representing the maximum reliability. The first letter marks our confidence in the correct identification of the optical counterpart, and the second letter indicates how confident we are in the evolutionary classification assigned.

The adopted selection criteria turned out to be very efficient in the detection of evolved stars. Up to 209 sources, representing 81% of the stars in the sample, were found to be evolved stars. Among them, the majority of these sources are considered to be post-AGB stars: 103 with an optical counterpart (see Table 4[1]), plus possibly 49 more heavily obscured ones, for which we did not find any optical counterpart during our observations, although most of which are believed to be obscured post-AGB stars. They are labeled as "No counterpart" in Table 3. We have also found 21 'transition sources' (see Table 5[1]).

Only 38 of the sources observed in the sample (∼17%) were identified as young stellar objects and 2 other ones as galaxies (less than 1%). Their identifications and the spectral type of the young objects are shown in Table 3.

4.2. Classification of the optical spectra

4.2.1. Spectral types in the MK system

The classification of the optical spectra in the MK system was performed taking several spectral libraries as references (Silva & Cornell 1992; Jacoby et al. 1984; Pickles 1998), and it was applied to all the observed sources showing a stellar continuum. By default, we always assumed a luminosity class I in our first try for the sources suspected to be post-AGB stars. To perform this classification, we first normalised both the spectral templates taken from these catalogues and our target spectra. This way we concentrate our attention on the spectral lines, rather than on the stellar continuum, which may appear extremely reddened in many stars of our sample.

We used Silva & Cornell's templates for the spectra with the lowest signal-to-noise ratios and for the young stellar objects. The estimated error in this classification is about plus or minus one subclass, which implies a total error of around five subtypes in the determination of the spectral type.

For the sources in our sample classified as evolved objects whose spectra had a good signal-to-noise ratio, we used the other two catalogues (Jacoby et al. 1984; Pickles 1998) to derive a more accurate spectral classification, as they provide one spectrum for each subtype and for a wide range of spectral types for stars with luminosity class I. We estimate that the stars classified using these catalogues are affected by errors that are always of the order of less than two spectral subtypes.

We have had difficulties classifying with accuracy the stars with the earliest spectral types showing the Balmer lines in emission. In many cases these lines show emission over absorption, making it impossible to use their strength for classification purposes.

In Table 4[1] we list all the sources in the sample classified as post-AGB stars together with their associated spectral classification, and in Table 5[1] we show the classification of the transition sources[2].

The spectral type in these two tables is given, as usual, by the letter and number corresponding to the MK classification system. Those spectra for which Silva's rough classification was used maintain the nomenclature followed in that catalogue, i.e, one letter followed by two numbers indicating the range of subtypes. The letter "e" appended to the spectral type indicates that the object shows emission lines. When the spectrum is dominated by emission lines,

[1] These tables are only available in electronic form.

[2] The rough spectral types assigned to the young stellar objects identified in our survey are shown in Table 3. Note that for these sources we did not try to make any luminosity class determination.

and the continuum is too faint to derive its spectral type, it is classified with the code "em".

4.2.2. Determination of the extinction constant, the excitation classes for PNe, and the WR type of the central stars

To determine the extinction corrected line intensities of the PNe, we calculated the extinction coefficient c, using the observed Balmer line decrement (see results in Table 6[1]). Then we dereddened the observed spectra using Whitford's extinction law (Whitford 1958), and we used the dereddened lines to calculate the excitation classes.

The excitation classes were determined using both Morgan (1984) and Dopita & Meatheringham (1990) criteria to provide a more reliable classification. Morgan (1984) based this classification on the value of the ratios [O III] (λ 4959 Å)/Hβ, Hβ/HeII (λ 4686 Å), and Hβ/[NeIII] (λ 3869 Å). It establishes 12 different classes, ranging from low (class 0) to high (class 10) excitation. The classification proposed by Dopita & Meatheringham (1990) is a continuous one, based on the ratios [O III] (λ 4959 Å)/Hβ and HeII (λ 4686 Å)/Hβ.

We grouped together all possible excitation classes in only three main subgroups: low, medium, and high excitation (see Table 6).

Note that some PNe were impossible to classify using these criteria, as they appeared so extinguished in the blue region that they did not show several of the lines needed for the classification.

In the case of the PNe with H-poor envelopes (i.e., with WR-type central stars), we used the criteria defined by Acker & Neiner (2003) which is, in turn, also based on the classification previously defined by Crowther et al. (1998). They identify [WO] subtypes ranging from [W01] to [W04] and [WC] subtypes ranging from [WC4] to [WC11]. This classification is based on the dereddened strength of several O and C lines with respect to the continuum, and implies a decrease in temperature from 100 000 K for [WO1-3] stars to 20 000 for [WC10].

The final classification derived for the PNe found in our spectroscopic survey and additional information on the morphology of individual sources is shown in Table 6.

5. Discussion

In the following we will concentrate our discussion on the subsample of evolved stars, e.g., the sources classified either as optically bright post-AGB stars, transition sources or PNe, plus the subsample of heavily obscured sources also tentatively classified as post-AGB stars.

5.1. Galactic latitude distribution

To study the evolutionary connection between the various types of evolved stars identified in this work (post-AGB stars with and without optical counterpart, transition sources, and PNe) we can compare their relative galactic latitude distribution. For a given class, this is expected to be an indicator of the average mass of the progenitor stars. The youngest, and thus more massive, stars are expected to appear more concentrated towards the galactic plane, while an older population of stars, with lower masses, should show a higher dispersion.

For this purpose, in Fig. 1, we have plotted the galactic latitude distribution of the optically bright post-AGB stars and transition sources, PNe, and obscured post-AGB stars identified in our sample.

To test if the apparent differences among the distributions shown in Fig. 1 are statistically significant, we have used the F-Snedecor test (or F-variance test). This test determines whether two samples are drawn from populations with the same variances.

The result of this study shows that there are no statistically significant differences between the galactic distribution of optically bright post-AGB stars (including the transition sources) and the galactic distribution of PNe with a 99% confidence. This can be interpreted as the confirmation that an evolutionary link exists between the two populations.

However, the galactic distribution of post-AGB stars with no optical counterparts seems to be different from both the post-AGB stars with optical counterparts and the PNe. The narrow galactic latitude distribution of the obscured post-AGB stars suggests that they represent a population of more massive progenitors. These stars may be evolving very rapidly to the PN stage and have very recently left the AGB phase, as they still preserve the optically thick envelopes formed in the mass-losing phase. In contrast, the post-AGB stars showing a bright optical counterpart may represent a less massive population of stars that would evolve more slowly. Alternatively, they may never develop optically thick envelopes, evolving all the way from the end of the AGB to the PN stage as optically bright stars.

5.2. Spectral type distribution of post-AGB stars

We have found post-AGB stars belonging to all spectral types from M to B, shown in Fig. 2, in what can be interpreted as an evolutionary sequence towards higher effective temperatures on their way to becoming PNe. If this interpretation is correct, the distribution of spectral types should be a good indicator of the time spent by these stars in each range of temperatures. The same analysis could be applied to high mass stars, but in this case, part of the evolution would take place while the central star is still heavily obscured by the circumstellar envelope, and by the time it could be observed in the optical, it would have already evolved significantly towards hotter temperatures.

The models developed by van Hoof et al. (1997) (VH97, hereafter) predict the relative number of stars that we should expect to find within each spectral type.

To test if the distribution of spectral types observed (see Fig. 2) is similar to any of the models produced by

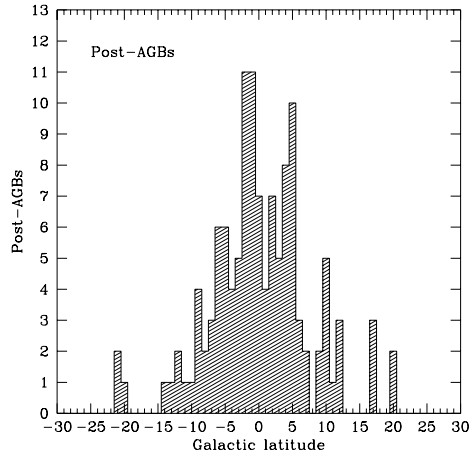

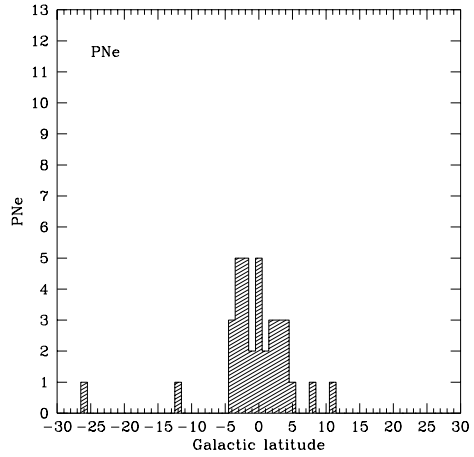

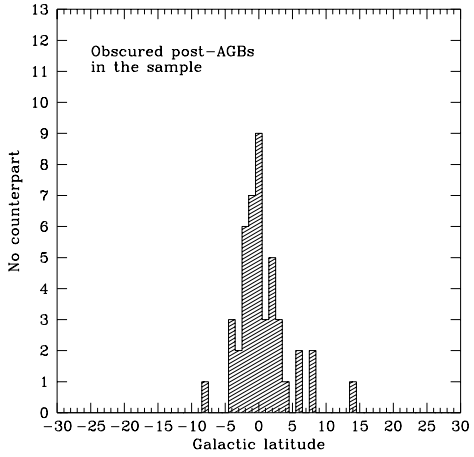

Fig. 1. Galactic latitude distribution of optically bright post-AGB stars, PNe, and obscured post-AGB stars identified in the sample.

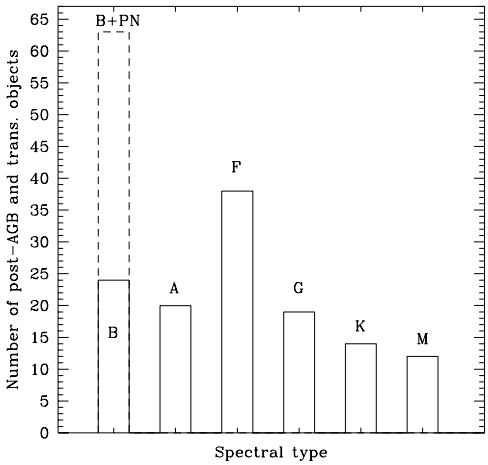

Fig. 2. Relative distribution of spectral types for the post-AGB stars in our sample.

VH97, we have applied the Pearson's Chi-square test. This test verifies if the shape of the distribution of a given variable fits a theoretical distribution with known parameters reasonably well.

The result of this analysis indicates that the distribution of spectral types observed in our sample of post-AGB stars and transition objects, excluding the M- and K- spectral types, is not compatible with any of the three theoretical models used by VH97 with a 95% confidence level.

We suggest that the incompatibility can be due to the fact that our sample is a combination of objects with different core masses, as is to be expected from the selection criteria chosen, which do not favour any particular core mass range.

5.3. Distribution in the IRAS colour-colour diagram

5.3.1. Overall distribution

In Fig. 3 in the IRAS colour-colour diagram, we show the distribution of all the sources included in our spectroscopic survey, where special symbols are used to distinguish between the different types of objects: PNe, optically bright post-AGB stars, galaxies, young stellar objects, and objects for which no counterpart was found (transition sources have again been included together with the post-AGB stars).

The boxes with dashed boundary lines indicate areas mostly populated by variable OH/IR stars (box *b*, dotted line), T-Tauri and Herbig Ae/Be stars (box *c*, short dash), and compact HII regions (box *e*, long dash) (see García-Lario et al. 1997 and references therein). In Fig. 3 we have maintained the labels used in that paper.

The two solid straight lines (vertical and horizontal) show the limits of the area defined by our selection criteria (see Sect. 2). The solid curve has been modeled by Bedijn (1987), and shows the location of O-rich stars as

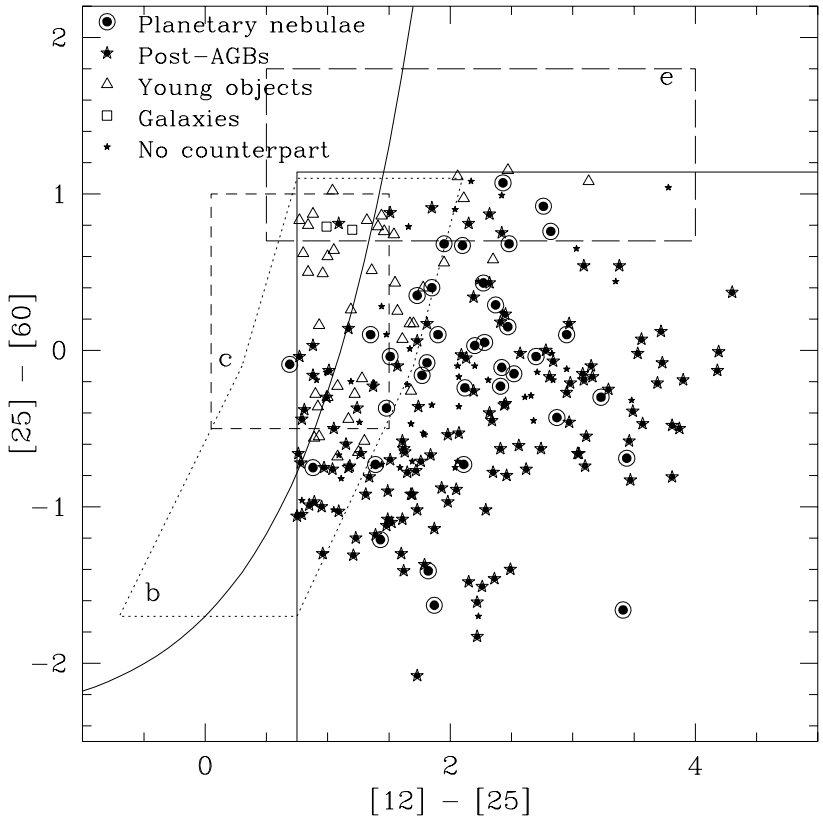

Fig. 3. IRAS colour-colour diagram showing the location of all the objects included in our spectroscopic survey.

they evolve along the AGB from M-type Miras to variable OH/IR stars.

We can see that PNe and post-AGB stars spread almost regularly over the diagram. However, it is important to remark that there is a high probability ($> 95\%$) of finding a post-AGB or a PN in the region that does not overlap with regions b, c, or e.

Almost all of young sources (marked with open triangles) are located, as expected, either in box c (T-Tauri, Herbig Ae/Be, and Vega-like stars) or e (usually populated by protostars and ultra-compact H II regions).

We have also plotted the objects for which we did not find any optical counterpart as small asterisks. A few of them are located in box e, suggesting that they could probably be heavily obscured young stellar objects, surrounded by thick protoplanetary discs or by their parent molecular cloud in which they are embedded. The rest of the sources with no counterpart are more or less clustered around a value of [25]−[60]~-0.2 and/or relatively close to box b, and these are the ones that have been classified as heavily obscured post-AGB stars in this paper.

5.3.2. Post-AGB stars and transition objects

In Fig. 4 we show more in detail the distribution of post-AGB stars and "transition sources" in the IRAS two-colour diagram as a function of the spectral type. Post-AGB stars with different spectral types are plotted with different colours, and a different symbol is used to plot the transition objects. Objects showing Hα emission are surrounded with a circle. Sources with emission, but for which we could not determine the spectral type because of their faint continuum, are plotted as open circles.

It is already known that there is not a one-to-one correspondence between the position of a post-AGB star in the IRAS two-colour diagram and its evolutionary stage (VH97), but this is the first time that a large sample of spectroscopically classified post-AGB stars show this evidence.

Neither the C-rich models nor the O-rich models predict an unambiguous relationship between the evolutionary stage in the post-AGB phase and the position in the IRAS two colour diagram. Perhaps models for different core masses and precise temporal marks could be used to create statistics and check whether there is an adequate correspondance between the position of our objects and their evolutionary status.

6. Conclusions

We have presented the results of an extensive spectroscopic survey carried out on a sample of 253 IRAS sources showing infrared colour characteristics of PNe. The selection criteria used turned out to be very efficient in discovering new post-AGB stars and transition sources evolving from the AGB to the PN stage, resulting in the identification of 152 post-AGB stars (49 of them without an optical

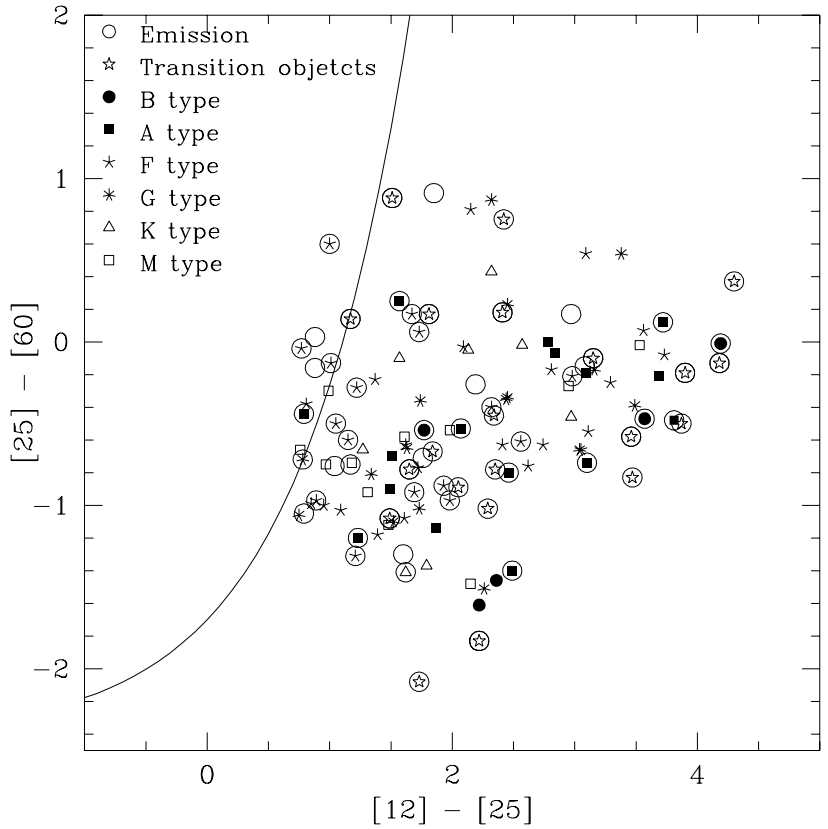

Fig. 4. IRAS colour-colour diagram showing the location of the post-AGB stars and transition objects in the survey.

counterpart), 21 transition sources, and 36 PNe. This constitutes the largest catalogue of post-AGB stars built so far.

The results from the survey are presented in an atlas format, including the spectroscopic data and finding charts. Improved astrometric information and spectral classification is also provided.

Our spectroscopic study has substantially increased the knowledge of the optical properties of galactic post-AGB stars, as can be seen in Table 4; only 35% of our 103 objects had their spectral types identified in the SIMBAD database.

An analysis of the galactic latitude distribution of the sources in the sample shows that the new population of obscured post-AGB stars identified in our spectroscopic survey must in general have higher progenitor masses than the population of post-AGB stars with optical counterparts for which spectroscopic data is presented in the atlas. The relatively large number of post-AGB stars showing optically thick envelopes suggests that many stars may evolve during a significant part of their post-AGB evolution hidden from detection in the optical.

The similar galactic latitude distribution shown by the PNe included in our sample and the population of post-AGB stars with optical counterparts suggests that many of these post-AGB stars will develop observable PNe, as they seem to belong to the same galactic population. Unfortunately, we do not know whether the small sample of PNe here studied is representative of the more general population of galactic PNe.

The spectral type distribution of the post-AGB stars observed is not compatible with any of the theoretical models developed by VH97 to predict the distribution expected for stars with several specific core masses. We suggest that this is due to our sample being a combination of sources with a wide variety of core masses.

The IRAS two-colour diagram has proved to be very useful in finding new post-AGB stars. The distribution of the post-AGB stars and the PNe in the diagram is similar, and suggests a direct evolutionary connection. We have also confirmed that the precise location of a given post-AGB star or a PNe in this diagram by itself cannot be directly interpreted as an indication of their evolutionary stage, as was suggested by previous theoretical works.

Acknowledgements. IRAF is distributed by the National Optical Astronomy Observatories, which are operated by the Association of Universities for Research in Astronomy, Inc., under cooperative agreement with the National Science Foundation

This research was funded through grant AYA-2003-09499 from the Spanish Ministerio de Ciencia y Tecnología. AM acknowledges support from grant AYA2004-03136 funded by the Spanish Ministerio de Educacion y Ciencia. It made extensive use of the Simbad database, operated at CDS, Strasbourg (France), as well as of the Space Telescope Science Institute Digitized Sky Survey (DSS). The STScI DSS is based on photographic data obtained using the UK Schmidt Telescope and

produced at the STScI under US Government grant NAG W-2166. Some images presented in the Appendices were obtained at the 2.5 m Nordic Optical Telescope, operated jointly by Denmark, Finland, Iceland, Norway, and Sweden, also at the Spanish Observatorio del Roque de los Muchachos of the Instituto de Astrofísica de Canarias.

References

Acker, A., Marcout, J., Ochsenbein, F., Stenholm, B., & Tylenda, R. 1992, Strasbourg - ESO catalogue of galactic planetary nebulae. Part 1; Part 2 (Garching: European Southern Observatory, 1992)
Acker, A. & Neiner, C. 2003, A&A, 403, 659
Allen, D. A., Hyland, A. R., & Caswell, J. L. 1980, MNRAS, 192, 505
Bedijn, P. J. 1987, A&A, 186, 136
Beichman, C. A., Neugebauer, G., Habing, H. J., Clegg, P. E., & Chester, T. J. 1988, NASA Reference Publication, 1190, 1
Bobrowsky, M., Sahu, K. C., Parthasarathy, M., & García-Lario, P. 1998, Nature, 392, 469
Crowther, P. A., de Marco, O., & Barlow, M. J. 1998, MNRAS, 296, 367
Cutri, R. M., Skrutskie, M. F., van Dyk, S., et al. 2003, VizieR Online Data Catalog, 2246, 0
de Gregorio-Monsalvo, I., Gómez, Y., Anglada, G., et al. 2004, ApJ, 601, 921
Dopita, M. A. & Meatheringham, S. J. 1990, ApJ, 357, 140
Draine, B. T. & Lee, H. M. 1984, ApJ, 285, 89
García-Lario, P. 1992, PhD thesis, Universidad de La Laguna, Spain
García-Lario, P., Manchado, A., Pych, W., & Pottasch, S. R. 1997, A&AS, 126, 479
García Lario, P., Manchado, A., Riera, A., Mampaso, A., & Pottasch, S. R. 1991, A&A, 249, 223
García-Lario, P., Manchado, A., Suso, S. R., Pottasch, S. R., & Olling, R. 1990, A&AS, 82, 497
García-Lario, P., Manchado, A., Ulla, A., & Manteiga, M. 1999a, ApJ, 513, 941
García-Lario, P., Riera, A., & Manchado, A. 1999b, ApJ, 526, 854
Habing, H. J. 1996, A&A Rev., 7, 97
Hu, J. Y., Slijkhuis, S., de Jong, T., & Jiang, B. W. 1993, A&AS, 100, 413
Jacoby, G. H., Hunter, D. A., & Christian, C. A. 1984, ApJS, 56, 257
Jacoby, G. H. & van de Steene, G. 2004, A&A, 419, 563
Kwok, S. 1993, ARA&A, 31, 63
Manchado, A., García-Lario, P., Esteban, C., Mampaso, A., & Pottasch, S. R. 1989a, A&A, 214, 139
Manchado, A., García-Lario, P., & Pottasch, S. R. 1989b, A&A, 218, 267
Morgan, D. H. 1984, MNRAS, 208, 633
Oudmaijer, R. D. 1996, A&A, 306, 823
Oudmaijer, R. D., van der Veen, W. E. C. J., Waters, L. B. F. M., et al. 1992, A&AS, 96, 625
Pickles, A. J. 1998, PASP, 110, 863
Pottasch, S. R., Olling, R., Bignell, C., & Zijlstra, A. A. 1988, A&A, 205, 248
Preite-Martinez, A. 1988, A&AS, 76, 317
Ratag, M. A., Pottasch, S. R., Zijlstra, A. A., & Menzies, J. 1990, A&A, 233, 181
Riera, A., García-Lario, P., Manchado, A., Pottasch, S. R., & Raga, A. C. 1995, A&A, 302, 137
Scoville, N. Z. & Kwan, J. 1976, ApJ, 206, 718
Silva, D. R. & Cornell, M. E. 1992, ApJS, 81, 865
van de Steene, G. C. M. & Pottasch, S. R. 1993, A&A, 274, 895
van der Veen, W. E. C. J. & Habing, H. J. 1988, A&A, 194, 125
van der Veen, W. E. C. J., Habing, H. J., & Geballe, T. R. 1989, A&A, 226, 108
van Hoof, P. A. M., Oudmaijer, R. D., & Waters, L. B. F. M. 1997, MNRAS, 289, 371
van Winckel, H. 2003, ARA&A, 41, 391
Vassiliadis, E. & Wood, P. R. 1994, ApJS, 92, 125
Whitford, A. E. 1958, AJ, 63, 201

Table 3: List of IRAS fields observed. The astrometric coordinates are given for all sources but for those without optical counterparts and without precise infrared measurements. IRAS colours are defined in Sect. 3. The run number is referred to Table 1.

GLMP	IRAS	RA (J2000)	Dec (J2000)	[12]−[25]	[25]−[60]	Classification	Spectral type/class (not evolved)	Run
12	00509+6623	00:54:07.7	66:40:12.8	1.05	−1.02	No counterpart		#11
15	01005+7910	01:04:45.5	79:26:46.3	1.98	−0.97	Post-AGB		#6
19	01156−5249	01:17:43.5	−52:33:30.8	1.22	−0.28	Young	F6e	#4,#15
20	01174+6110	01:20:44.2	61:26:15.9	1.54	0.74	Young	em	#6
23	01259+6823	01:29:33.4	68:39:16.9	1.05	−0.50	Post-AGB		#6
26	02143+5852	02:17:57.8	59:05:52.0	1.21	−1.31	Post-AGB		#6,#11
34	02528+4350	02:56:11.3	44:02:52.2	1.57	0.25	Young	A0e	#6
53	04101+3103	04:13:20.0	31:10:47.3	0.90	−0.28	Young	A5e	#6
58	04137+7016	...	...	1.26	−0.46	No counterpart		#6,#11
63	04189+2650	04:22:02.2	26:57:30.5	1.05	0.64	Young	em	#8
74	04296+3429	04:32:57.0	34:36:12.4	1.39	−1.18	Post-AGB		#11
87	05089+0459	05:11:36.2	05:03:26.3	1.18	−0.74	Post-AGB		#1
88	05113+1347	05:14:07.8	13:50:28.3	1.52	−1.10	Post-AGB		#2
91	05209−0107	05:23:31.0	−01:04:23.8	1.19	0.26	Young	F7e	#2,#7
95	05238−0626	05:26:19.8	−06:23:57.4	1.17	−0.44	Young	F4	#7,#6
96	05245+0022	05:27:05.5	00:25:07.5	1.00	−0.30	Young	A03	#7
100	05273+2517	05:30:27.5	25:19:57.1	0.88	0.87	Young	A5e	#6
106	05341+0852	05:36:55.1	08:54:08.7	0.85	−0.99	Post-AGB		#7,#6
109	05357−0217	05:38:14.1	−02:15:59.7	1.25	−0.65	Young	F6e	#2,#6,#7
117	05381+1012	05:40:57.1	10:14:25.0	1.34	−0.81	Post-AGB		#6,#11
131	05471+2351	05:50:13.9	23:52:17.7	2.00	0.96	Peculiar	BQ[ ]	#6,#11
136	05573+3156	06:00:33.4	31:56:44.5	1.95	0.56	No counterpart		#6
138	06013−1452	06:03:37.1	−14:53:02.5	0.92	−0.36	Young	A03	#7,#6,#11
155	06464−1644	06:48:41.7	−16:48:05.6	0.89	−0.56	Young	A0e	#6,#8
159	06499+0145	06:52:28.2	01:42:12.0	3.03	0.65	No counterpart		#12
160	06518−1041	06:54:13.4	−10:45:38.2	1.77	−0.16	PN		#2,#12
161	06530−0213	06:55:31.8	−02:17:28.3	1.63	−0.65	Post-AGB		#3
162	06549−2330	06:57:06.5	−23:34:09.2	1.70	0.17	Young	F4	#3
163	06556+1623	06:58:30.4	16:19:26.1	1.77	−0.54	Peculiar	BeI-BQ[ ]	#3,#10
165	06562−0337	06:58:44.4	−03:41:10.0	1.55	0.43	Young	em	#6,#7,#8,#10,#12

Table 3: List of IRAS fields observed (continued).

GLMP	IRAS	RA (J2000)	Dec (J2000)	[12]−[25]	[25]−[60]	Classification	Spectral type/class (not evolved)	Run
170	07027−7934	06:59:26.4	−79:38:47.0	1.39	−0.73	PN		#3
175	07134+1005	07:16:10.3	09:59:48.0	1.69	−0.92	Post-AGB		#3,#6
178	07173−1733	07:19:35.9	−17:39:18.0	0.84	0.50	Young	Be	#2
182	07227−1320	07:25:03.1	−13:26:19.9	0.76	−0.66	Post-AGB		#2
183	07253−2001	07:27:33.0	−20:07:19.6	0.95	−1.00	Post-AGB		#2
186	07280−1829	07:30:16.7	−18:35:49.1	2.11	0.97	Young	Ae	#2
188	07331+0021	07:35:41.2	00:14:57.9	1.62	−1.41	Post-AGB		#3
192	07430+1115	07:45:51.4	11:08:19.6	1.48	−1.12	Post-AGB		#2
197	07506−0345	07:53:07.4	−03:53:32.2	0.93	−0.55	Young	B7e	#2,#10
201	07582−4059	07:59:57.7	−41:07:23.3	1.74	−0.36	Post-AGB		#3
202	08005−2356	08:02:40.7	−24:04:42.7	1.15	−0.60	Post-AGB		#1,#8,#12
-	08046−3844	08:06:28.4	−38:53:24.0	≥2.41	−0.23	PN		#10
206	08143−4406	08:16:03.0	−44:16:04.6	2.97	−0.46	Post-AGB		#1,#3
209	08187−1905	08:20:57.1	−19:15:03.4	3.49	−0.39	Post-AGB		#2,#3
212	08213−3857	08:23:12.1	−39:07:07.4	1.73	0.06	Post-AGB		#3
214	08242−3828	08:26:03.8	−38:38:47.5	0.91	−0.19	No counterpart		#12
218	08281−4850	08:29:40.6	−49:00:04.3	1.61	−1.08	Post-AGB		#2,#12
222	08351−4634	...	...	0.79	−0.96	No counterpart		#12
223	08355−4027	08:37:24.7	−40:38:04.2	2.70	−0.04	PN		#3,#8
227	08418−4843	08:43:29.5	−48:54:46.8	2.47	0.15	PN		#3
236	08574−5011	08:59:02.3	−50:23:40.2	1.81	−0.08	PN		#8
251	09149−6206	09:16:09.4	−62:19:29.6	0.99	0.79	Galaxy		#1
254	09362−5413	09:37:51.8	−54:27:08.7	1.43	−1.21	PN		#8
255	09370−4826	...	...	1.11	−0.82	No counterpart		#2
260	09425−6040	09:44:01.7	−60:54:25.7	0.79	−1.05	Post-AGB		#3
261	09500−5236	09:51:49.2	−52:50:52.7	1.46	0.76	No counterpart		#2
-	09517−5438	...	...	≥1.95	0.68	PN		#10
262	10001−5857	10:01:48.1	−59:12:12.5	1.00	0.60	Young	F3e	#1
263	10029−5553	10:04:40.1	−56:08:37.2	2.11	−0.73	PN		#8
268	10115−5640	10:13:19.7	−56:55:32.3	2.12	−0.24	PN		#8,#10
270	10178−5958	10:19:32.5	−60:13:29.3	2.42	0.75	Transition		#3,#10,#12
272	10197−5750	10:21:33.9	−58:05:47.7	1.84	−0.67	Transition		#10

Table 3: List of IRAS fields observed (continued).

GLMP	IRAS	RA (J2000)	Dec (J2000)	[12]−[25]	[25]−[60]	Classification	Spectral type/class (not evolved)	Run
273	10211−5922	10:22:53.9	−59:37:28.4	1.72	−0.40	Peculiar	LBV	#2
275	10215−5916	10:23:19.5	−59:32:04.7	2.35	−0.78	Transition		#3,#8,#10,#12
277	10256−5628	10:27:35.2	−56:44:19.8	2.74	−0.63	Post-AGB		#3,#15
285	10594−3426	11:01:51.9	−34:42:17.0	1.36	0.51	Young	K1e	#2
289	11065−6026	11:08:40.1	−60:42:51.7	3.02	−0.50	Peculiar	LBV	#1,#8,#12
294	11195−2430	11:22:05.3	−24:46:39.4	1.68	−0.26	Young	K5	#3
295	11201−6545	11:22:18.9	−66:01:50.7	3.10	−0.74	Post-AGB		#2
300	11307−5402	11:33:05.6	−54:19:28.5	1.67	0.17	Young	F0e	#2,#3
303	11339−6004	11:36:20.7	−60:20:53.3	1.59	−0.75	No counterpart		#7,#12
-	11353−6037	11:37:42.9	−60:53:51.4	≥4.30	0.37	Transition		#10,#15
306	11381−6401	11:40:32.0	−64:18:34.9	1.78	−0.53	No counterpart		#3
307	11387−6113	11:41:08.7	−61:30:17.3	2.07	−0.53	Post-AGB		#3
312	11472−7834	11:49:31.8	−78:51:01.1	1.28	−0.18	Young	M	#10
-	11531−6111	11:55:38.0	−61:28:16.8	≥2.34	−0.45	Transition		#10,#15
317	12002−5333	12:02:47.6	−53:50:07.8	1.20	0.77	Galaxy		#8
318	12067−4508	12:09:23.8	−45:25:34.7	0.78	−0.72	Post-AGB		#2
-	12145−5834	12:17:16.1	−58:51:29.5	≥2.19	−0.26	Post-AGB		#10
323	12262−6417	...	...	1.38	−0.21	No counterpart		#10
326	12302−6317	12:33:07.0	−63:33:42.7	0.96	−1.30	Post-AGB		#12,#15
327	12309−5928	12:33:44.6	−59:45:18.5	1.09	−0.67	No counterpart		#8
328	12316−6401	12:34:36.0	−64:18:16.8	1.85	0.40	PN		#7
335	12405−6219	12:43:31.5	−62:36:13.5	2.04	0.90	No counterpart		#2,#8
339	13010−6012	13:04:05.5	−60:28:45.6	1.61	−0.58	Post-AGB		#3,#15
343	13185−6922	13:22:07.5	−69:38:12.2	0.93	0.16	Young	K0e	#2
345	13203−5917	13:23:32.2	−59:32:49.7	2.26	−1.51	Post-AGB		#12
346	13208−6020	13:24:04.4	−60:36:30.7	0.84	0.80	Young	em	#4
347	13245−5036	13:27:36.1	−50:52:05.7	1.23	−1.20	Post-AGB		#2
348	13266−5551	13:29:51.0	−56:06:53.7	4.19	−0.01	Post-AGB		#10
349	13293−6000	13:32:39.2	−60:15:39.2	1.04	1.02	No counterpart		#4
352	13313−5838	13:34:37.4	−58:53:32.3	1.27	−0.66	Post-AGB		#8
353	13356−6249	...	...	3.48	−0.32	No counterpart		#3,#12
360	13416−6243	13:45:07.3	−62:58:16.9	1.24	−0.37	Post-AGB		#2,#15

Table 3: List of IRAS fields observed (continued).

GLMP	IRAS	RA (J2000)	Dec (J2000)	[12]−[25]	[25]−[60]	Classification	Spectral type/class (not evolved)	Run
362	13427−6531	13:46:25.7	−65:46:24.4	2.68	−0.45	No counterpart		#3
363	13428−6232	13:46:20.5	−62:47:59.6	2.97	0.17	Post-AGB		#15
366	13483−6232	13:51:55.1	−62:46:56.6	2.06	1.11	Young	-	#8
368	13500−6106	...	...	1.65	−0.22	No counterpart		#12
371	13529−5934	13:56:24.6	−59:48:57.2	2.20	−0.10	No counterpart		#3
374	14079−6402	14:11:46.3	−64:16:24.0	1.82	−1.41	PN		#3
377	14122−5947	14:15:53.3	−60:01:37.9	1.48	−0.37	PN		#7,#8,#12
381	14177−5824	14:21:19.9	−58:38:22.5	2.37	0.29	PN		#1,#7,#8
384	14325−6428	14:36:34.4	−64:41:31.1	2.41	−0.63	Post-AGB		#1
385	14331−6435	14:37:10.1	−64:48:04.7	3.57	−0.47	Post-AGB		#10
386	14341−6211	14:38:05.0	−62:24:47.6	1.68	−0.92	Post-AGB		#3,#15
387	14345−5858	14:38:20.0	−59:11:46.1	2.20	0.03	PN		#10
388	14346−5952	14:38:24.6	−60:04:53.0	0.88	0.03	Post-AGB		#8
391	14429−4539	14:46:13.8	−45:52:05.1	0.89	−0.97	Post-AGB		#1,#15
393	14482−5725	14:51:57.3	−57:38:19.0	1.49	−0.90	Post-AGB		#3
394	14488−5405	14:52:28.7	−54:17:42.7	2.458	−0.81	Post-AGB		#2
399	14592−6311	15:03:23.8	−63:22:58.9	0.80	0.62	Young	em	#1
-	15039−4806	15:07:27.4	−48:17:53.8	≥3.09	−0.19	Post-AGB		#7,#15
403	15066−5532	15:10:26.0	−55:44:13.3	3.90	−0.19	Transition		#3
404	15093−5732	...	...	1.48	0.10	No counterpart		#10,#15
405	15103−5754	15:14:18.5	−58:05:20.3	2.43	0.24	No counterpart		#8
408	15144−5812	15:18:21.9	−58:23:12.0	1.67	0.01	No counterpart		#3
409	15154−5258	15:19:08.2	−53:09:46.6	1.90	0.10	PN		#1,#7
411	15210−6554	15:25:31.7	−66:05:20.0	1.79	−1.37	Post-AGB		#3,#15
416	15310−6149	15:35:17.1	−61:59:04.1	1.51	−0.70	Post-AGB		#3
422	15373−4220	15:40:46.4	−42:29:53.6	1.61	0.07	Young	A79	#3
424	15406−4946	15:44:20.5	−49:56:24.1	0.99	−0.30	Post-AGB		#3
431	15482−5741	15:52:19.4	−57:50:53.2	2.56	−0.61	Post-AGB		#12
437	15534−5422	15:57:21.1	−54:30:46.1	2.23	0.44	No counterpart		#10
441	15556−2248	15:58:36.9	−22:57:15.3	1.41	0.79	Young	G8e	#1,#7,#13
442	15559−5546	15:59:57.4	−55:55:34.0	0.88	−0.75	PN		#3

Table 3: List of IRAS fields observed (continued).

GLMP	IRAS	RA (J2000)	Dec (J2000)	[12]−[25]	[25]−[60]	Classification	Spectral type/class (not evolved)	Run
444	15579−5445	16:01:50.8	−54:53:40.1	2.52	−0.15	PN		#3,#10
446	16053−5528	16:09:20.2	−55:36:10.0	2.76	0.92	PN		#7,#12
456	16114−4504	16:15:03.0	−45:11:54.5	2.27	0.43	PN		#7
457	16115−5044	16:15:18.0	−50:52:19.7	3.13	1.08	Young	-	#4
-	16206−5956	16:25:02.6	−60:03:32.3	≥3.72	0.12	Post-AGB		#7
464	16228−5014	16:26:31.3	−50:21:26.9	3.78	1.04	No counterpart		#4
466	16241−2412	16:27:10.3	−24:19:18.9	2.35	0.58	Young	G1	#3
469	16279−4757	16:31:38.7	−48:04:05.7	1.98	−0.54	Post-AGB		#10
472	16283−4424	16:31:58.4	−44:31:18.6	2.49	−1.40	Post-AGB		#8
474	16289−4449	16:32:32.2	−44:55:30.7	1.32	0.83	Young	em	#7
478	16333−4807	...	...	1.66	0.79	No counterpart		#7
488	16476−1122	16:50:24.3	−11:27:57.8	1.31	−0.92	Post-AGB		#11
490	16494−3930	16:52:55.4	−39:34:56.2	1.73	−1.02	Post-AGB		#12,#15
494	16518−3425	...	...	2.23	−1.70	No counterpart		#10
495	16529−4341	16:56:34.0	−43:46:14.7	2.95	0.10	PN		#7,#8,#15
498	16552−3050	16:58:27.8	−30:55:06.2	1.57	−0.10	Post-AGB		#3
500	16559−2957	16:59:08.2	−30:01:40.3	1.37	−0.74	No counterpart		#7,#8,#9
504	16584−3710	17:01:52.1	−37:14:53.8	2.07	−0.36	No counterpart		#10
507	16594−4656	17:03:11.2	−47:00:21.0	2.05	−0.89	Transition		#3
509	17009−4154	17:04:29.6	−41:58:38.7	2.66	−0.29	No counterpart		#10,#15
510	17010−3810	17:04:27.3	−38:14:41.7	2.06	−0.71	No counterpart		#10
522	17074−1845	17:10:24.2	−18:49:00.7	3.47	−0.83	Transition		#10,#13,#15
525	17086−2403	17:11:38.9	−24:07:33.1	2.22	−1.83	Transition		#4,#13
527	17088−4221	...	...	1.19	−0.20	No counterpart		#7
526	17088−4227	17:12:21.8	−42:30:50.3	3.23	−0.30	PN		#8
531	17106−3046	17:13:51.8	−30:49:40.7	2.98	−0.21	Post-AGB		#10,#15
535	17119−5926	17:16:21.1	−59:29:23.3	3.44	−0.69	PN		#7,#8,#10,#12,#15
537	17130−4029	...	...	2.83	−0.02	No counterpart		#4
538	17131−3330	17:16:26.2	−33:33:23.8	2.43	1.07	PN		#8
542	17153−3814	17:18:44.7	−38:17:21.2	2.17	1.08	No counterpart		#3
546	17164−3226	17:19:40.8	−32:29:52.7	2.48	0.68	PN		#8,#15
547	17168−3736	...	...	1.44	0.28	No counterpart		#3,#15

Table 3: List of IRAS fields observed (continued).

GLMP	IRAS	RA (J2000)	Dec (J2000)	[12]−[25]	[25]−[60]	Classification	Spectral type/class (not evolved)	Run
554	17195−2710	17:22:43.6	−27:13:36.9	1.17	−0.75	Post-AGB		#11
-	17203−1534	17:23:11.9	−15:37:15.1	3.81	−0.48	Post-AGB		#7
556	17208−3859	17:24:19.5	−39:01:46.0	2.84	−0.07	Post-AGB		#4
558	17223−2659	17:25:25.2	−27:02:03.3	2.15	−1.48	Post-AGB		#3,#15
563	17234−4008	17:26:56.1	−40:11:03.7	2.31	−0.19	No counterpart		#10,#15
565	17245−3951	17:28:04.6	−39:53:44.3	2.81	−0.17	Post-AGB		#4,#15
567	17253−2831	17:28:33.0	−28:33:25.8	2.95	−0.27	Post-AGB		#4
572	17269−2235	17:29:58.7	−22:37:44.5	3.35	0.44	No counterpart		#7
574	17287−3443	17:32:04.8	−34:45:32.6	3.81	−0.81	Post-AGB		#10,#15
575	17291−2402	17:32:12.8	−24:04:59.9	2.41	0.18	Transition		#7
578	17300−3509	17:33:22.6	−35:11:03.7	2.32	0.87	Post-AGB		#4
580	17310−3432	17:34:20.8	−34:34:54.9	2.78	0.00	Post-AGB		#10,#15
581	17311−4924	17:35:02.5	−49:26:26.4	2.29	−1.02	Transition		#8
584	17317−2743	17:34:53.3	−27:45:11.5	3.56	0.07	Post-AGB		#11,#15
588	17332−2215	17:36:17.7	−22:17:24.9	2.57	−0.02	Post-AGB		#4,#15
591	17347−3139	17:38:00.6	−31:40:55.2	1.81	0.17	Transition		#15
-	17364−1238	17:39:16.9	−12:40:29.7	$\geq$1.76	−0.71	Post-AGB		#9
607	17370−3357	17:40:20.2	−33:59:14.4	2.45	0.23	Post-AGB		#15
608	17371−2747	17:40:23.3	−27:49:11.7	1.73	0.35	PN		#4,#15
611	17376−2040	17:40:38.6	−20:41:52.6	0.81	−0.38	Post-AGB		#11
-	17381−1616	17:40:59.8	−16:17:58.9	$\geq$3.41	−1.66	PN		#9
616	17388−2203	17:41:49.0	−22:05:15.9	3.16	−0.17	Post-AGB		#7,#15
619	17392−3020	17:42:30.4	−30:22:10.7	1.09	0.81	Post-AGB		#15
621	17395−0841	17:42:14.4	−08:43:19.5	2.82	0.76	PN		#4,#15
631	17418−3335	17:45:08.7	−33:36:06.2	2.25	−0.21	No counterpart		#15
632	17423−1755	17:45:14.2	−17:56:46.9	1.51	0.88	Transition		#4
639	17436+5003	17:44:55.5	50:02:39.5	3.69	−0.21	Post-AGB		#13
640	17441−2411	17:47:13.5	−24:12:51.4	1.62	−0.63	Post-AGB		#15
641	17443−2949	...	...	0.99	−0.14	No counterpart		#4
646	17460−3114	17:49:16.6	−31:15:18.1	1.30	−0.58	Young	B3	#8
647	17466−3031	17:49:52.5	−30:33:02.5	1.17	0.14	Transition		#15
651	17476−4446	17:51:16.4	−44:47:28.9	2.22	−1.61	Post-AGB		#10

Table 3: List of IRAS fields observed (continued).

GLMP	IRAS	RA (J2000)	Dec (J2000)	[12]−[25]	[25]−[60]	Classification	Spectral type/class (not evolved)	Run
-	17488−1741	17:51:48.9	−17:42:25.8	≥3.09	0.54	Post-AGB		#9
661	17514−1555	17:54:21.1	−15:55:52.0	1.51	−0.04	PN		#4
662	17516−2526	17:54:43.4	−25:26:28.0	0.88	−0.16	Post-AGB		#11
669	17542−0603	17:56:56.0	−06:04:09.7	1.60	−1.30	Post-AGB		#11
684	17576−2653	18:00:49.6	−26:53:12.7	1.87	−1.14	Post-AGB		#11,#15
686	17579−3121	18:01:12.8	−31:21:59.7	3.73	−0.08	Post-AGB		#4
687	17580−3111	18:01:19.6	−31:11:22.2	1.69	−0.71	No counterpart		#4
689	17582−2619	18:01:21.6	−26:19:37.3	2.07	−0.17	No counterpart		#4
698	17597−1442	18:02:38.3	−14:42:02.8	2.28	0.05	PN		#8,#11
711	18019−3403	18:05:13.7	−34:03:16.4	2.36	−1.46	Post-AGB		#10
713	18025−3906	18:06:03.3	−39:05:56.6	2.45	−0.34	Post-AGB		#4
-	18044−1303	18:07:15.3	−13:03:29.0	≥2.15	0.81	Post-AGB		#9
723	18061−2505	18:09:12.4	−25:04:34.5	1.35	0.10	PN		#10,#11
724	18062+2410	18:08:20.1	24:10:43.3	1.73	−2.08	Transition		#5,#8,#12,#13
726	18075−0924	18:10:15.1	−09:23:35.1	2.44	−0.35	Post-AGB		#4
737	18096−3230	18:12:57.5	−32:30:08.9	3.38	0.54	Post-AGB		#4
744	18108−3248	18:14:10.5	−32:47:34.4	1.44	0.86	Young	K1e	#7
759	18186−0833	18:21:21.1	−08:31:42.4	2.87	−0.43	PN		#4
771	18216−0156	18:24:14.3	−01:54:24.2	2.47	1.15	Young	em	#4
777	18246−1032	...	...	2.42	0.99	No counterpart		#4
-	18401−1109	18:42:57.1	−11:06:53.0	2.10	0.67	PN		#10
822	18415−2100	18:44:32.0	−20:57:12.8	1.04	−0.76	Peculiar	RCrB star	#10
823	18420−0512	18:44:41.7	−05:09:17.0	3.53	−0.02	Post-AGB		#11
829	18442−1144	18:47:04.0	−11:41:12.0	3.15	−0.10	Transition		#7
844	18520+0007	18:54:34.8	00:11:04.4	2.42	−0.11	PN		#14
845	18524+0544	18:54:54.1	05:48:11.3	2.95	−0.12	No counterpart		#10
849	18533+0523	18:55:46.7	05:27:03	2.61	−0.30	No counterpart		#7,#14
855	18576+0341	...	...	1.68	−0.47	No counterpart		#15
858	18582+0001	19:00:49.0	00:06:14.1	2.32	0.43	Post-AGB		#11,#15
869	19016−2330	19:04:43.6	−23:26:09.1	1.65	−0.78	Transition		#4,#6,#7,#15
879	19024+0044	19:05:02.1	00:48:50.9	3.08	−0.15	Post-AGB		#11,#15

Table 3: List of IRAS fields observed (continued).

GLMP	IRAS	RA (J2000)	Dec (J2000)	[12]−[25]	[25]−[60]	Classification	Spectral type/class (not evolved)	Run
875	19063−3709	19:09:45.9	−37:04:26.1	0.96	0.49	Young	K5e	#4
883	19083+0119	19:10:54.5	01:24:45.0	2.06	−0.10	No counterpart		#4
890	19114+0002	19:13:58.6	00:07:31.9	3.29	−0.25	Post-AGB		#4,#13
895	19154+0809	19:17:50.6	08:15:08.5	1.87	−1.63	PN		#11
-	19200+3457	19:21:55.3	35:02:55.1	2.32	≥−0.41	Post-AGB		#9
907	19207+2023	19:22:55.8	20:28:54.8	3.05	−0.66	Post-AGB		#4
908	19208+1541	19:23:05.9	15:47:31.3	0.77	0.83	No counterpart		#4
914	19225+3013	19:24:26.9	30:19:26.7	0.97	−0.75	Post-AGB		#11
923	19306+1407	19:32:55.1	14:13:36.9	3.04	−0.66	Post-AGB		#4
935	19356+0754	19:38:02.2	08:01:33.8	2.13	−0.05	Post-AGB		#4
941	19386+0155	19:41:08.3	02:02:31.3	1.09	−1.03	Post-AGB		#11,#15
-	19422+1438	19:44:31.7	14:45:24.6	≥2.09	−0.03	Post-AGB		#9
950	19454+2920	...	...	1.79	−0.54	No counterpart		#11
952	19477+2401	19:49:54.9	24:08:53.3	1.72	−0.77	Post-AGB		#11
954	19500−1709	19:52:52.7	−17:01:50.4	1.93	−0.88	Post-AGB		#14,#15
961	19589+4020	20:00:43.0	40:29:09.6	2.62	−0.76	Post-AGB		#11
962	19589+3419	20:00:52.9	34:28:22.2	0.69	−0.09	PN		#11
-	19590−1249	20:01:49.8	−12:41:17.8	3.87	−0.50	Transition		#7,#8
987	20160+2734	20:18:05.9	27:44:03.6	0.77	−0.04	Post-AGB		#13
988	20174+3222	20:19:27.8	32:32:15.2	2.04	−0.75	No counterpart		#5,#6
998	20259+4206	20:27:42.3	42:16:44.1	1.37	−0.23	Post-AGB		#11
1003	20406+2953	20:42:46.0	30:04:06.4	1.85	−0.35	No counterpart		#6
1008	20462+3416	20:48:16.6	34:27:24.3	4.18	−0.13	Transition		#11,#13,#14
1012	20490+5934	20:50:13.6	59:45:51.2	1.78	0.40	Young	A3e	#11
1013	20559+6416	20:15:58.4	47:05:35.9	1.08	−0.23	Young	A3e	#6,#11
1015	20572+4919	20:58:55.6	49:31:13.2	1.01	−0.13	Post-AGB		#9,#11
1034	21289+5815	21:30:22.8	58:28:52.0	0.79	−0.44	Post-AGB		#6
1044	21537+6435	...	...	1.44	−0.73	No counterpart		#6
1047	21546+4721	21:56:33.0	47:36:12.8	1.49	−1.08	Transition		#5
1051	22023+5249	22:05:30.3	53:21:33	3.46	−0.58	Transition		#5,#6
1052	22036+5306	22:05:30.3	53:21:32.8	1.85	0.91	Post-AGB		#6
1058	22223+4327	22:24:31.4	43:43:10.9	3.11	−0.55	Post-AGB		#13

Table 3: List of IRAS fields observed (continued).

GLMP	IRAS	RA (J2000)	Dec (J2000)	[12]−[25]	[25]−[60]	Classification	Spectral type/class (not evolved)	Run
1073	23198−0230	23:22:24.7	−02:13:41.4	1.08	−0.68	Young	G2e	#6,#7,#15

Table 4: Main characteristics derived for the IRAS sources identified as post-AGB stars.

IRAS name	Other identifications	Spectral type our survey	Spectral type (SIMBAD)	Reliability code†
01005+7910		Fe	B2Iab:e	AA
01259+6823		F5Ie	GIab:	AA
02143+5852		F7Ie	A5	AA
04296+3429		F7I	G0Ia	AA
05089+0459		M3I	M	AB
05113+1347	PM 2-4	G5I	G8Ia	AA
05341+0852		F5I	F4Iab:	AA
05381+1012		G2I	G	AA
06530−0213	PM 1-24	G1I	F0Iab:	AA
07134+1005		F7Ie	F5Iab:	AA
07227−1320		M1I		AA
07253−2001		F2I		AA
07331+0021		K35I	G5Iab	AA
07430+1115		M2I	G5Ia	AA
07582−4059	PM 1-35	G5I		AA
08005−2356		F5Ie	F5e	AA
08143−4406	PM 1-39	K12I		AA
08187−1905		G1I	F6Ib/II	AA
08213−3857		F2Ie	F3V	AA
08281−4850	PM 1-40	F0I		AA
09425−6040		C		AA
10256−5628	PM 2-11	F5I		AA
11201−6545	PM 1-56	A3Ie		AA
11387−6113		A3Ie		AA
12067−4508	Hen 3-755	G1Ie	G2w...	AA
12145−5834	PM 1-64	em		AA
12302−6317		*		AA
13010−6012	PM 1-72	M2I		CA
13203−5917		G2I		AA
13245−5036		A79Ie		AA
13266−5551		B1Ie	O+...	AA
13313−5838		K5I	K1III	AA
13416−6243		*		AA
13428−6232	PM 2-14	em		AA
14325−6428		F5I		AA
14331−6435	Hen 3-1013	B8Ie	B3Iab:e	AA
14341−6211	PM 1-85	*		BA
14346−5952		em		AA
14429−4539		F4Ie	M	AA
14482−5725	PM 1-86	A2I		AA
14488−5405		A0Ie		AA
15039−4806		A0I	A1/A2Ib/	AA
15210−6554	PM 2-16	K2I		BA
15310−6149		A7I	F0V	AA

Table 4: Main characteristics derived of the IRAS sources identified as Post AGB stars (continued).

IRAS name	Other identifications	Spectral type our survey	Spectral type (SIMBAD)	Reliability code†
15406−4946		M4II		AA
15482−5741		F7I		AA
16206−5956		A3Ie	A3Iab:e	AA
16279−4757	PM 2-18	M3II		AA
16283−4424	PM 2-19	A2Ie		AA
16476−1122		M1I		AA
16494−3930		G2I		CA
16552−3050	PM 1-120	K0I		AA
17106−3046	PM 2-23	F5I		AA
17195−2710	PN G358.7+05.1	em		AA
17203−1534		A0Ie	B1IIIpe	AA
17208−3859	RPZM 14	A2I		AA
17223−2659	PM 2-26	M5III		AA
17245−3951	PM 2-27	F6I		AA
17253−2831		M4II		AA
17287−3443		*		CA
17300−3509	PM 1-156	G2I		AA
17310−3432	PM 1-157	A2I		AA
17317−2743	PM 1-158	F5I		CA
17332−2215	PM 1-160	K2I		AA
17364−1238	PM 1-167	em		BB
17370−3357	PM 1-169	G3I		AA
17376−2040		F6I		BA
17388−2203		G0I		AA
17392−3020		*		AA
17436+5003		A7I	F3Ib	AA
17441−2411		F4I	F5:	AA
17476−4446	PM 2-29	B7I		AA
17488−1741	PM 1-184	F7I		BA
17516−2526		em		AB
17542−0603	PM 2-32	em	Ge	AA
17576−2653	PM 1-198	A7I		BA
17579−3121	RPZM 44 PM 2-33	F4I		AA
18019−3403		B8I		AA
18025−3906	PM 2-34	G1I	G2	AA
18044−1303	PM 1-212	F7I		AA
18075−0924		G2I		AA
18096−3230	PM 1-218	G3I		AA
18420−0512	PM 1-255	M1I		AA
18582+0001	PM 1-272	K2I		AA
19024+0044		em		AA
19114+0002		F7I	G5Ia	AA
19200+3457	PM 1-300	Fe	B...	AA
19207+2023		F6I		AA

Table 4: Main characteristics derived of the IRAS sources identified as Post AGB stars (continued).

IRAS name	Other identifications	Spectral type our survey	Spectral type (SIMBAD)	Reliability code†
19225+3013		M2II		AA
19306+1407		G5I	B0:e	AA
19356+0754		K2I		AA
19386+0155		F5I	F	AA
19422+1438	PM 1-312	F5I		AA
19477+2401		F4I-F7I		AA
19500−1709		F0Ie	F2/F3Iab	AA
19589+4020	PM 1-315	F5I		AA
20160+2734		F3Ie		AA
20259+4206		F3I		AA
20572+4919		F3Ie	Fe	AA
21289+5815		A2Ie		AA
22036+5306		em		AA
22223+4327		F7I	G0Ia	AA

† This code rates our confidence in the data presented, with A representing the maximum reliability. The first letter marks our confidence in the correct identification of the optical counterpart, and the second letter indicates how confident we are in the evolutionary classification assigned.
* Faint and red continuum.

Table 5. Main characteristics derived for the IRAS sources identified as transition objects.

IRAS name	Other names	Spectral type our survey	Spectral type (SIMBAD)	Reliability code†	Morphology
10178−5958	PN G285.1-02.7 Hen 3-401	BeI	Be	AA	Bipolar [1]
10197−5750	Hen 3-404	A0Ie	A2Iabe	AA	Bipolar [2]
10215−5916		A7eI	K0	AA	
11353−6037	PM 1-60	B5Ie		AA	
11531−6111	PM 1-61	B8eI		AA	
15066−5532	PM 2-15			AA	
16594−4656	PN G340.3-03.2	Ae	B7	AA	Multipolar [3]
17074−1845	Hen 3-1347	B3eI	B3IIIe	AA	
17086−2403	PN G359.8+08.9 PM 2-22		G5IV-V	AA	
17291−2402	PN G002.5+05.1 PM 1-155			AA	
17311−4924	PN G341.4-09.0 Hen 3-1428	B3Ie	B1IIe	AA	
17347−3139	RPZM 28			AA	Bipolar [4]
17423−1755	PN G009.3+05.7 Hen 3-1475		Be	AA	Bipolar [5]
17466−3031	RPZM 42			AA	
18062+2410	PN G050.6+19.7	B3e	B1IIIpe	AA	
18442−1144	PN G022.0-04.3		A3V	AA	
19016−2330	PN G013.1-13.2			AA	
19590−1249	PN G029.1-21.2	B2eI	B1Ibe	AA	
20462+3416	PN G076.6-05.7		B1Iae	AA	
21546+4721	PN G095.0-05.5			AA	
22023+5249	PN G099.3-01.9		Be	AA	

† This code rates our confidence in the data presented, with A representing the maximum reliability. The first letter marks our confidence in the correct identification of the optical counterpart, and the second letter indicates how confident we are in the evolutionary classification assigned.
[1] García-Lario et al. (1999a); [2] Allen et al. (1980); [3] García-Lario et al. (1999b); [4] de Gregorio-Monsalvo et al. (2004); [5] Riera et al. (1995).

Table 6: Main characteristics derived from the optical images and spectra of the IRAS sources identified as PNe.

IRAS name	PN G name	Other names	Morphology	Size (″)	c	Excitation class	WR subtype	Code†
06518−1041	222.8−04.2	PM 1-23	Bipolar	20	1.1		[WC7]	AA
07027−7934	291.3−26.2		Round	<15	2.3		[WC10]	AA
08046−3844	255.3-03.6		Compact	-	1.5	Medium		AA
08355−4027	260.7+00.9	PM 1-41	Round	12	3.0	Medium		AA
08418−4843			-	-	2.5	Medium		AA
08574−5011	270.1−02.9		Round	10	2.7	Medium		AA
09362−5413	277.1−01.5		Compact	<2	2.8	Low		AA
09517−5438	279.1-00.4		-	-	2.4	Medium		AA
10029−5553	281.1−00.4	PM 2-10	Compact	<3.4	High	-		AB
10115−5640	282.6−00.4	PM 1-51	Compact	<6.1	High	-		AB
12316−6401	301.1−01.4	PM 1-68	Compact	<2.3	1.1	Medium		AA
14079−6402			Compact	-	2.2	Low		AA
14122−5947	313.3+01.1		Elliptical/Bipolar	<4.5	High	-		AA
14177−5824	314.4+02.2	PM 1-81	Bipolar	6	4.9	Medium		AA
14345−5858	316.2+00.8		-	<9.9	High	-		AA
15154−5258	324.0+03.5	PM 1-89	Round	10	0.9		[WC4]	AA
15559−5546	327.1-02.2	Hen 2-142	Elliptical/Bipolar	5.3×3.2	1.4		[WC9]	AA
15579−5445	328.0−01.6	PM 1-105	-	<1.8	High	-		AA
16053−5528	328.4−02.8	PM 1-106	-	-	2.8	Low		AA
16114−4504	336.1+04.1	PM 2-17	Elliptical?	8	3.0	High		AA
16529−4341	342.2−00.3	PM 1-119	-	<4.7	High	-		AA
17088−4227	344.9−01.9	PM 1-131	-	<2.2	High	-		AA
17119−5926	331.3-12.1	Hen 3-1357	Elliptical/Bipolar	2.1×1.9	0.3	Medium		AA
17131−3330		PM 1-136 RPZM 10	-	<1.6	High	-		AA
17164−3226		PM 1-140 RPZM 12	-	<2.1	2.84	Medium		CA
17371−2747		OH6	-	-	4.7	Low		AA
17381−1616	010.2+07.5	PM 2-28	-	-	High	-		AA
17395−0841	017.0+11.1		Bipolar	5×8	1.9	Low		AA
17514−1555	012.2+04.9	PM 1-188	Round	18	1.2		[WC9]	AA
17597−1442	014.2+03.8	PM 1-205	Round	20	0.8		[WC9]	AA
18061−2505	005.9−02.6	PM 1-213	Bipolar	15×46	2.1	Low		AA
18186−0833	021.9+02.7	PM 1-226	Round	8	2.31	Medium		AA

Table 6: Characteristics of PNe (continued).

IRAS name	PN G name	Other names	Morphology	Size (″)	c	Excitation class	WR subtype	Code†
18401−1109	022.0−03.1	PM 1-252	Elliptical	9×11	1.0	High		AA
18520+0007			Compact	-	High	-		AB
19154+0809	043.2−02.0	PM 2-40	Compact	-	2.7	Low		AA
19589+3419	070.9+02.2	PM 1-316	Compact?	-	-	Low		AA

† This code rates our confidence in the data presented, with A representing the maximum reliability. The first letter marks our confidence in the correct identification of the optical counterpart, and the second letter indicates how confident we are in the evolutionary classification assigned.
* Spectroscopic range covered not enough to assign a classification.

Appendix A: Atlas of post-AGB stars

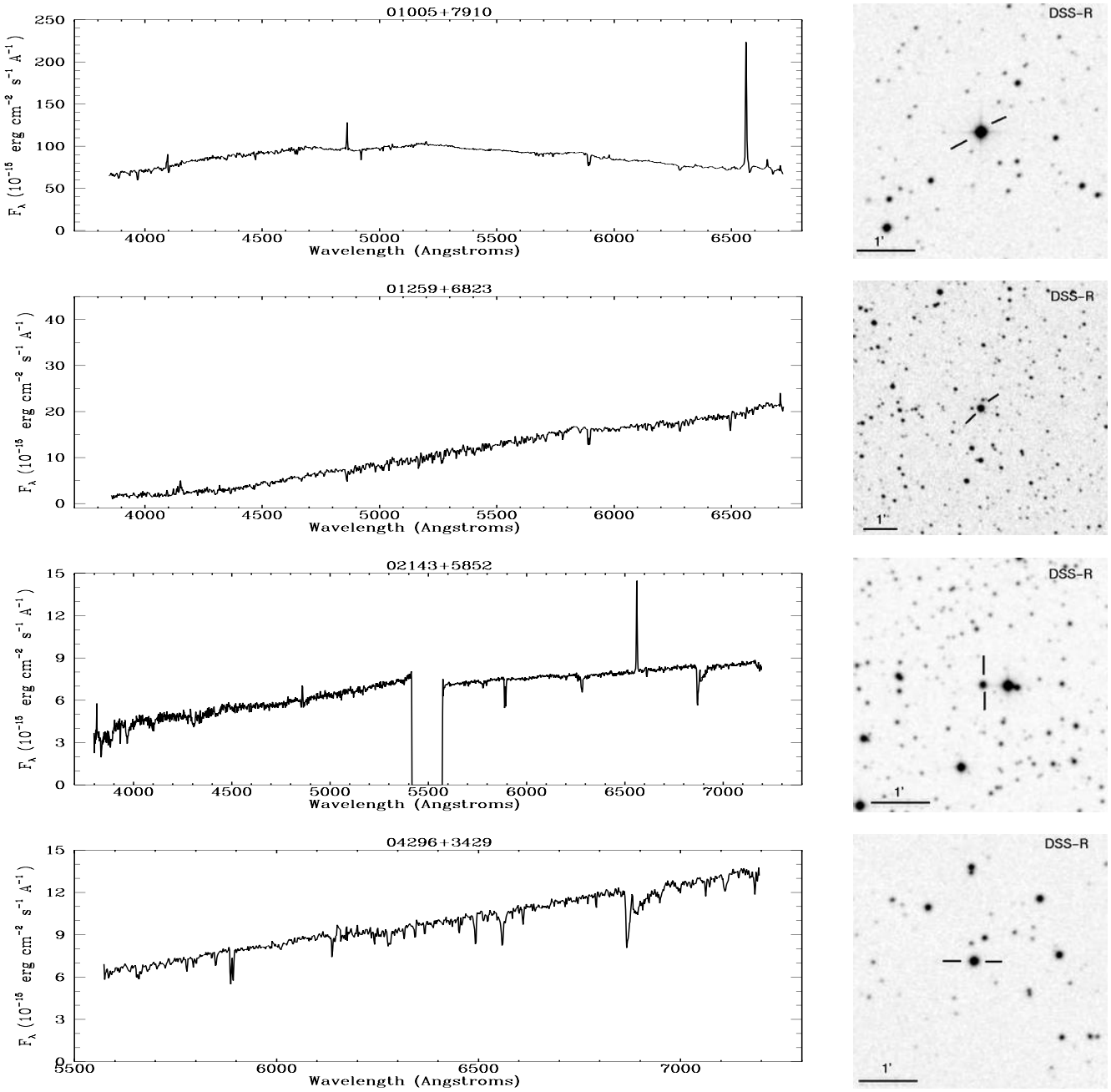

Fig. A.1. Spectra of the objects classified as post-AGB in the sample together with their corresponding identification charts.

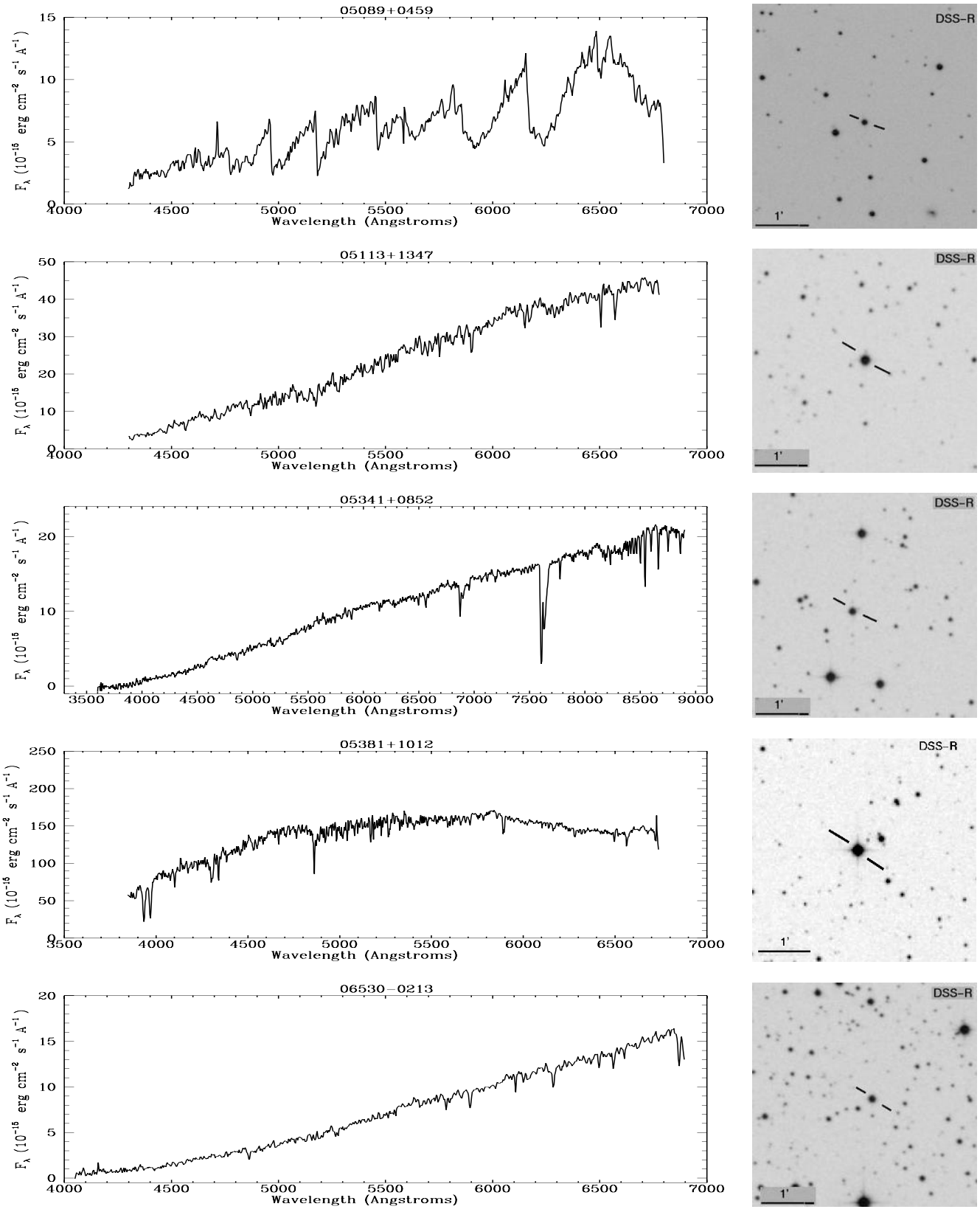

Fig. A.1. Spectra of the objects classified as post-AGB in the sample together with their corresponding identification charts (continued).

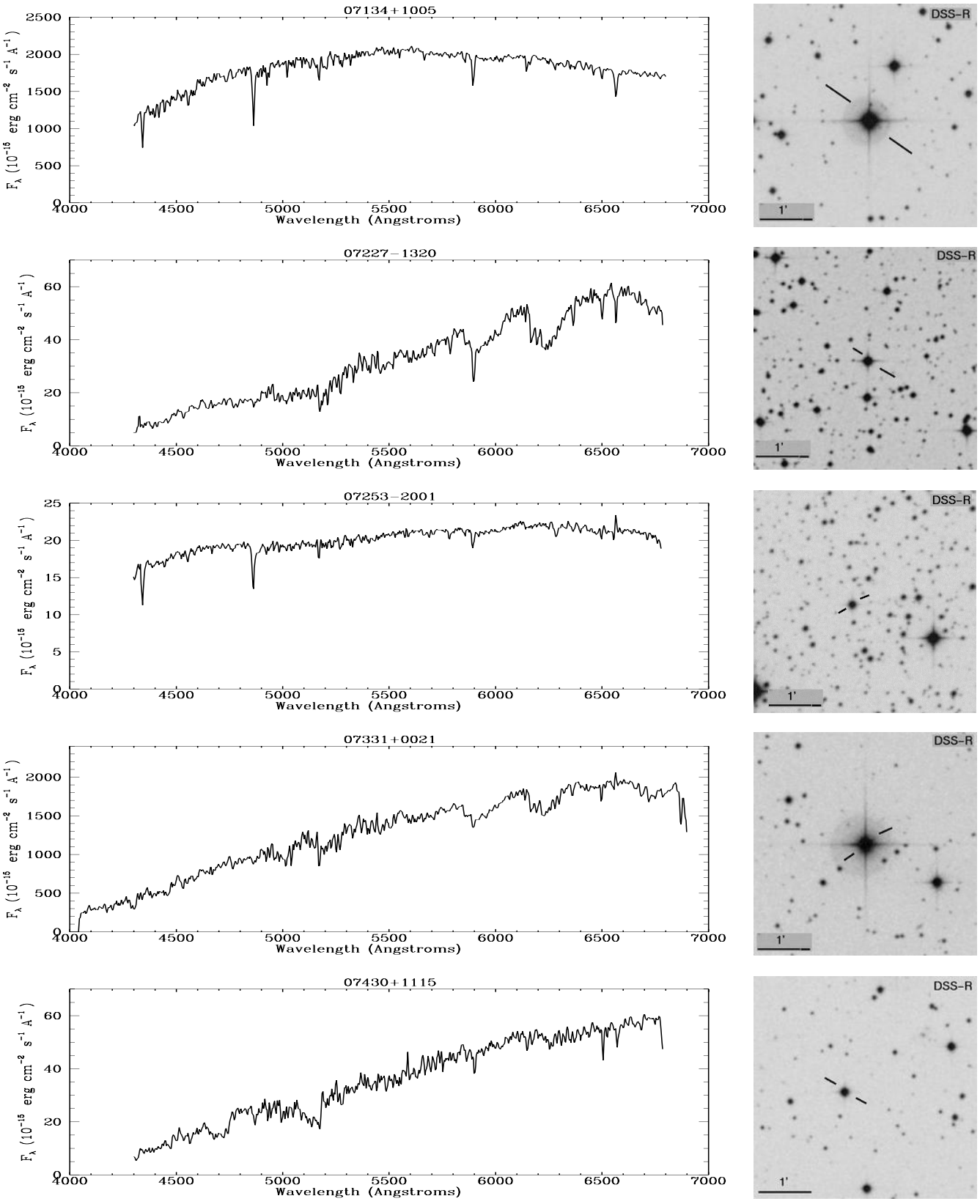

Fig. A.1. Spectra of the objects classified as post-AGB in the sample together with their corresponding identification charts (continued).

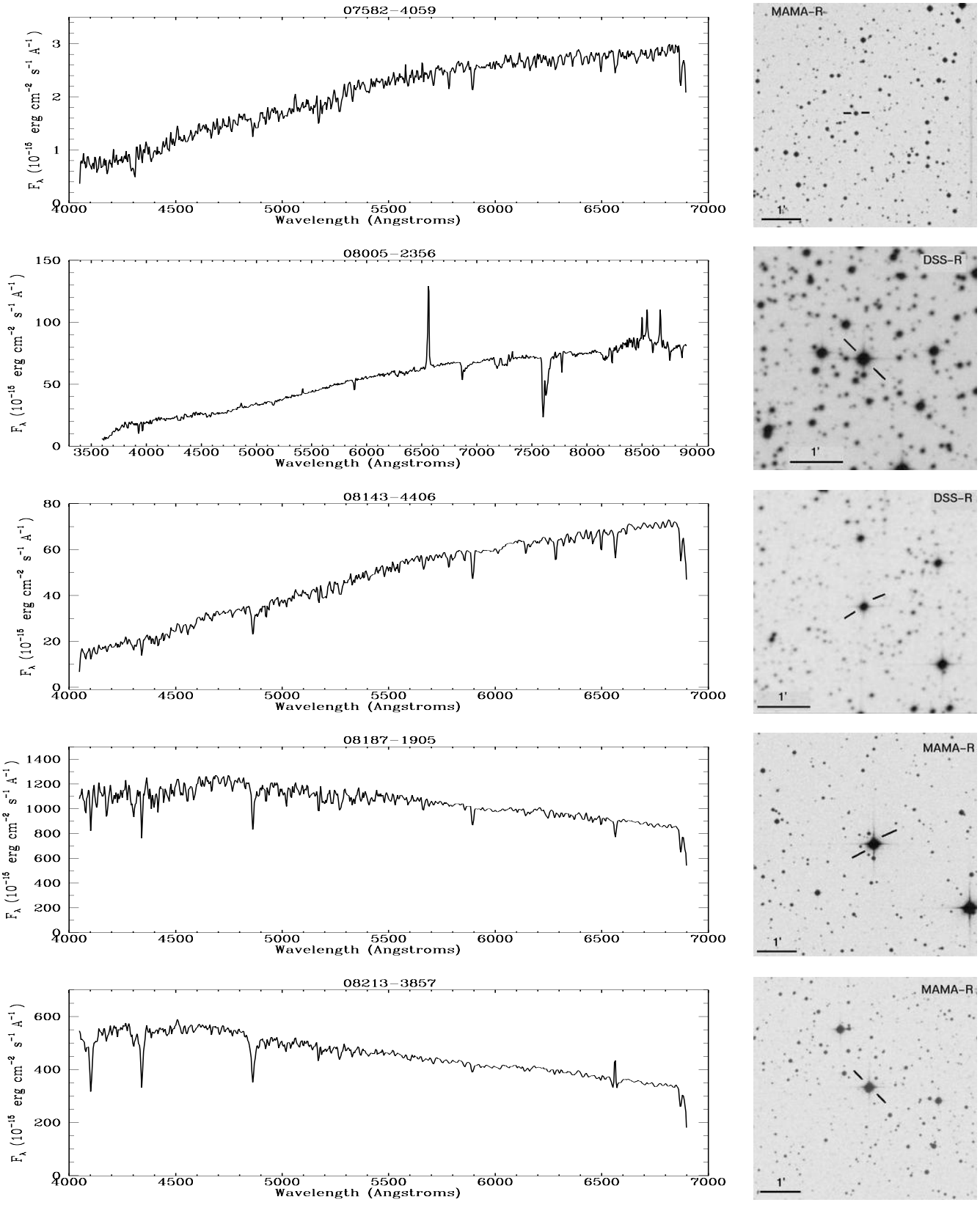

Fig. A.1. Spectra of the objects classified as post-AGB in the sample together with their corresponding identification charts (continued).

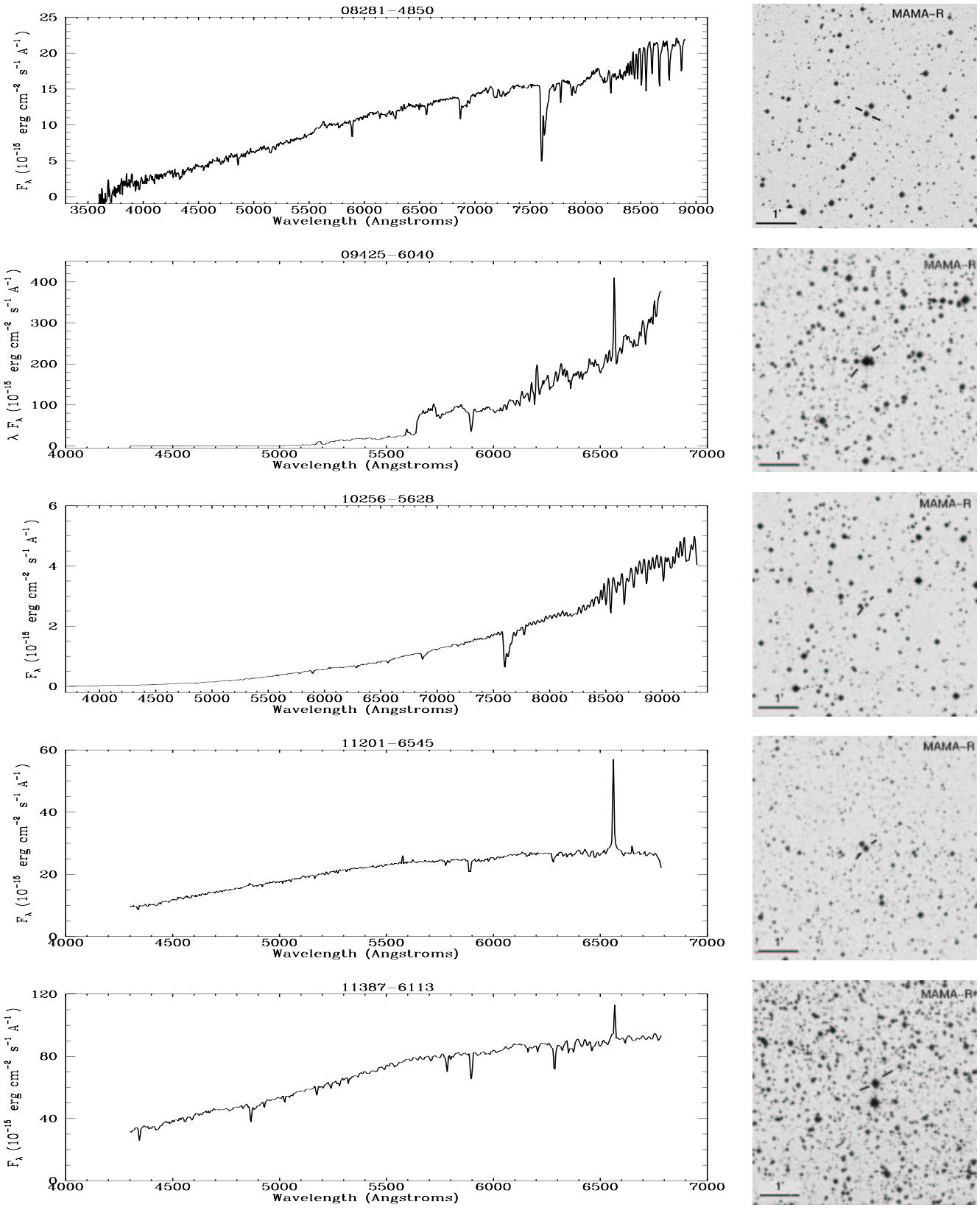

Fig. A.1. Spectra of the objects classified as post-AGB in the sample together with their corresponding identification charts (continued).

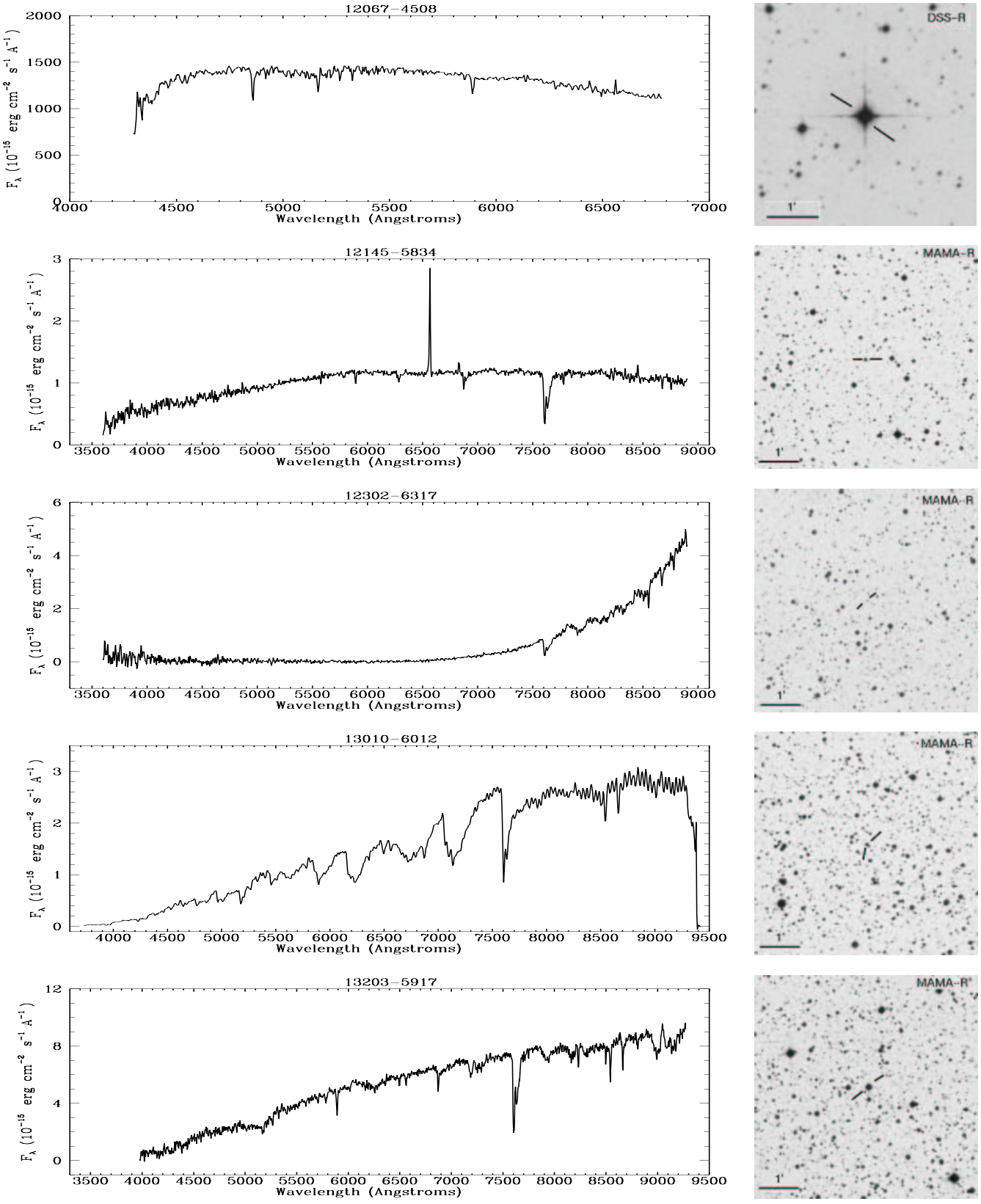

Fig. A.1. Spectra of the objects classified as post-AGB in the sample together with their corresponding identification charts (continued).

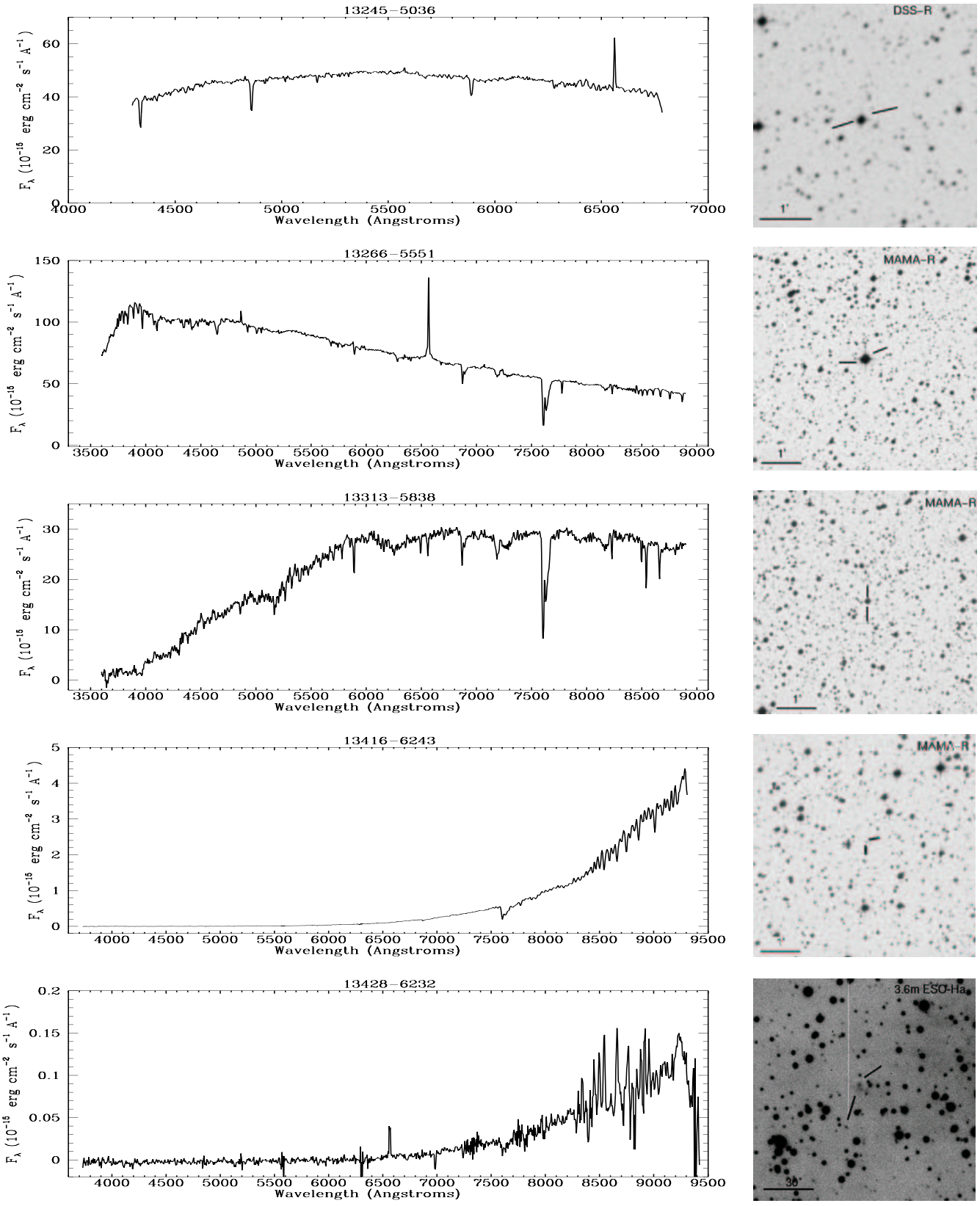

Fig. A.1. Spectra of the objects classified as post-AGB in the sample together with their corresponding identification charts (continued).

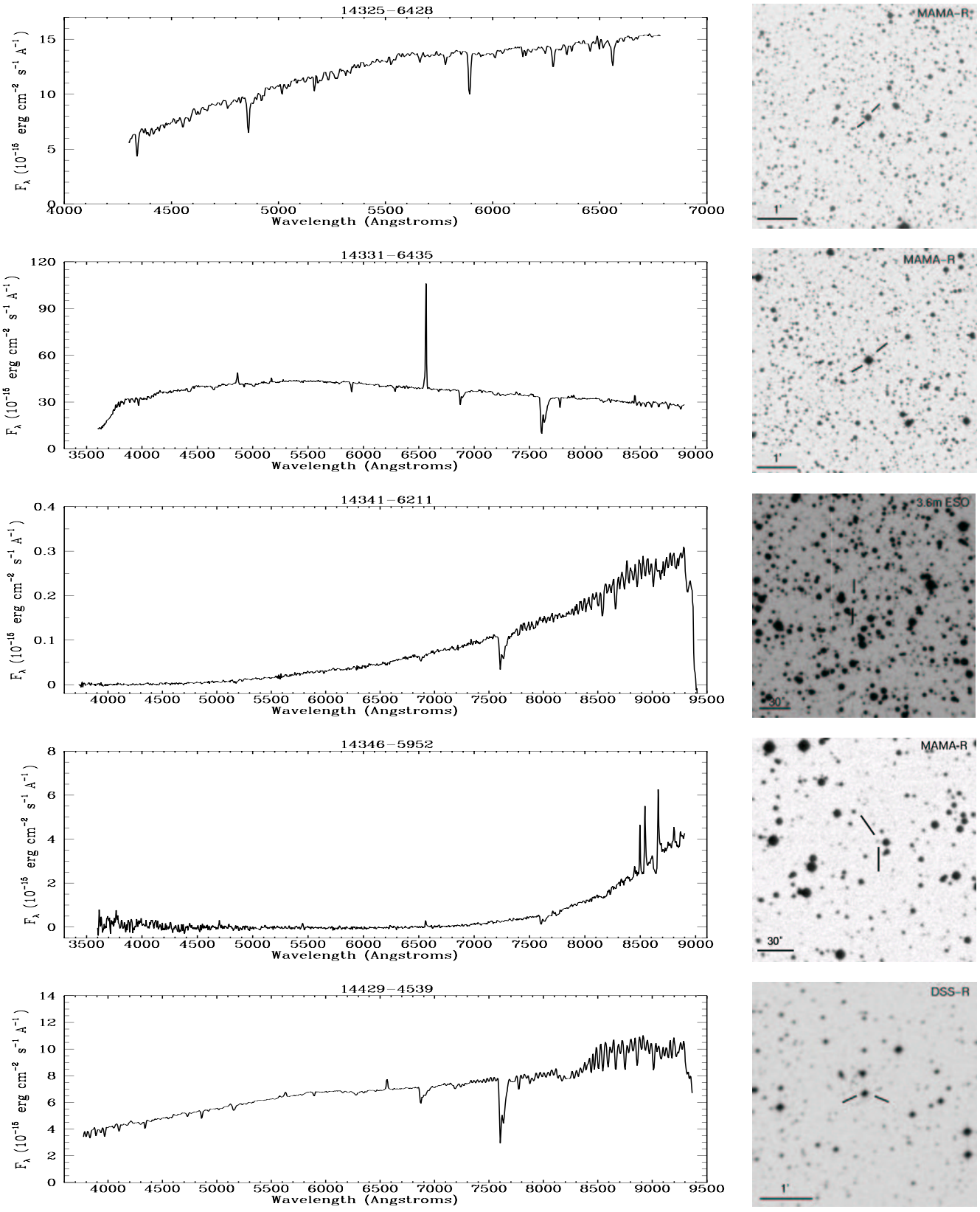

Fig. A.1. Spectra of the objects classified as post-AGB in the sample together with their corresponding identification charts (continued).

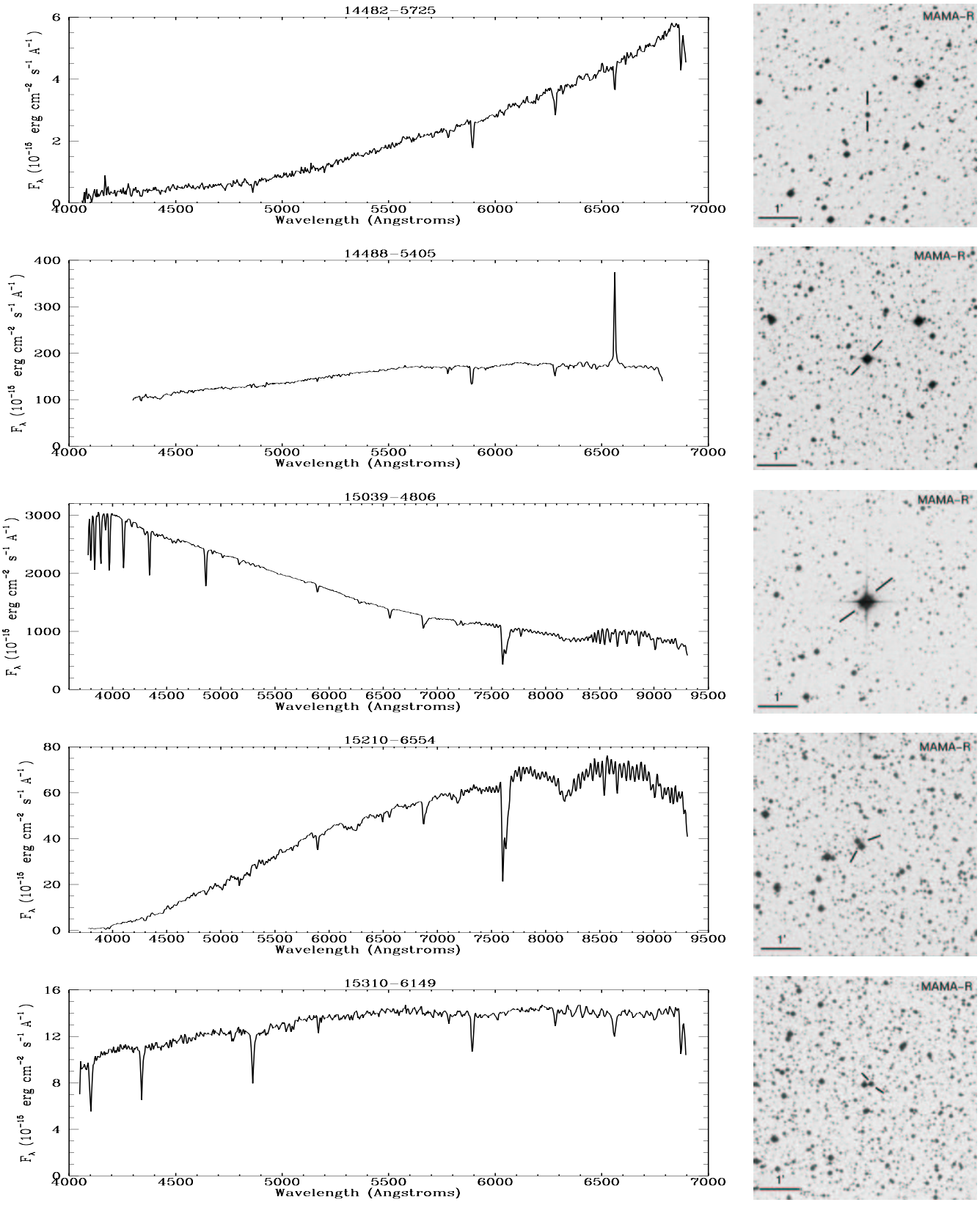

Fig. A.1. Spectra of the objects classified as post-AGB in the sample together with their corresponding identification charts (continued).

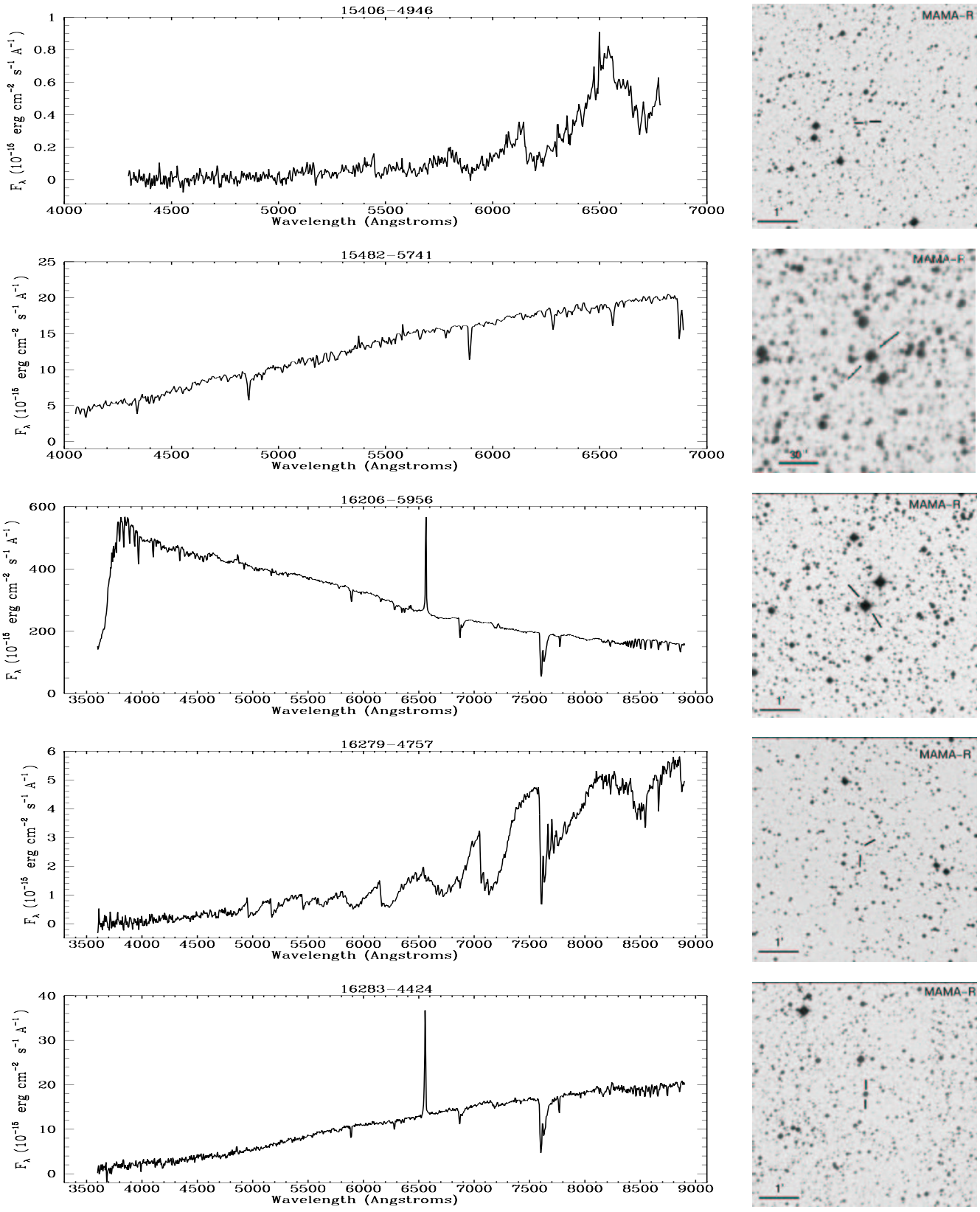

Fig. A.1. Spectra of the objects classified as post-AGB in the sample together with their corresponding identification charts (continued).

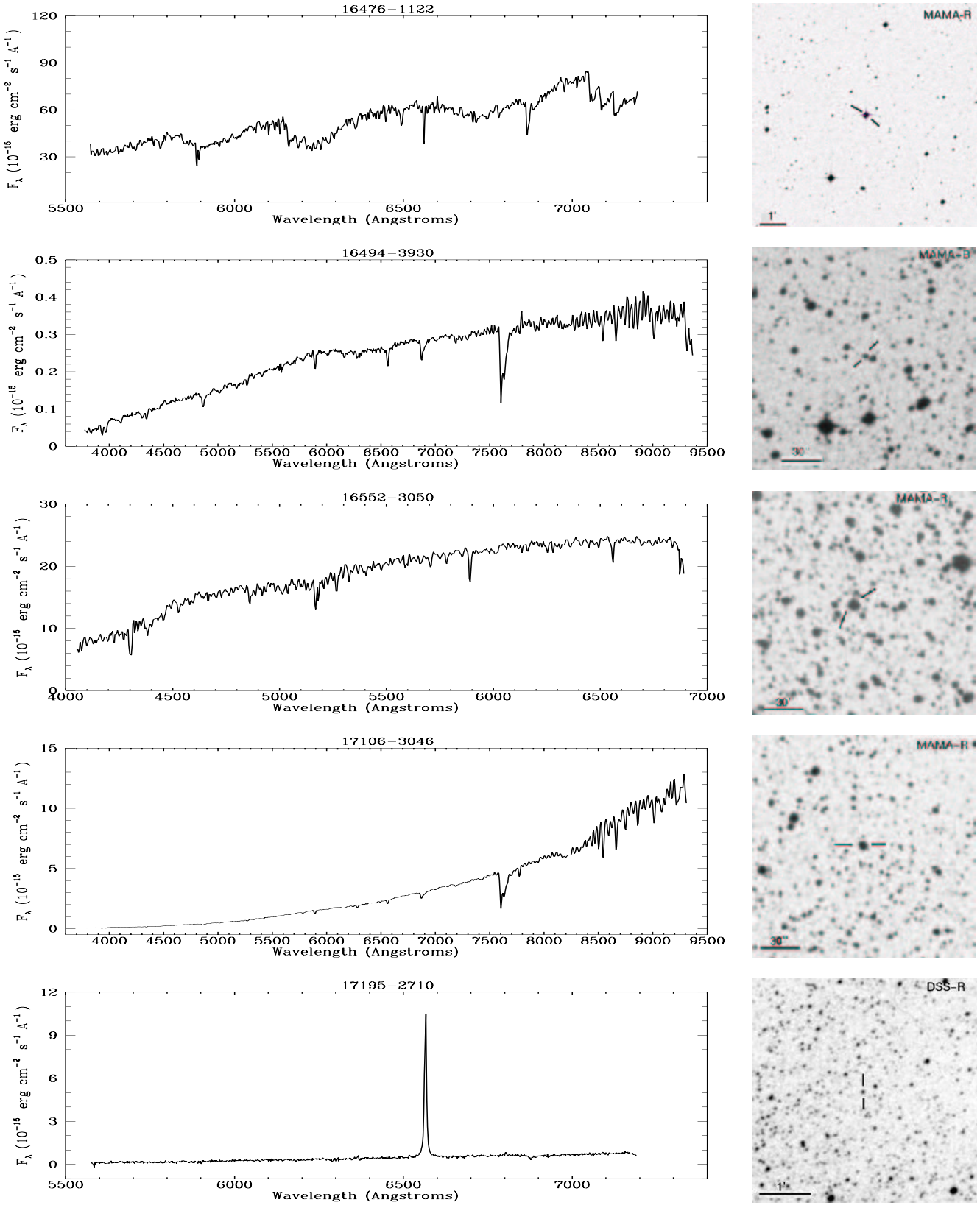

Fig. A.1. Spectra of the objects classified as post-AGB in the sample together with their corresponding identification charts (continued).

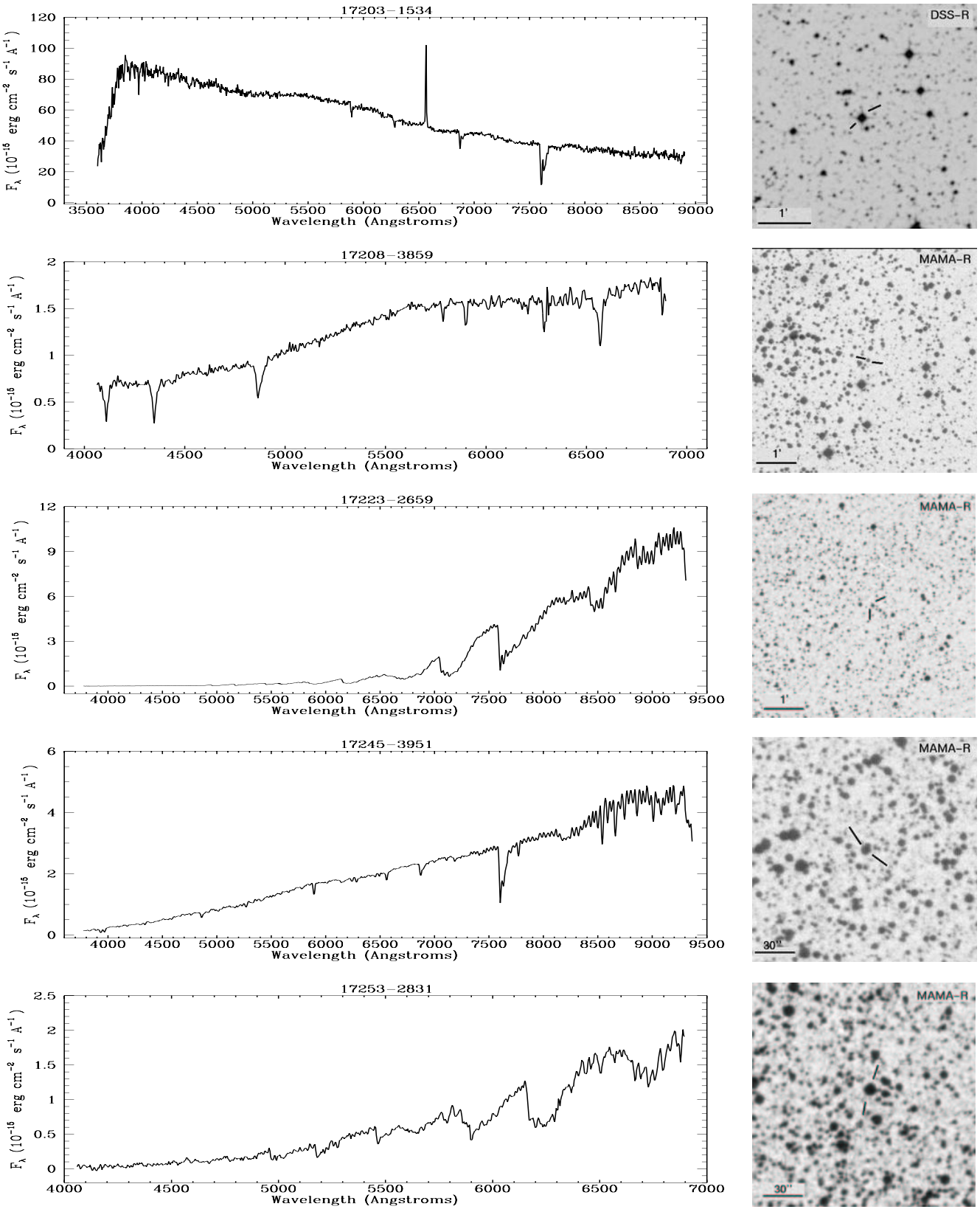

Fig. A.1. Spectra of the objects classified as post-AGB in the sample together with their corresponding identification charts (continued).

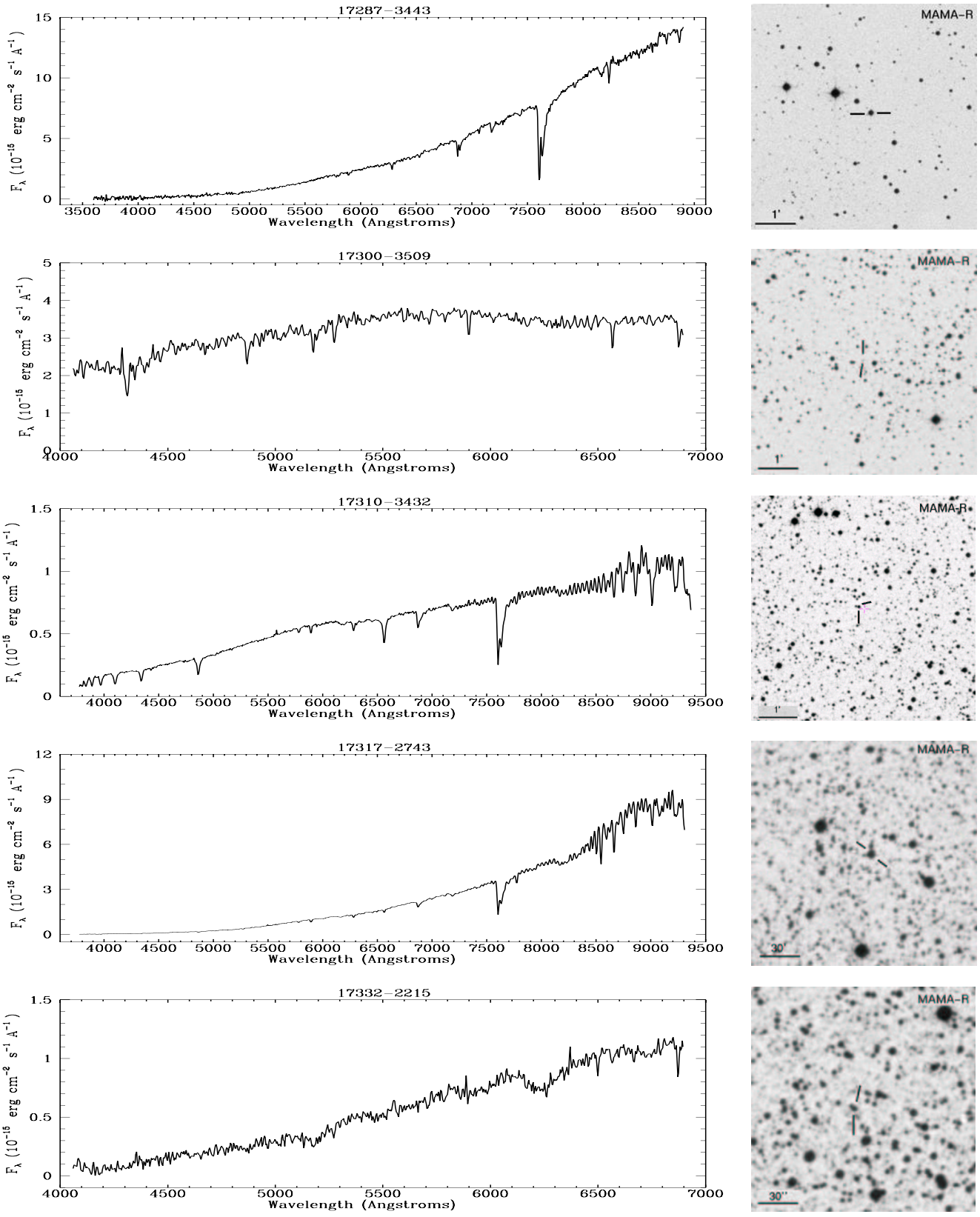

Fig. A.1. Spectra of the objects classified as post-AGB in the sample together with their corresponding identification charts (continued).

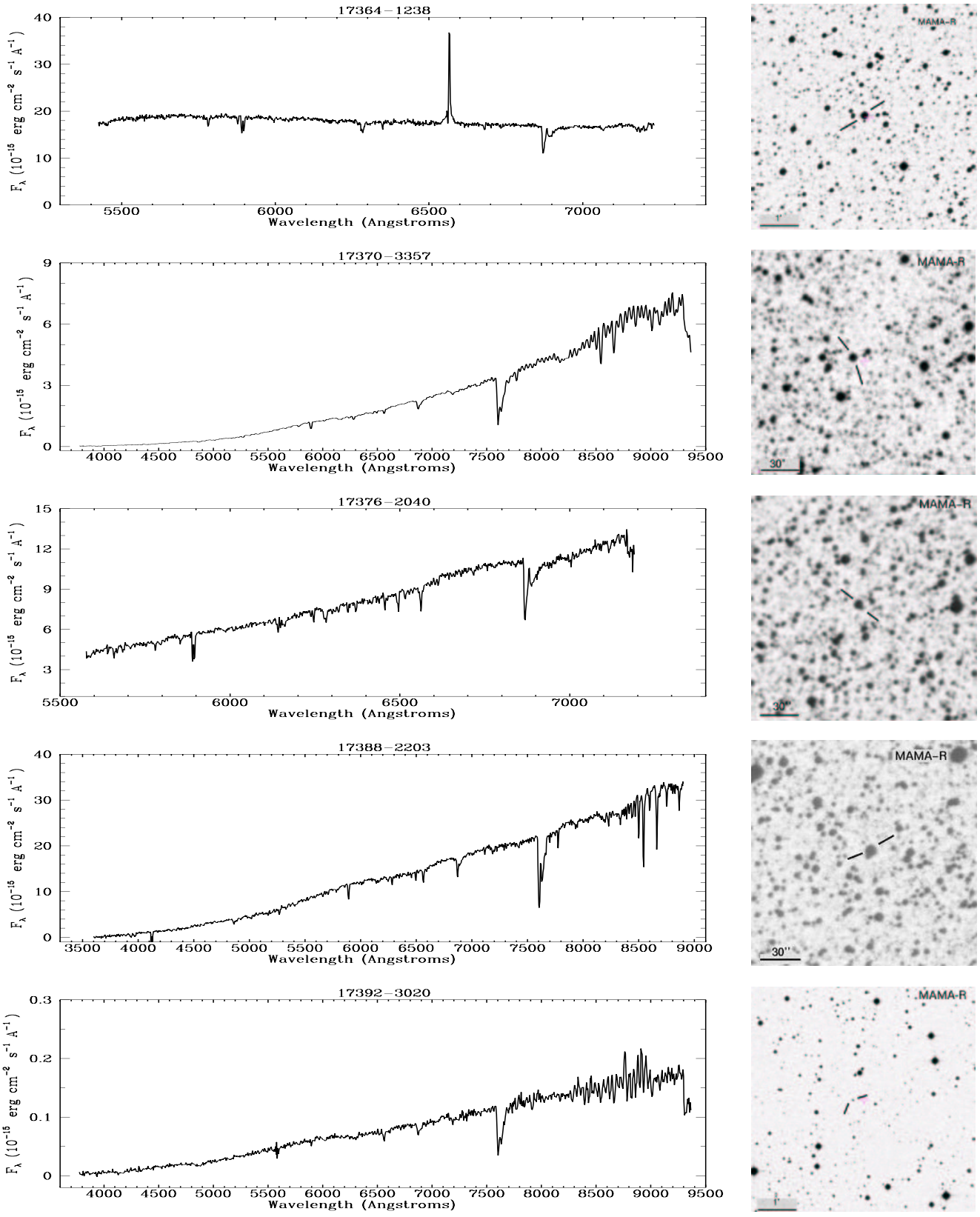

Fig. A.1. Spectra of the objects classified as post-AGB in the sample together with their corresponding identification charts (continued).

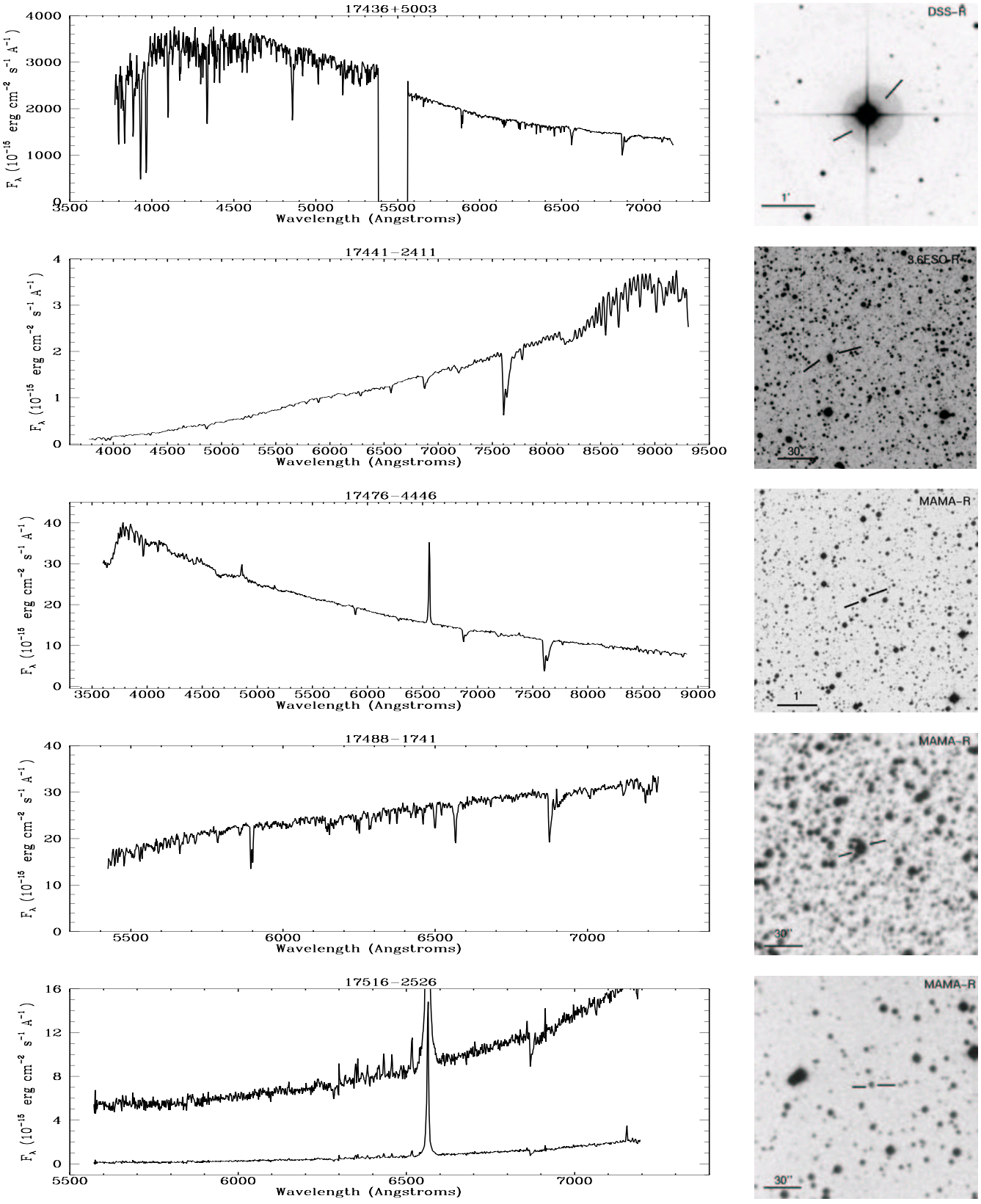

Fig. A.1. Spectra of the objects classified as post-AGB in the sample together with their corresponding identification charts (continued).

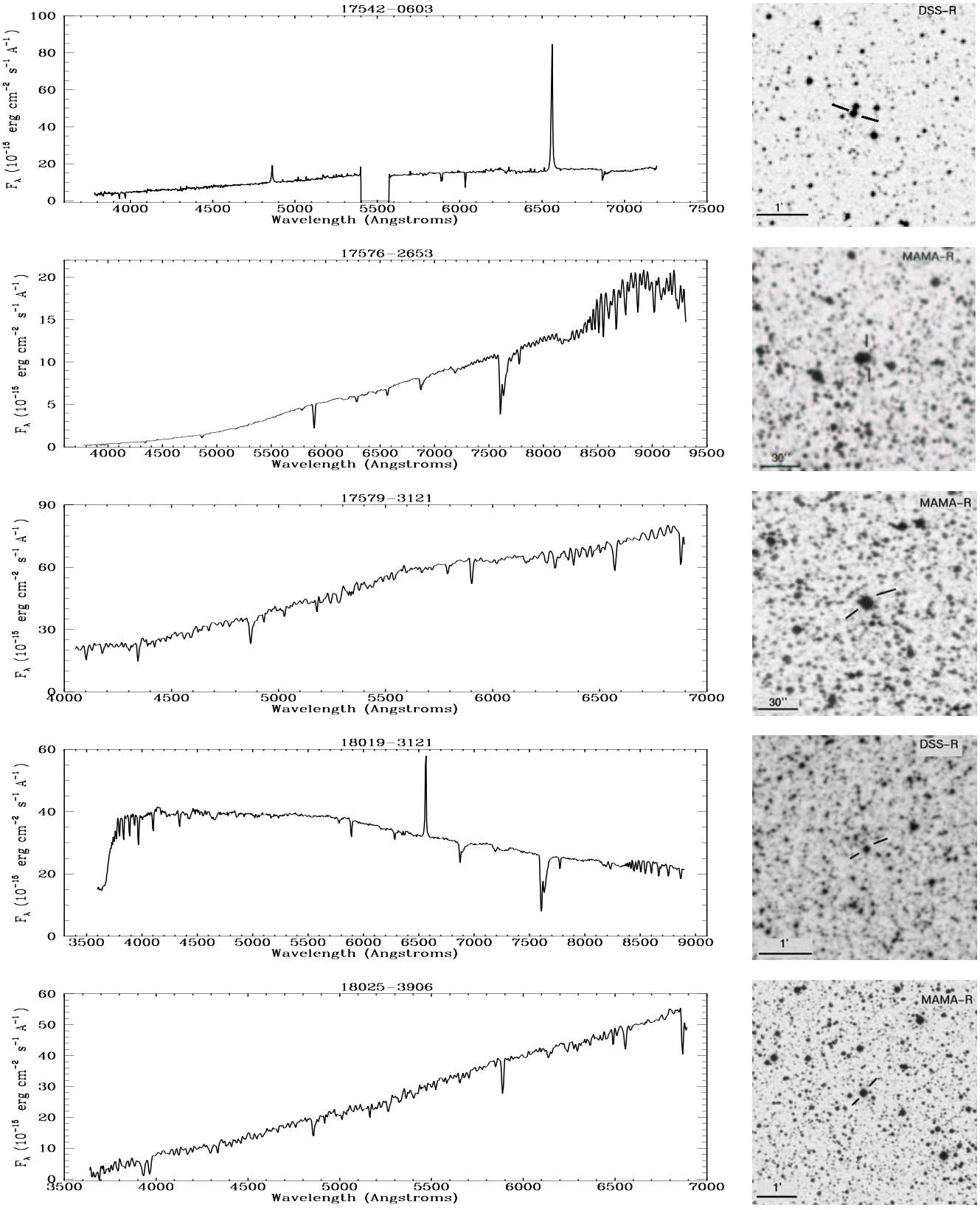

Fig. A.1. Spectra of the objects classified as post-AGB in the sample together with their corresponding identification charts (continued).

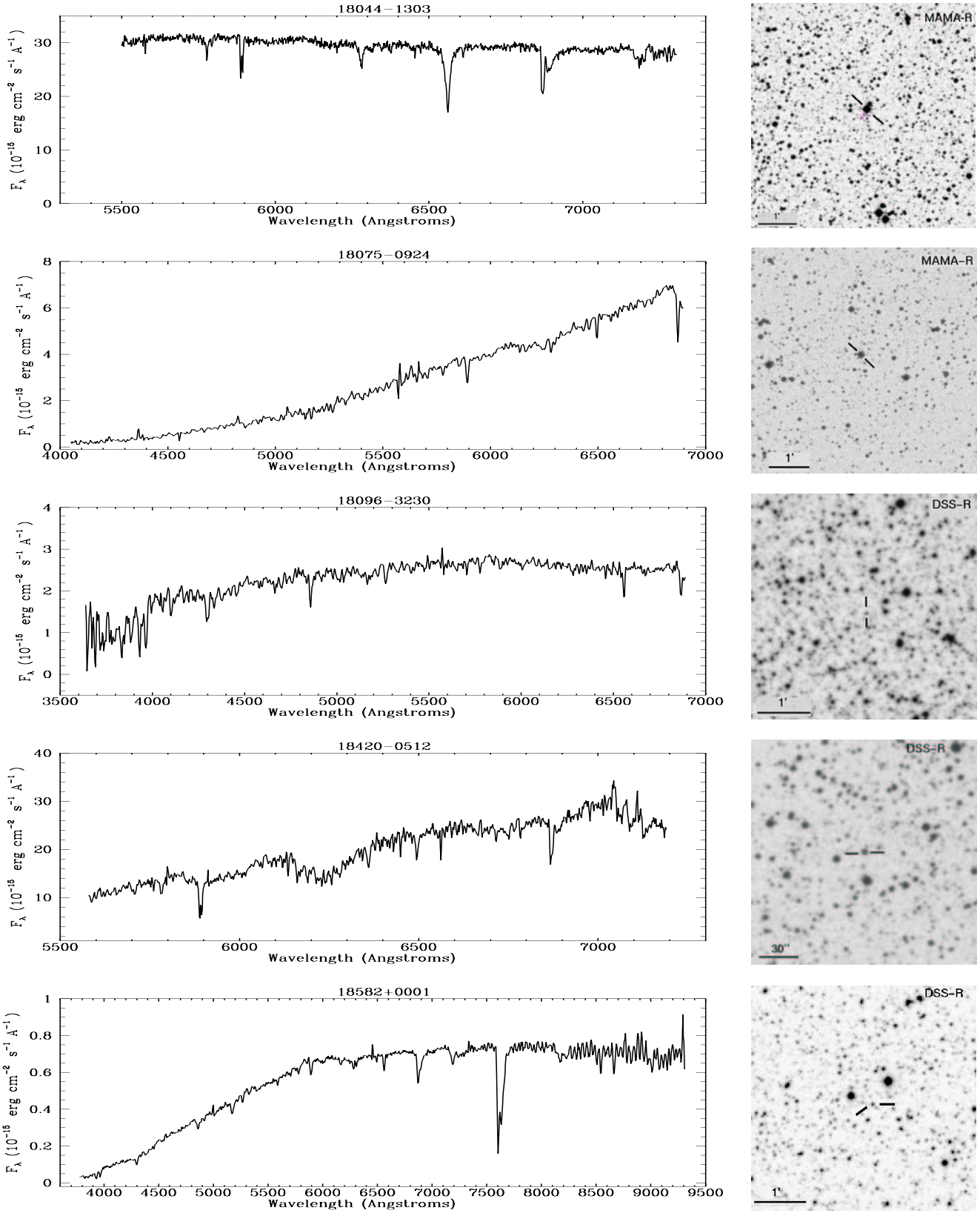

Fig. A.1. Spectra of the objects classified as post-AGB in the sample together with their corresponding identification charts (continued).

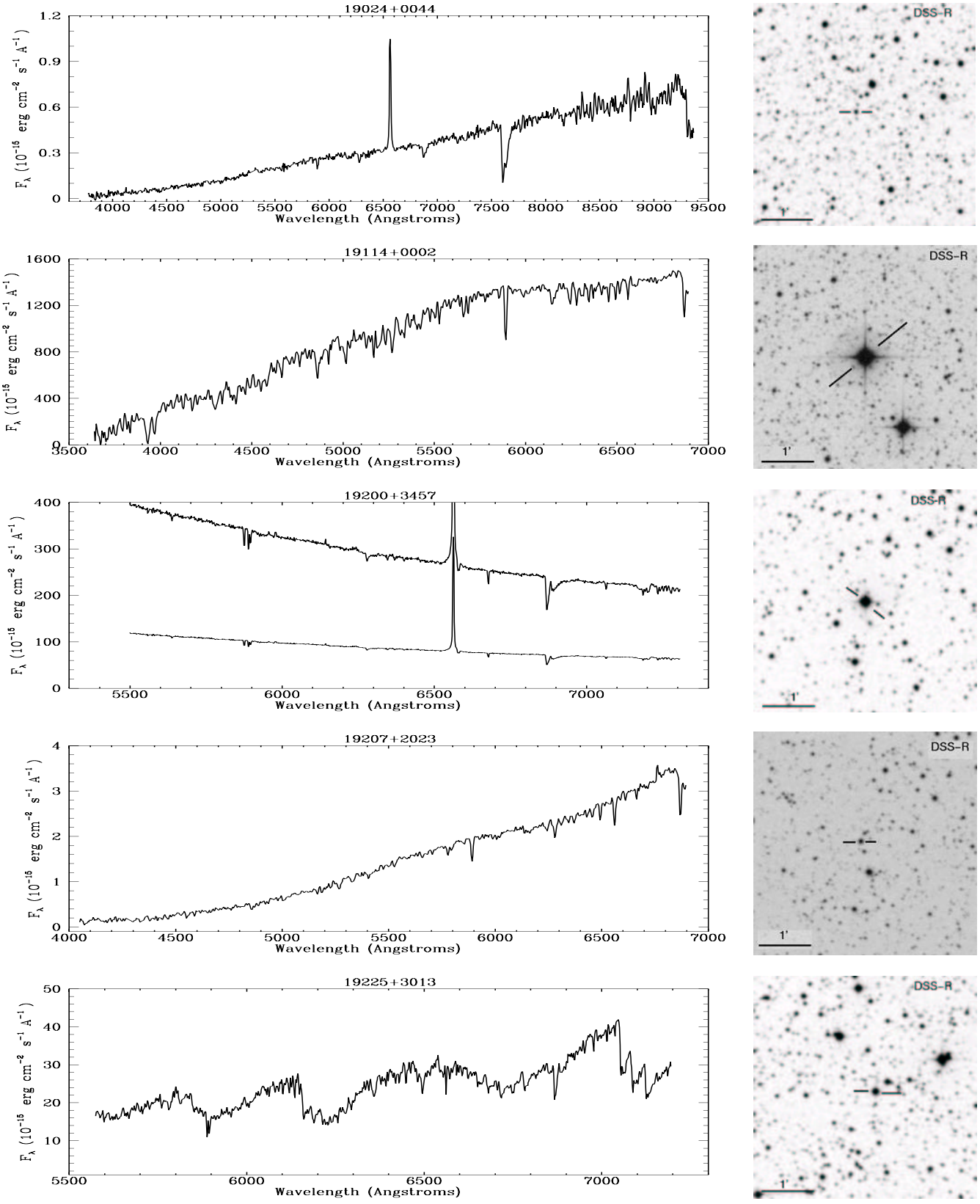

Fig. A.1. Spectra of the objects classified as post-AGB in the sample together with their corresponding identification charts (continued).

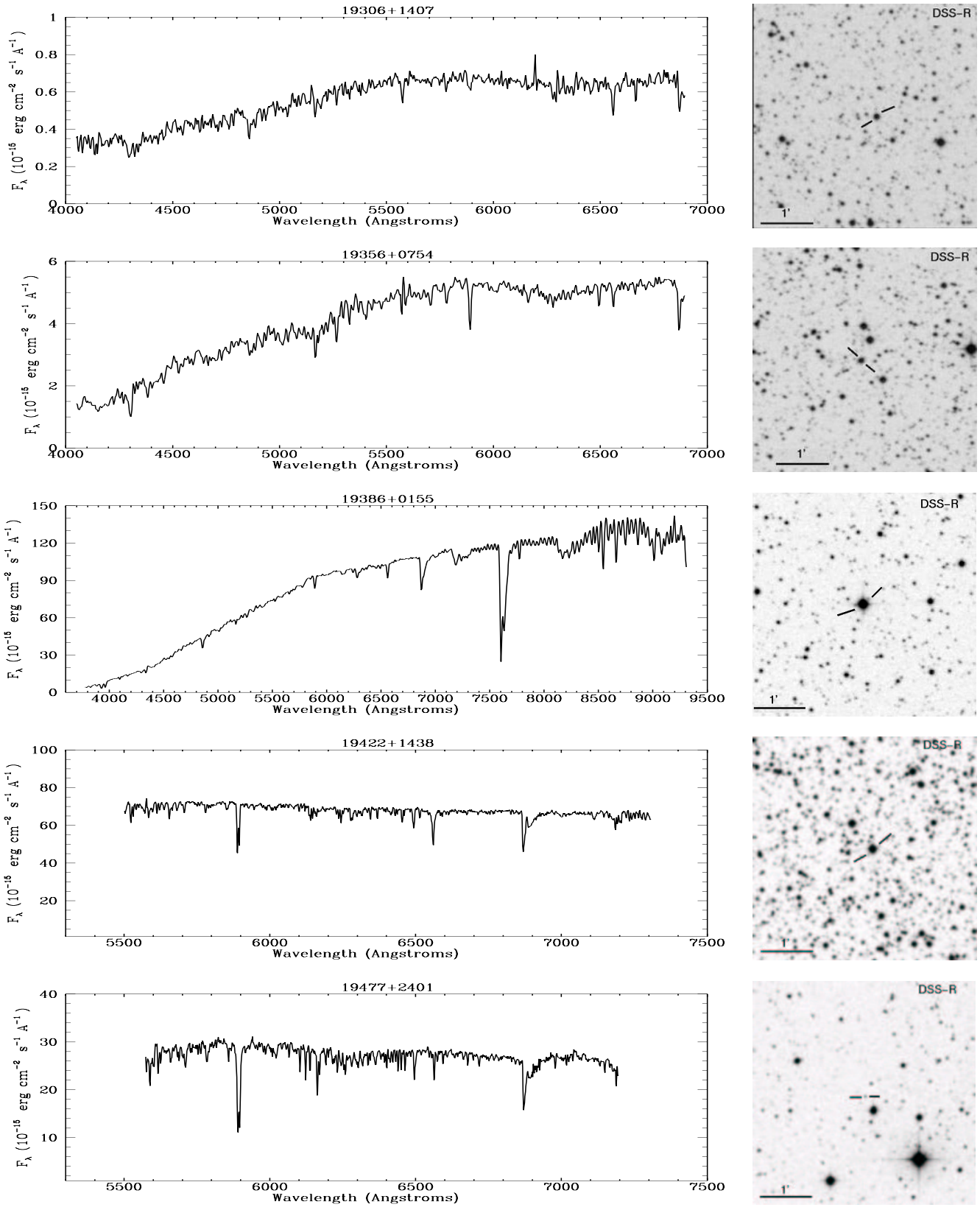

Fig. A.1. Spectra of the objects classified as post-AGB in the sample together with their corresponding identification charts (continued).

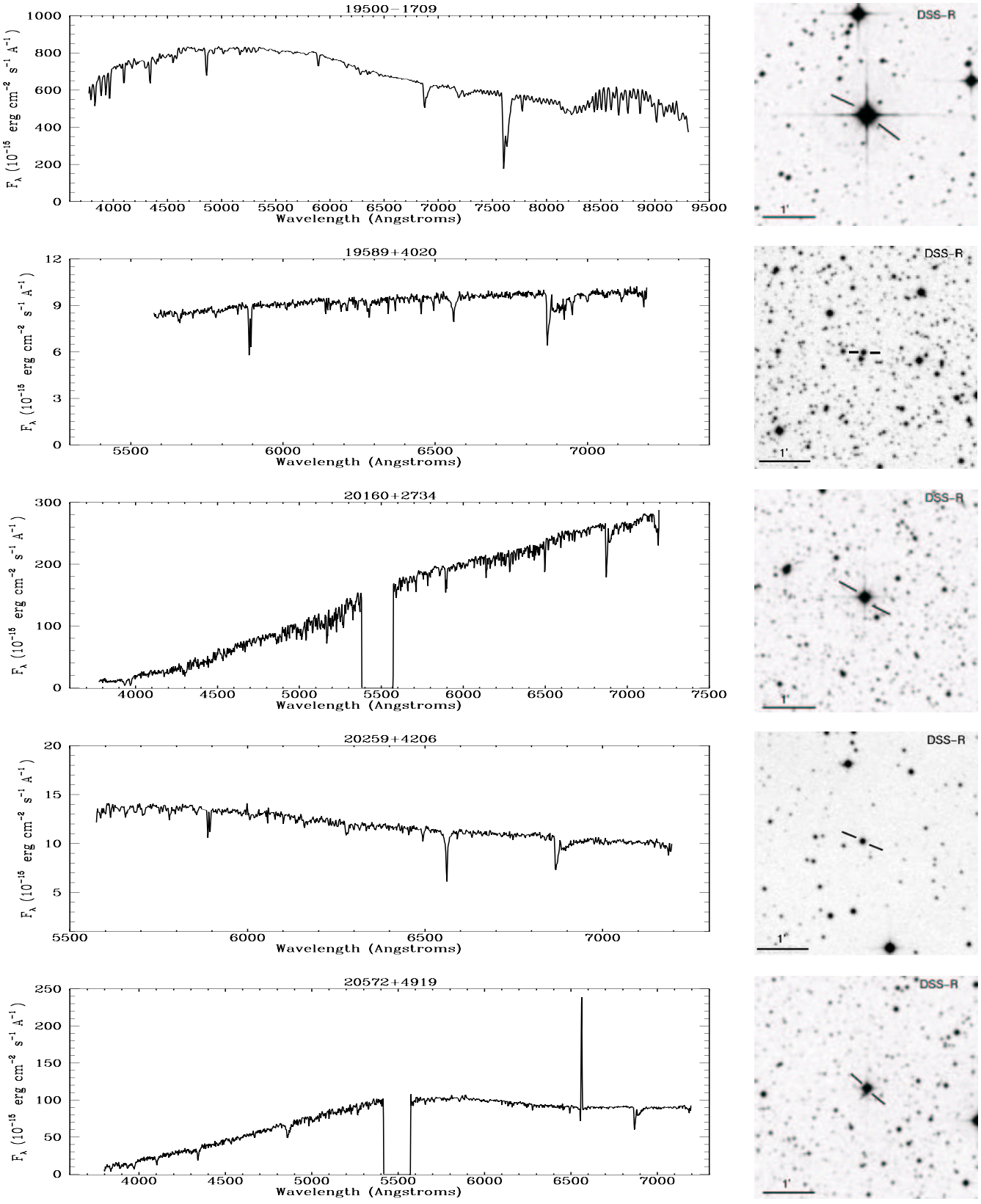

Fig. A.1. Spectra of the objects classified as post-AGB in the sample together with their corresponding identification charts (continued).

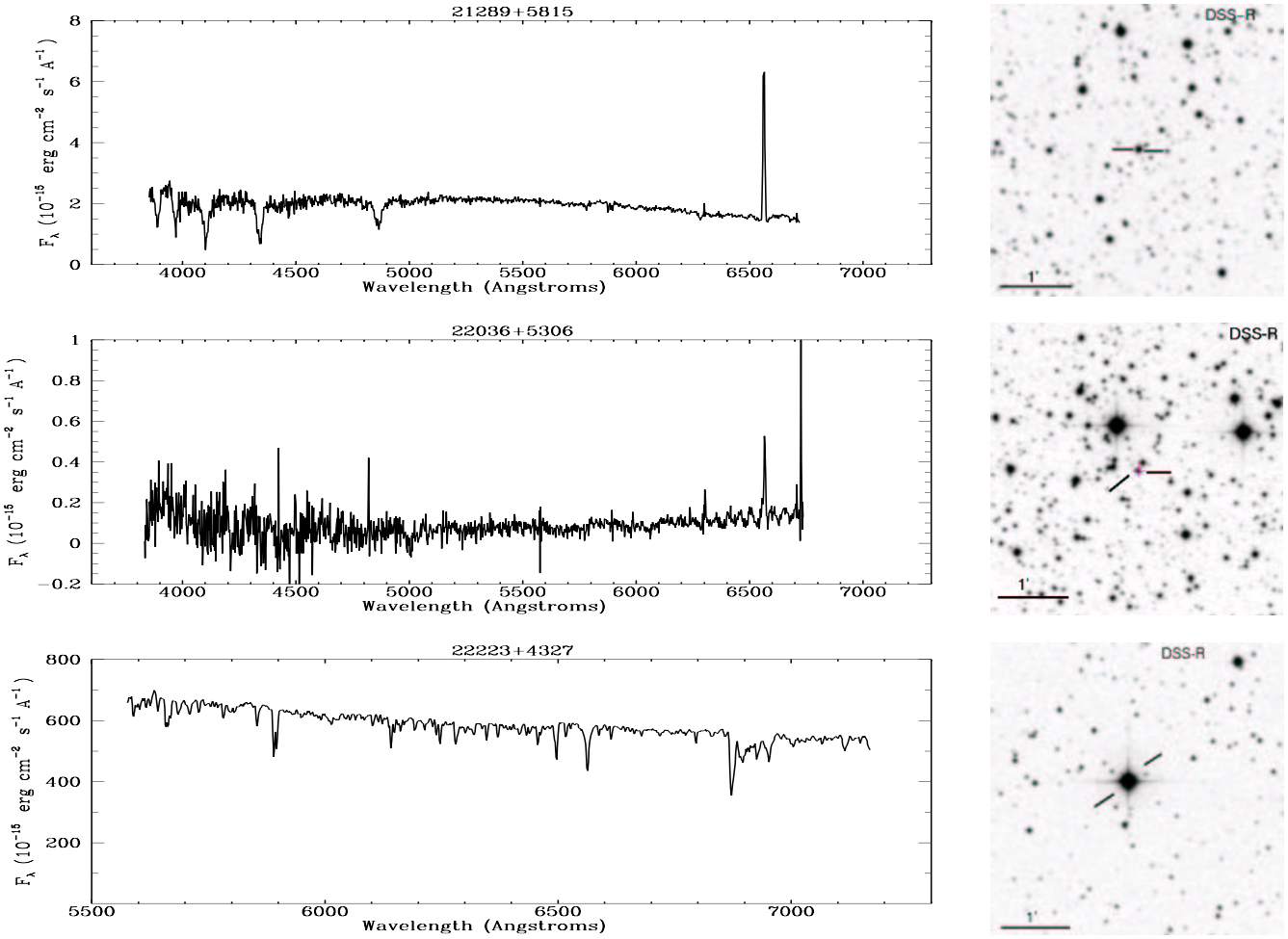

Fig. A.1. Spectra of the objects classified as post-AGB in the sample together with their corresponding identification charts (continued).

Appendix B: Atlas of transition sources

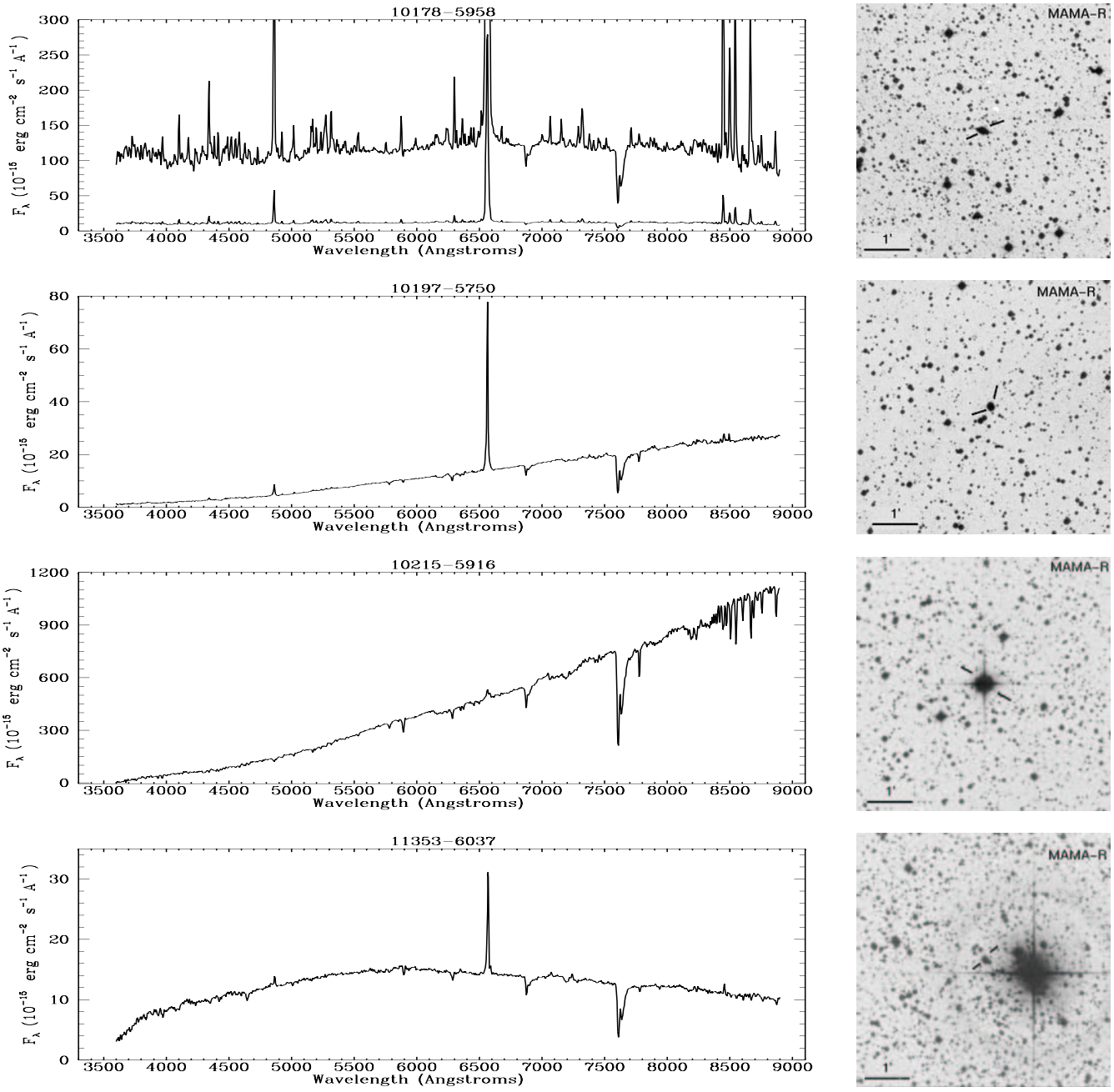

Fig. B.1. Spectra of the transition objects together with their corresponding identification charts.

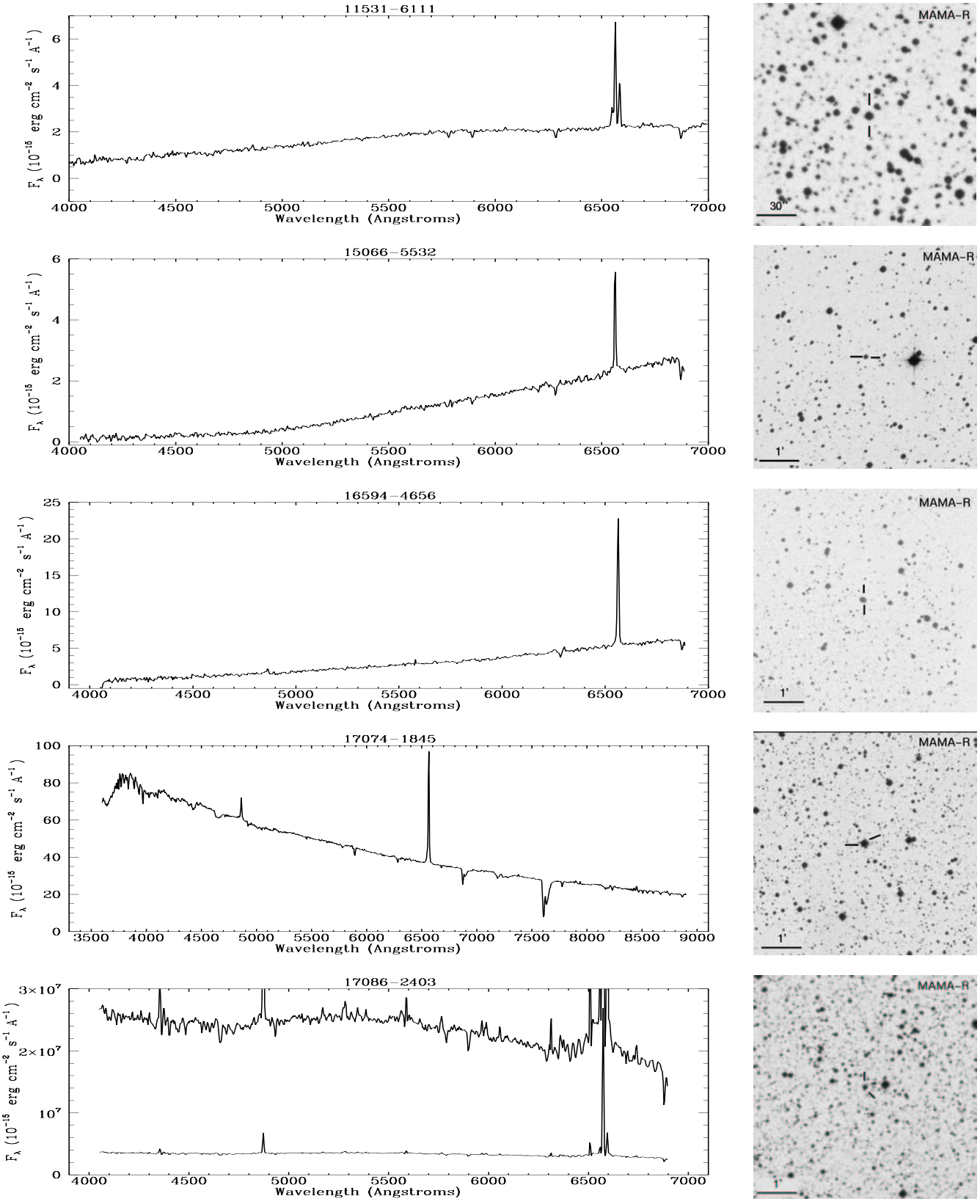

Fig. B.1. Spectra of the transition objects together with their corresponding identification charts (continued).

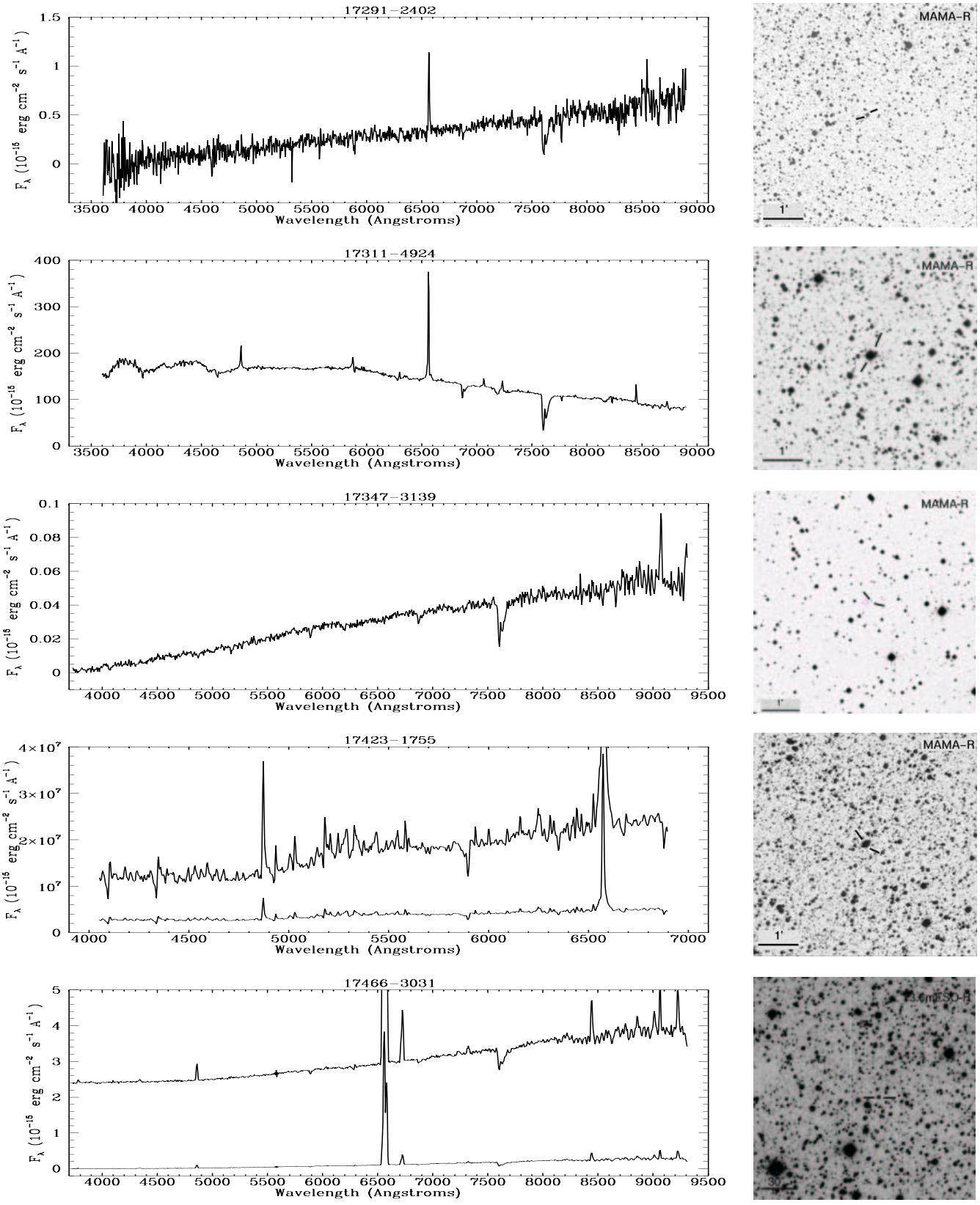

Fig. B.1. Spectra of the transition objects together with their corresponding identification charts (continued).

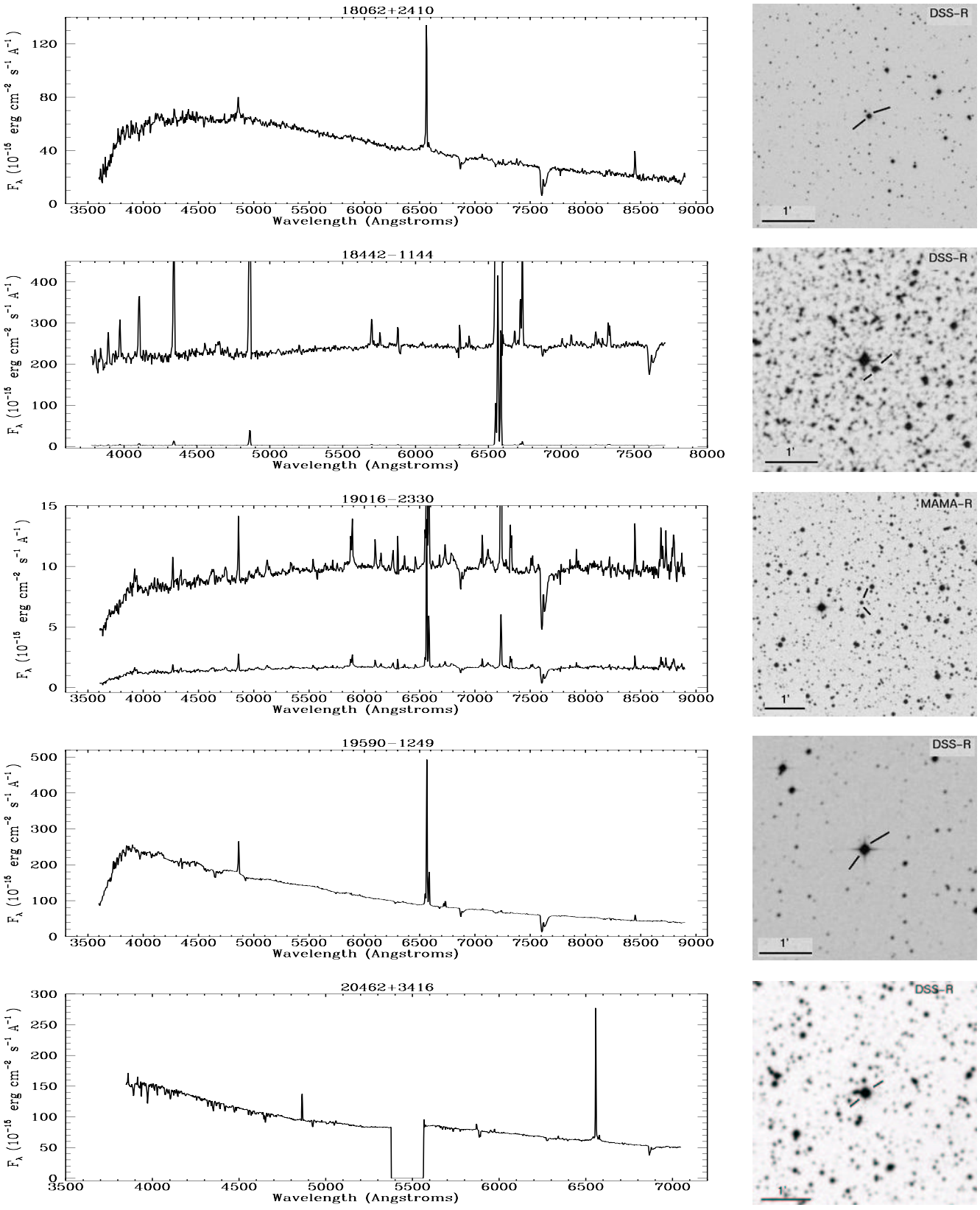

Fig. B.1. Spectra of the transition objects together with their corresponding identification charts (continued).

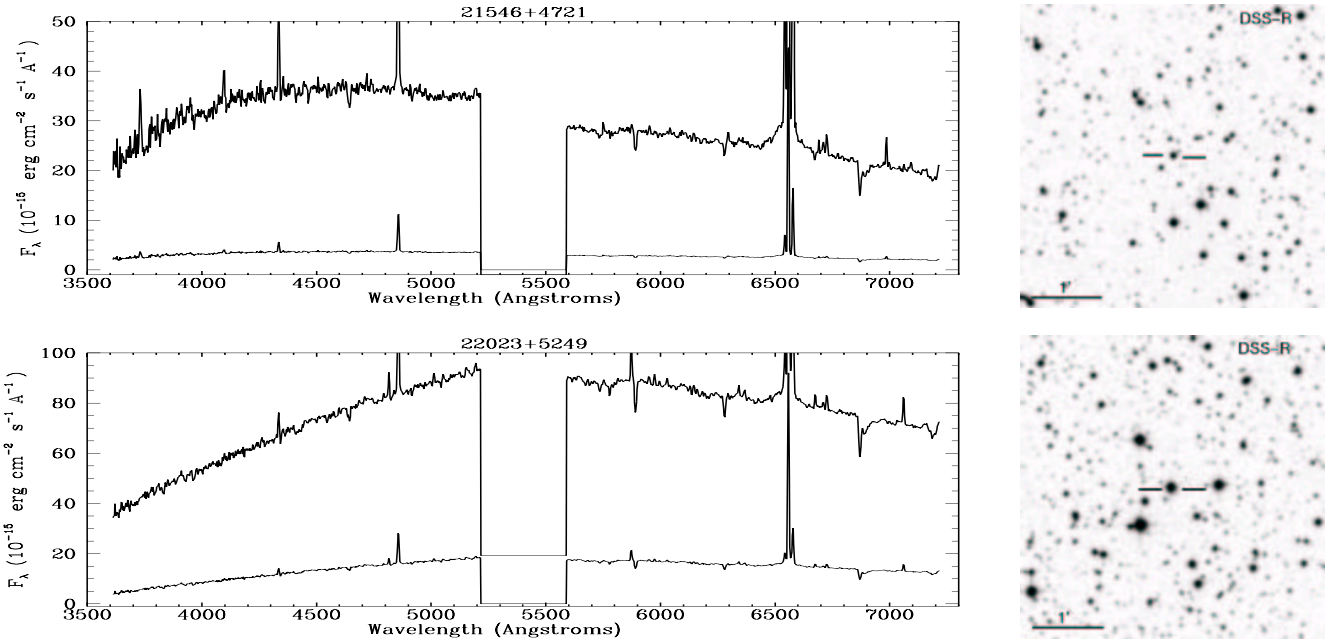

Fig. B.1. Spectra of the transition objects together with their corresponding identification charts (continued).

Appendix C: Atlas of PNe

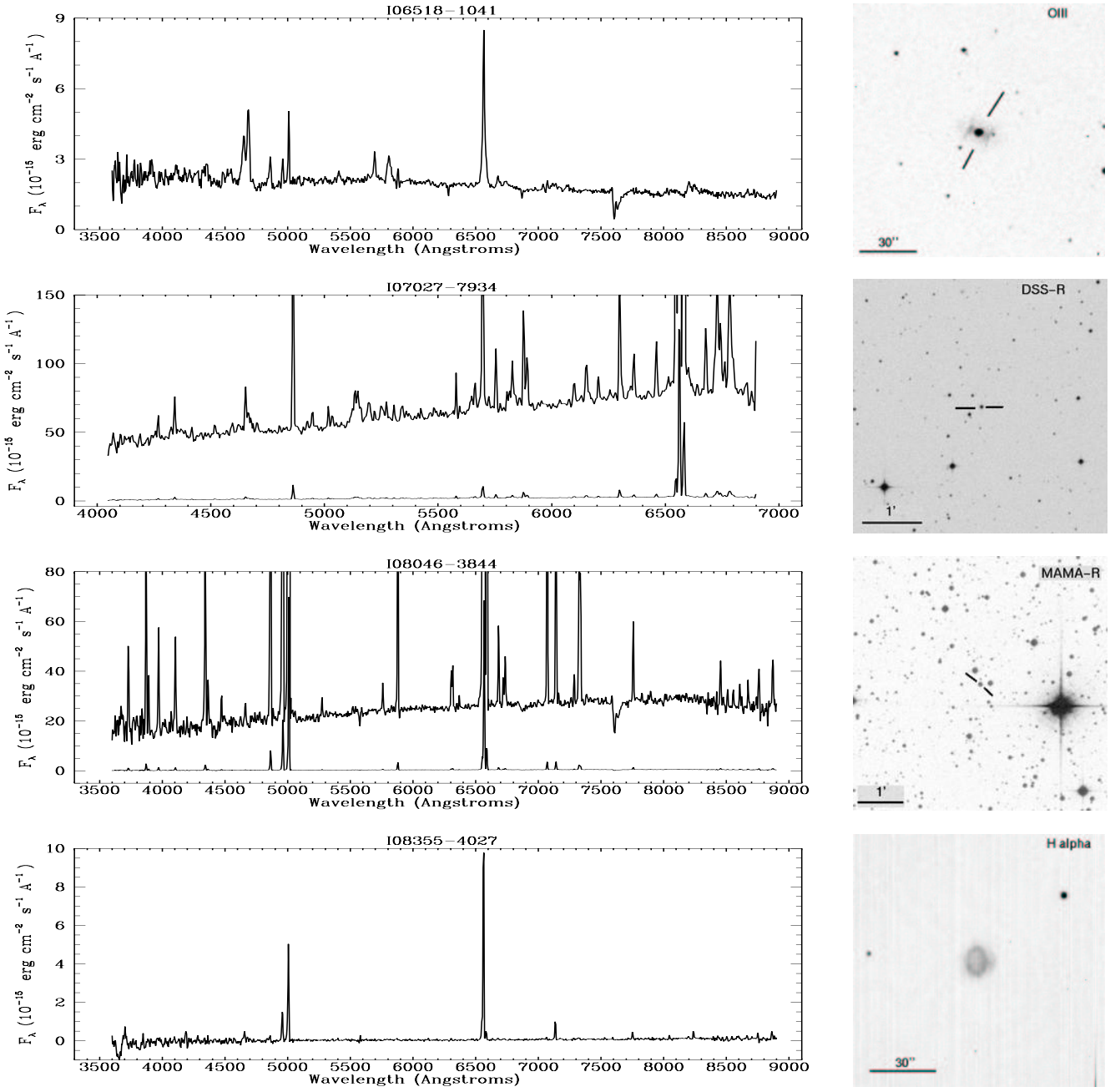

Fig. C.3. Spectra of the PNe in the sample together with their corresponding identification charts.

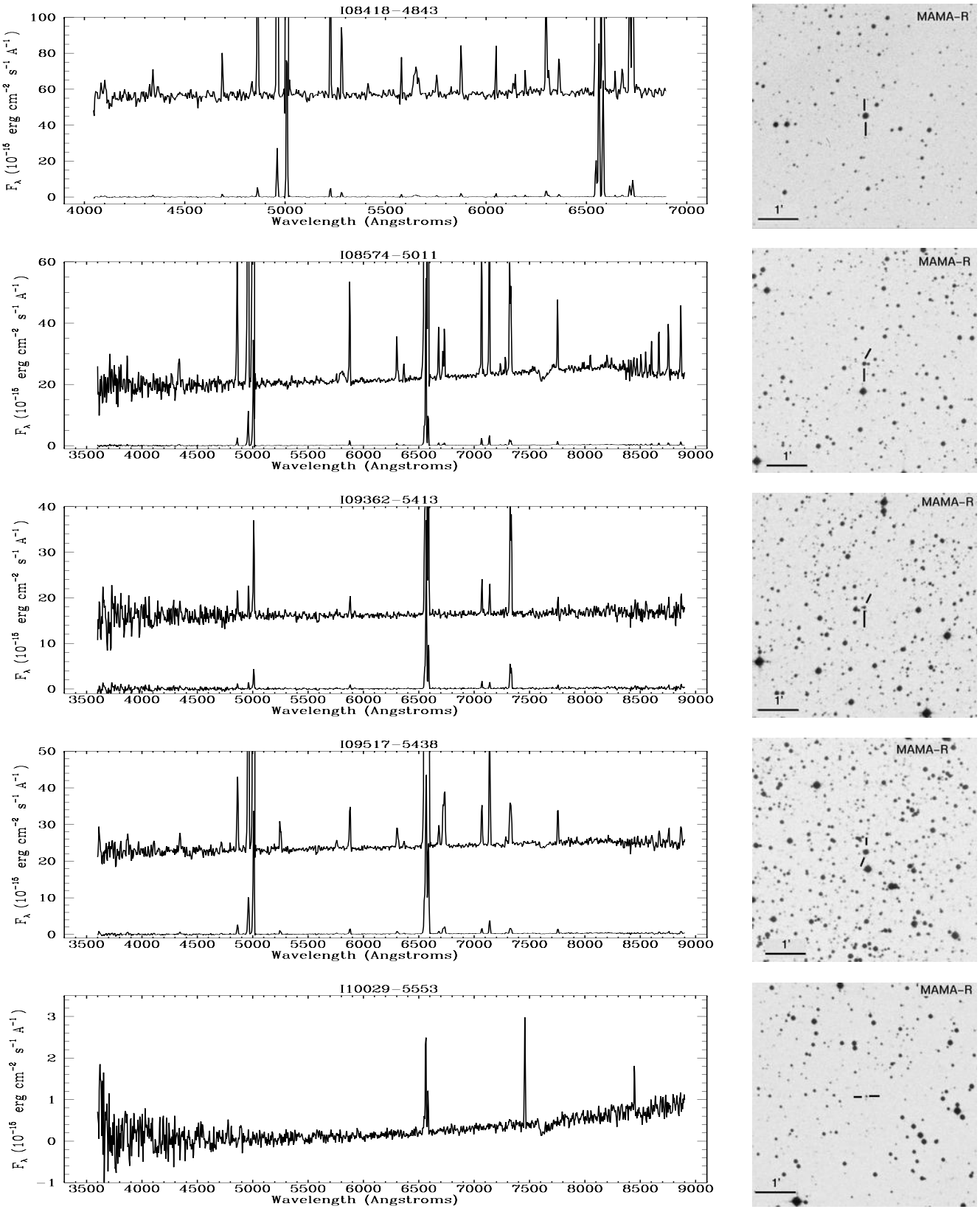

Fig. C.3. Spectra of the PNe in the sample together with their corresponding identification charts (continued).

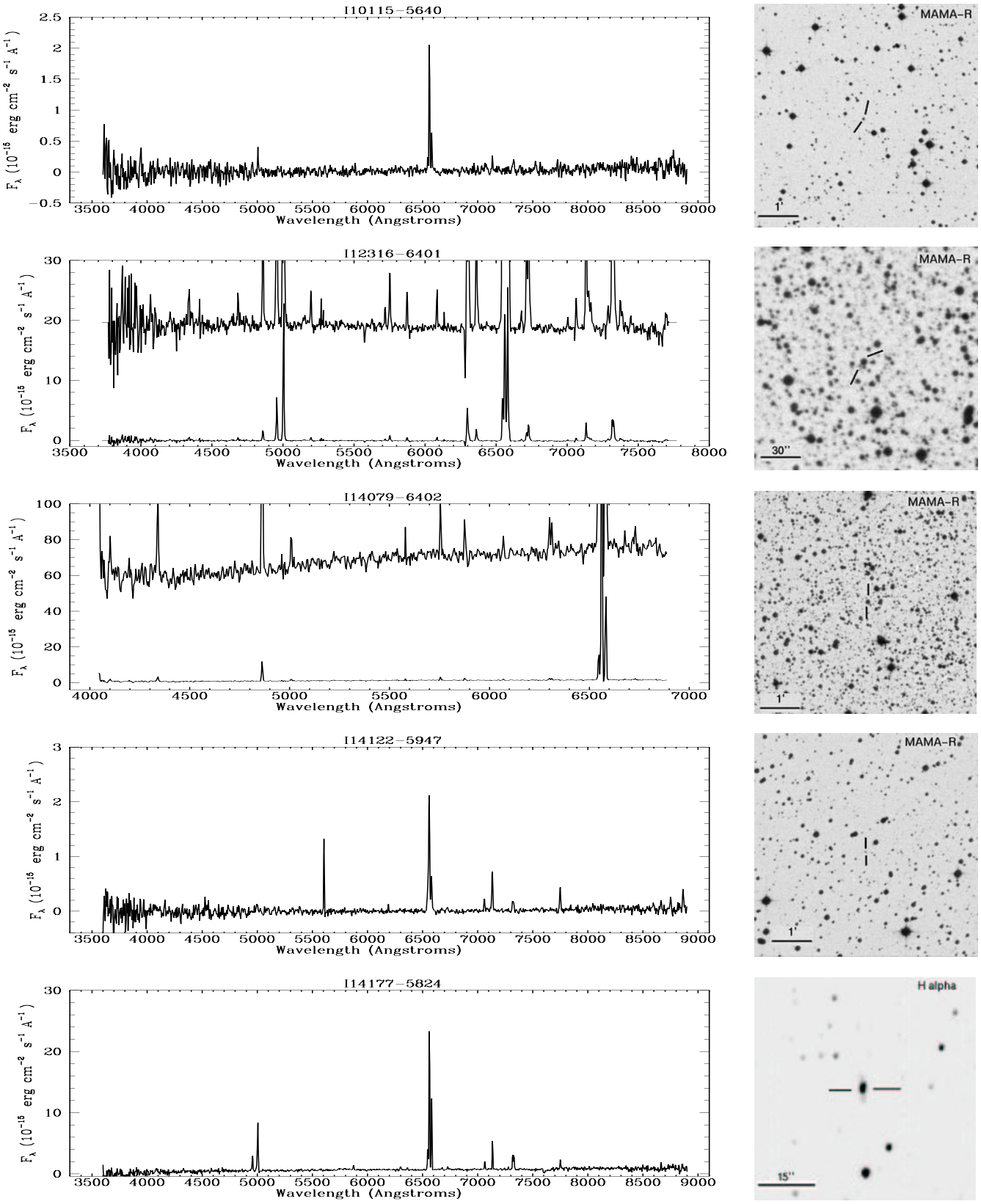

Fig. C.3. Spectra of the PNe in the sample together with their corresponding identification charts (continued).

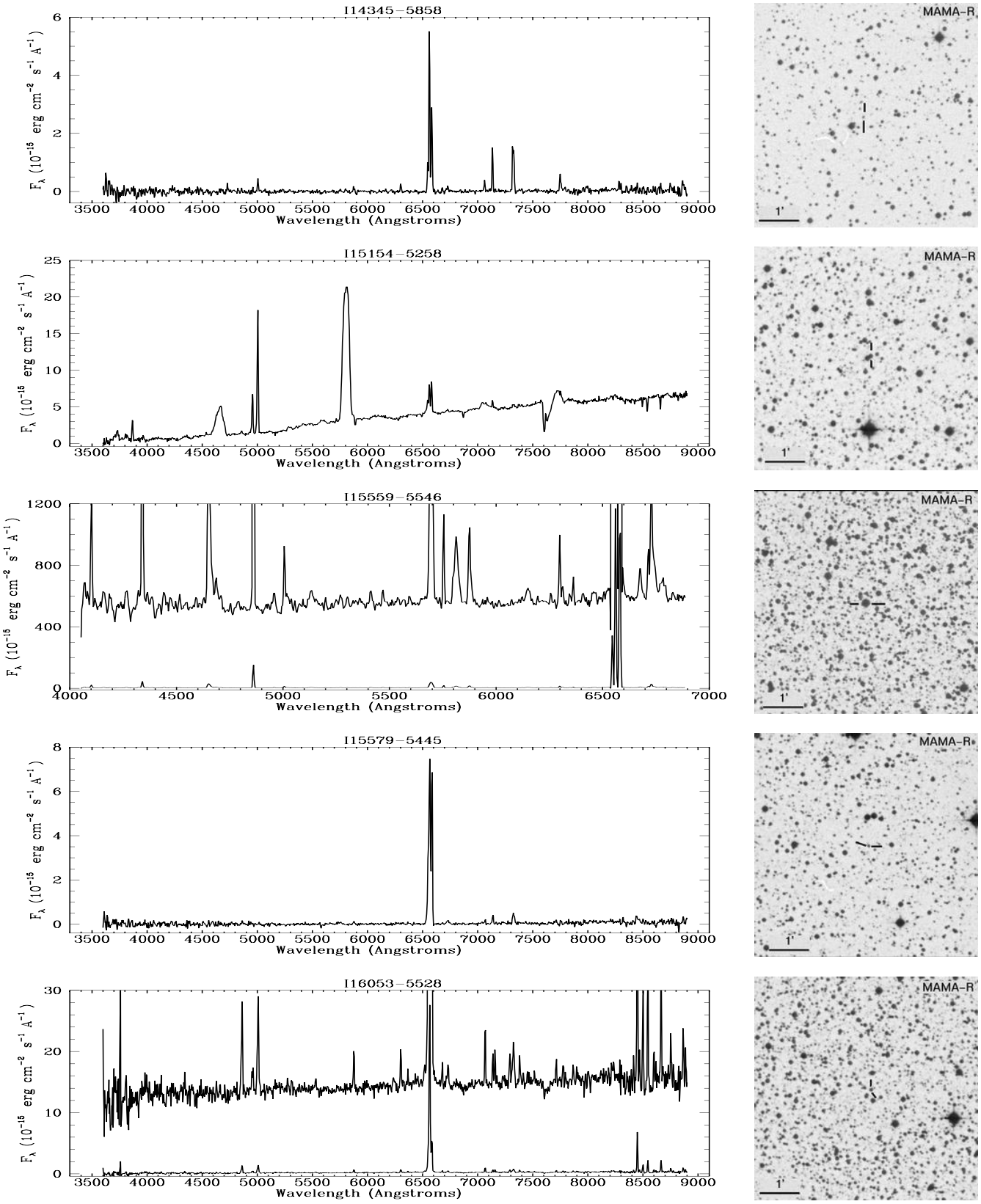

Fig. C.3. Spectra of the PNe in the sample together with their corresponding identification charts (continued).

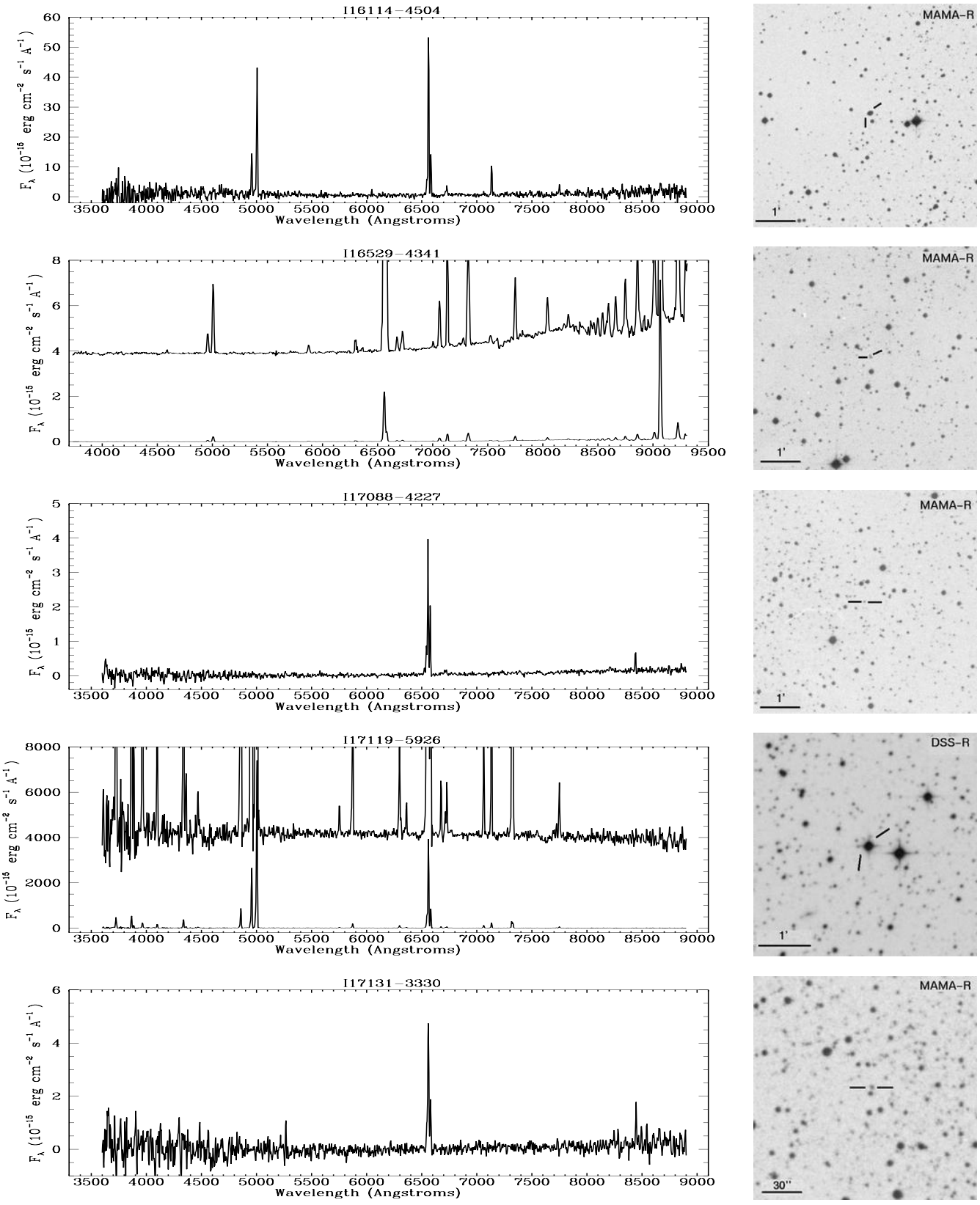

Fig. C.3. Spectra of the PNe in the sample together with their corresponding identification charts (continued).

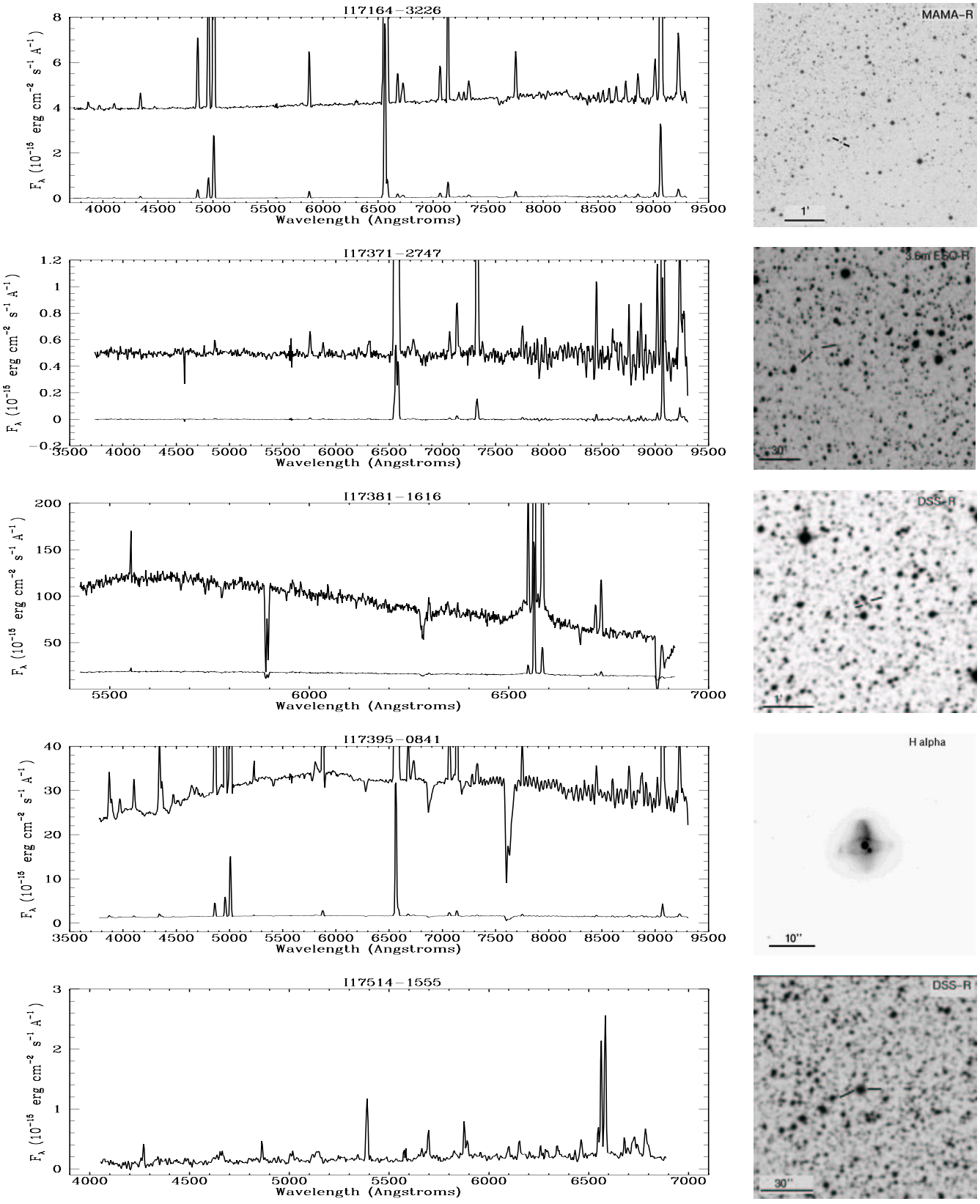

Fig. C.3. Spectra of the PNe in the sample together with their corresponding identification charts (continued).

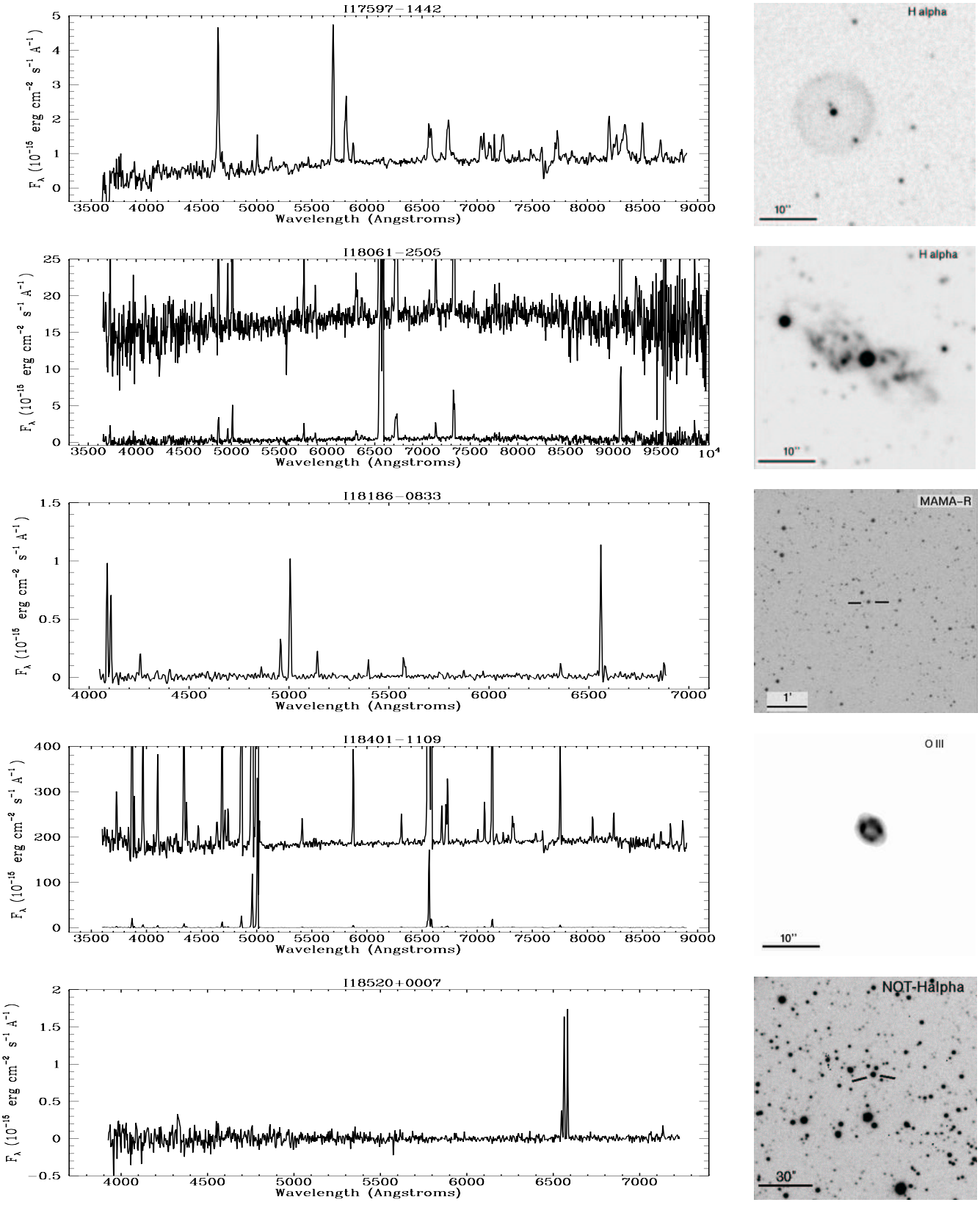

Fig. C.3. Spectra of the PNe in the sample together with their corresponding identification charts (continued).

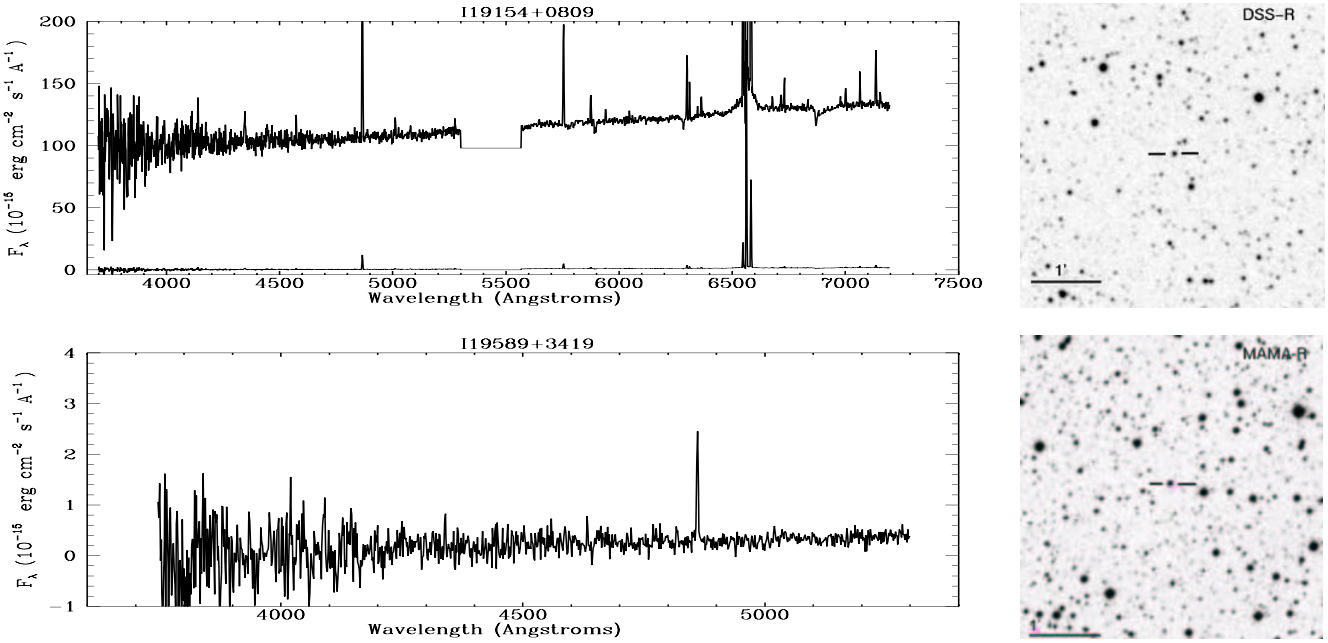

Fig. C.3. Spectra of the PNe in the sample together with their corresponding identification charts (continued).

Appendix D: Atlas of young stellar objects

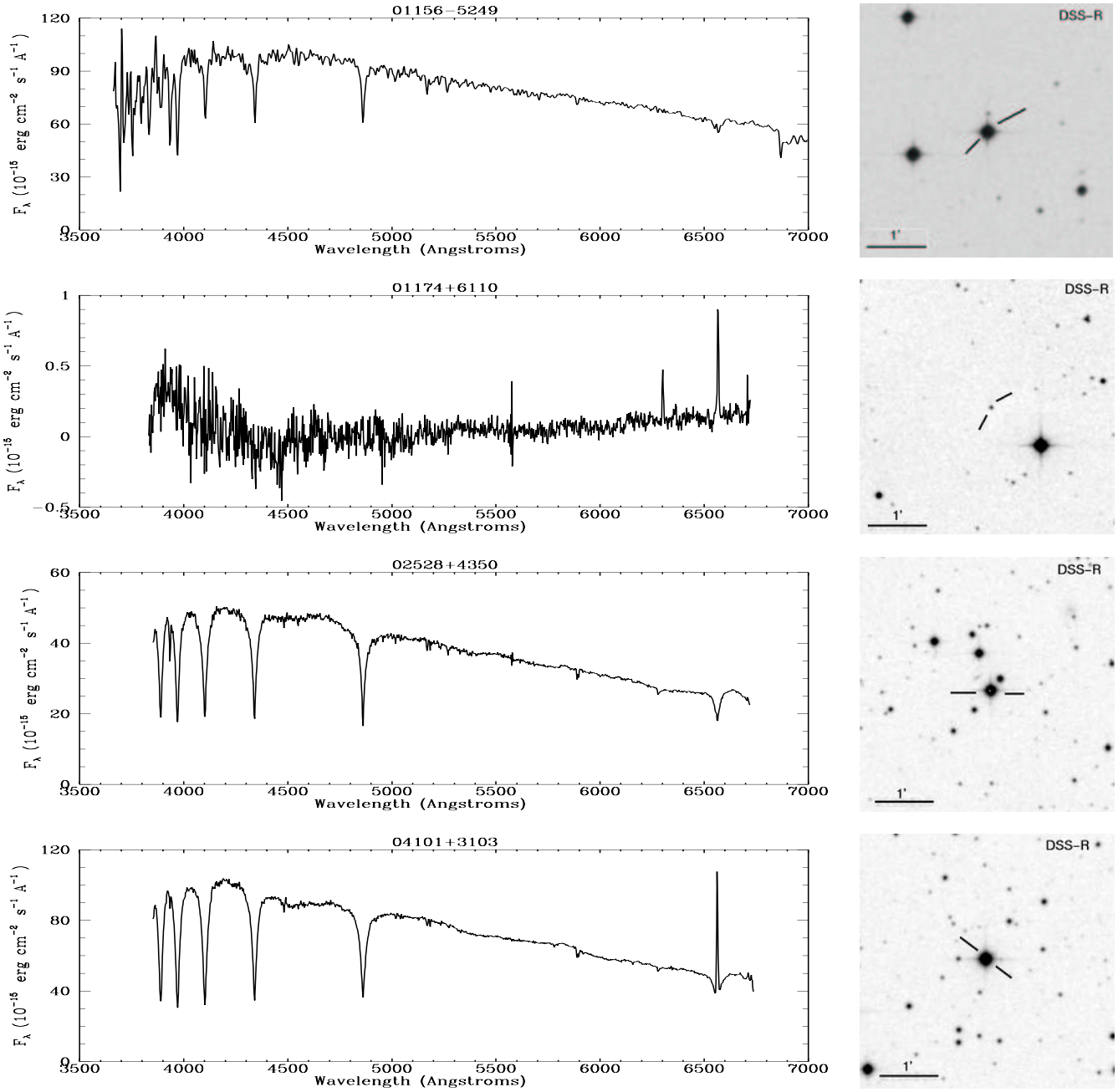

Fig. D.1. Spectra of the objects classified as young stars in the sample together with their corresponding identification charts.

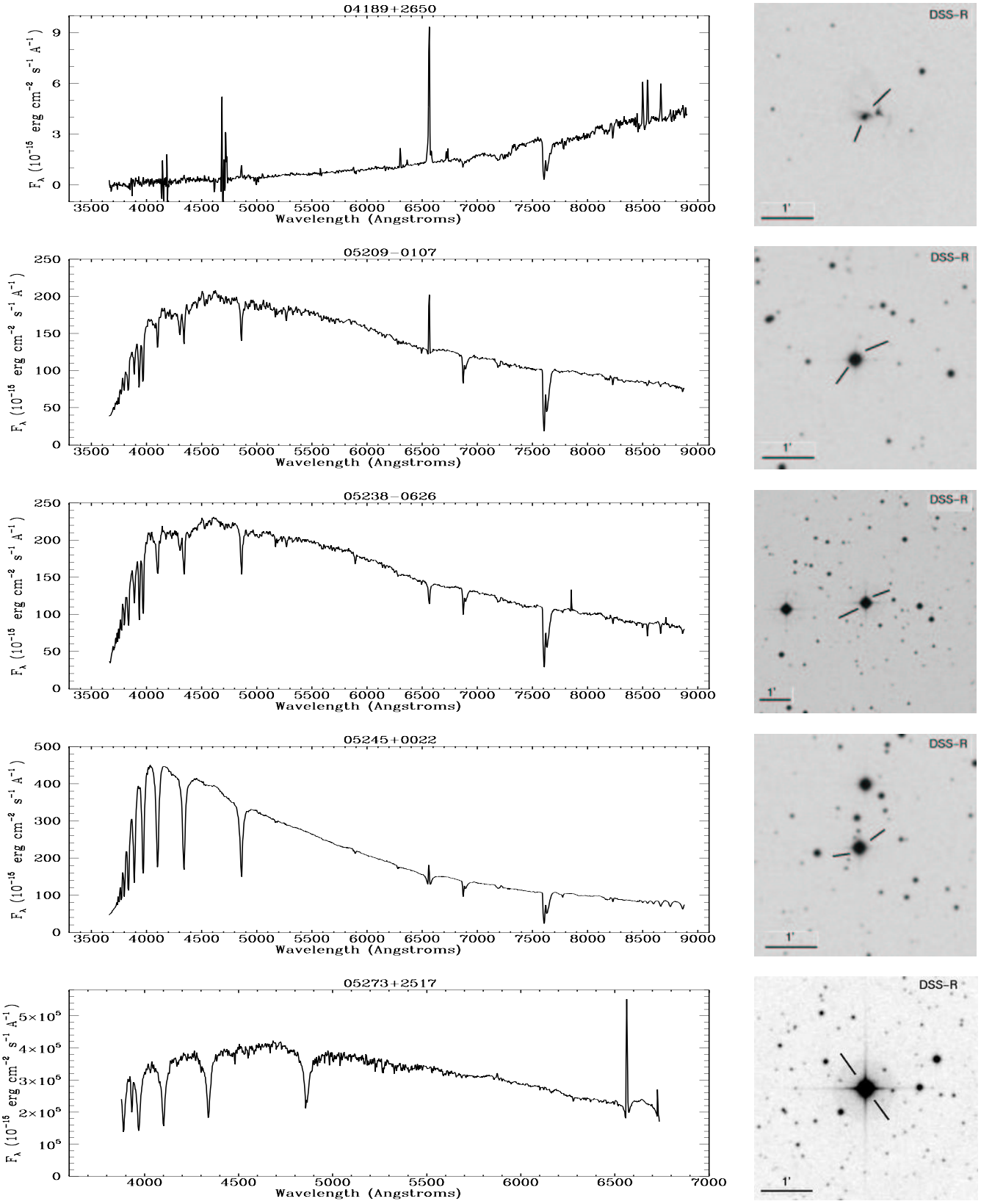

Fig. D.1. Spectra of the objects classified as young stars in the sample together with their corresponding identification charts (continued).

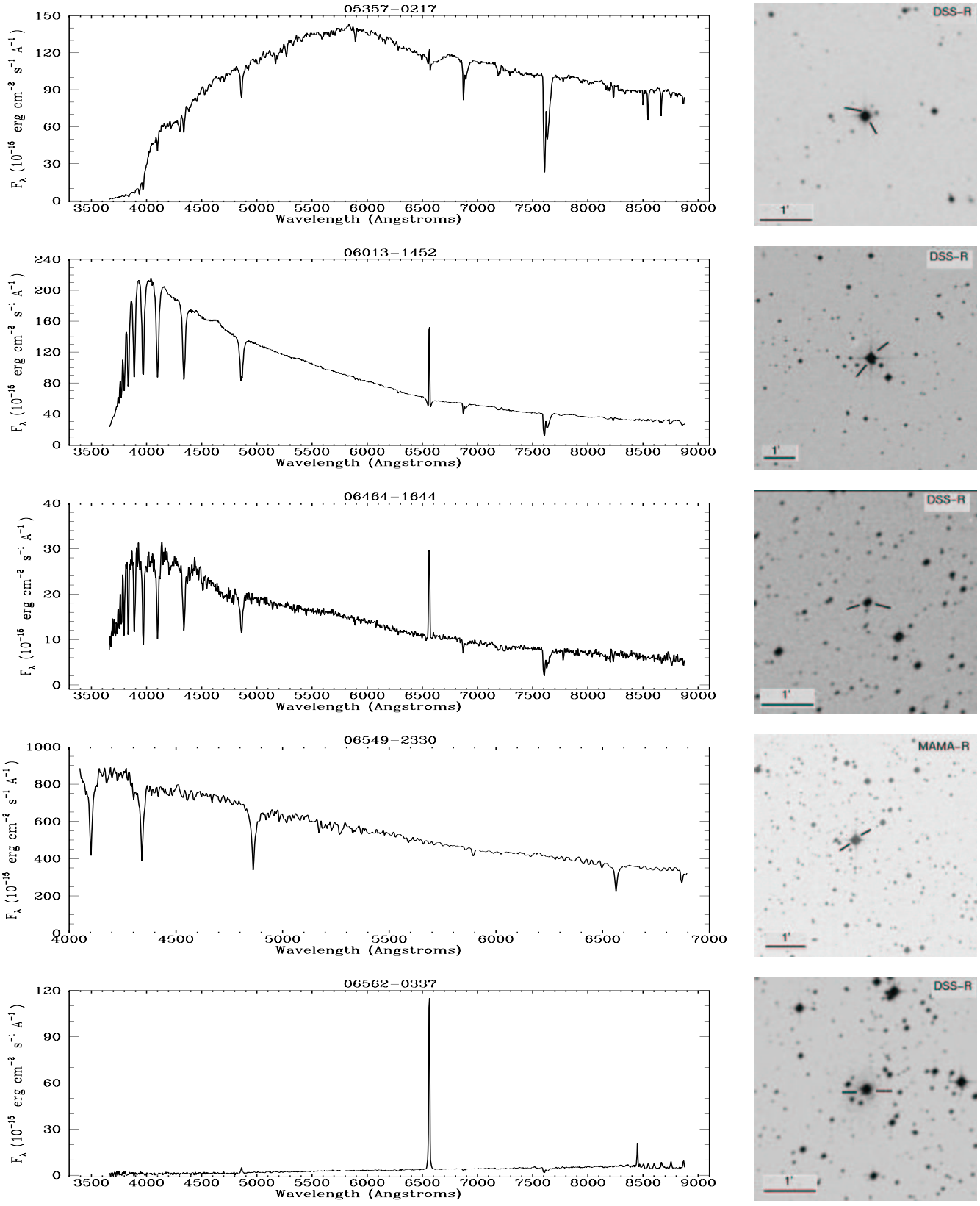

Fig. D.1. Spectra of the objects classified as young stars in the sample together with their corresponding identification charts (continued).

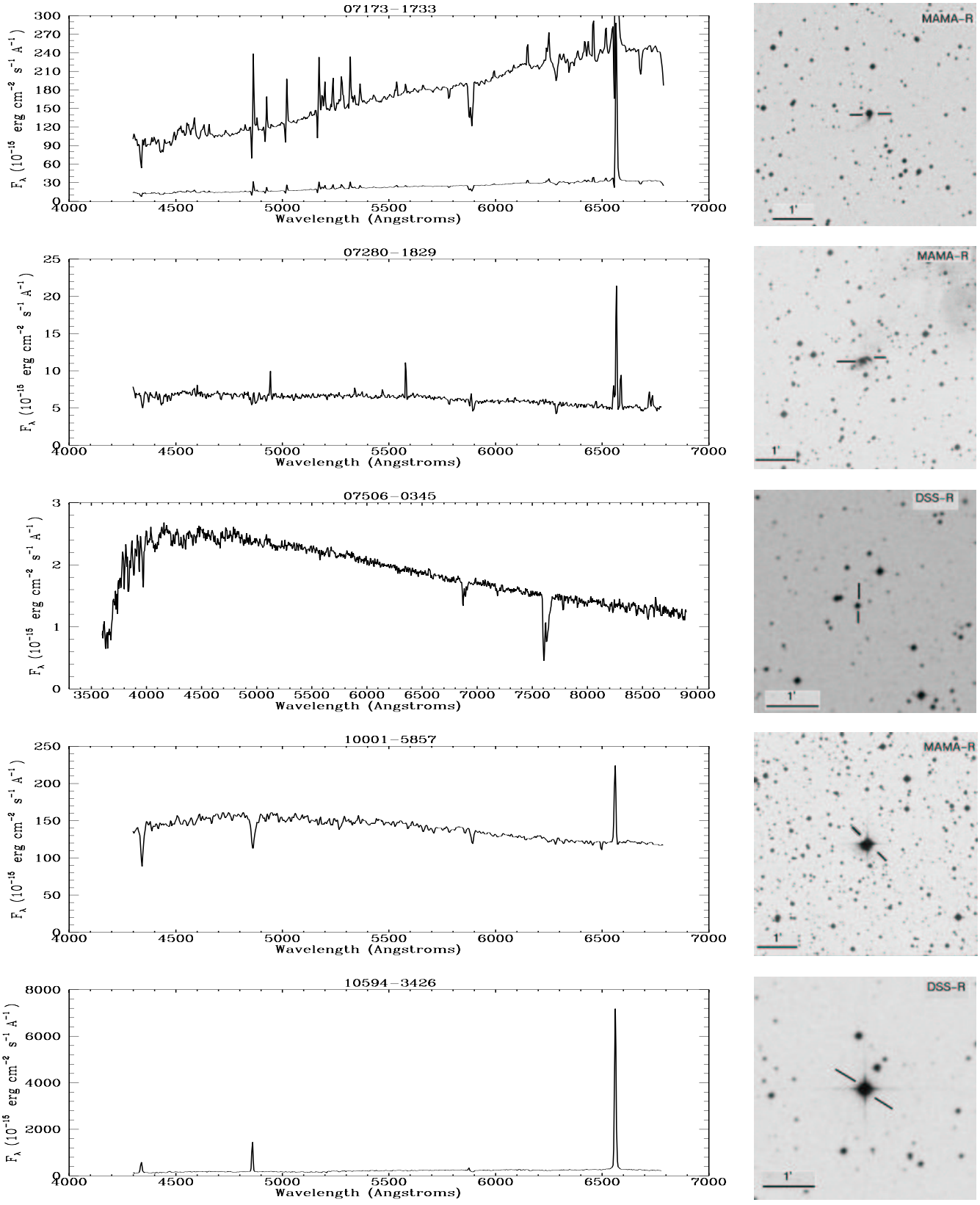

Fig. D.1. Spectra of the objects classified as young stars in the sample together with their corresponding identification charts (continued).

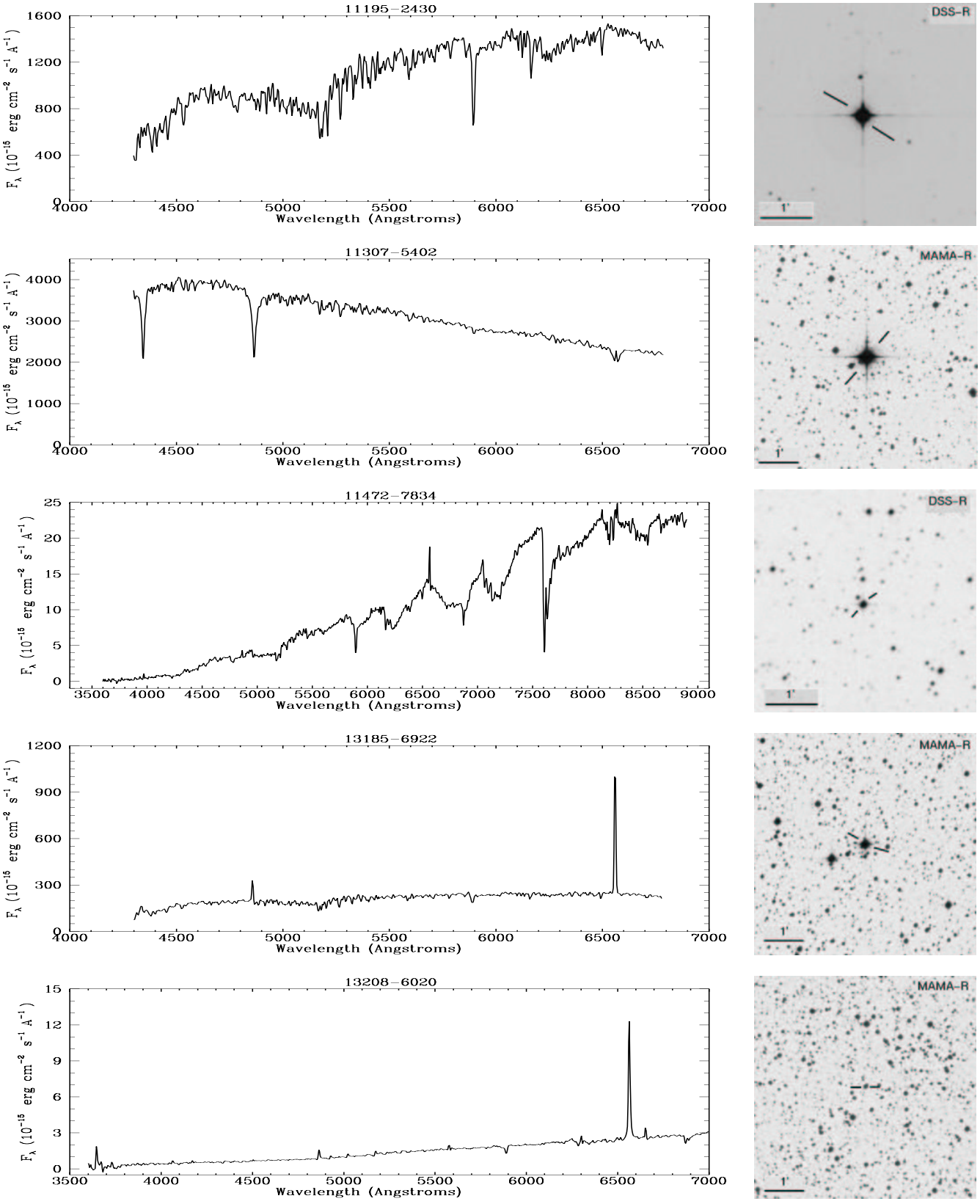

Fig. D.1. Spectra of the objects classified as young stars in the sample together with their corresponding identification charts (continued).

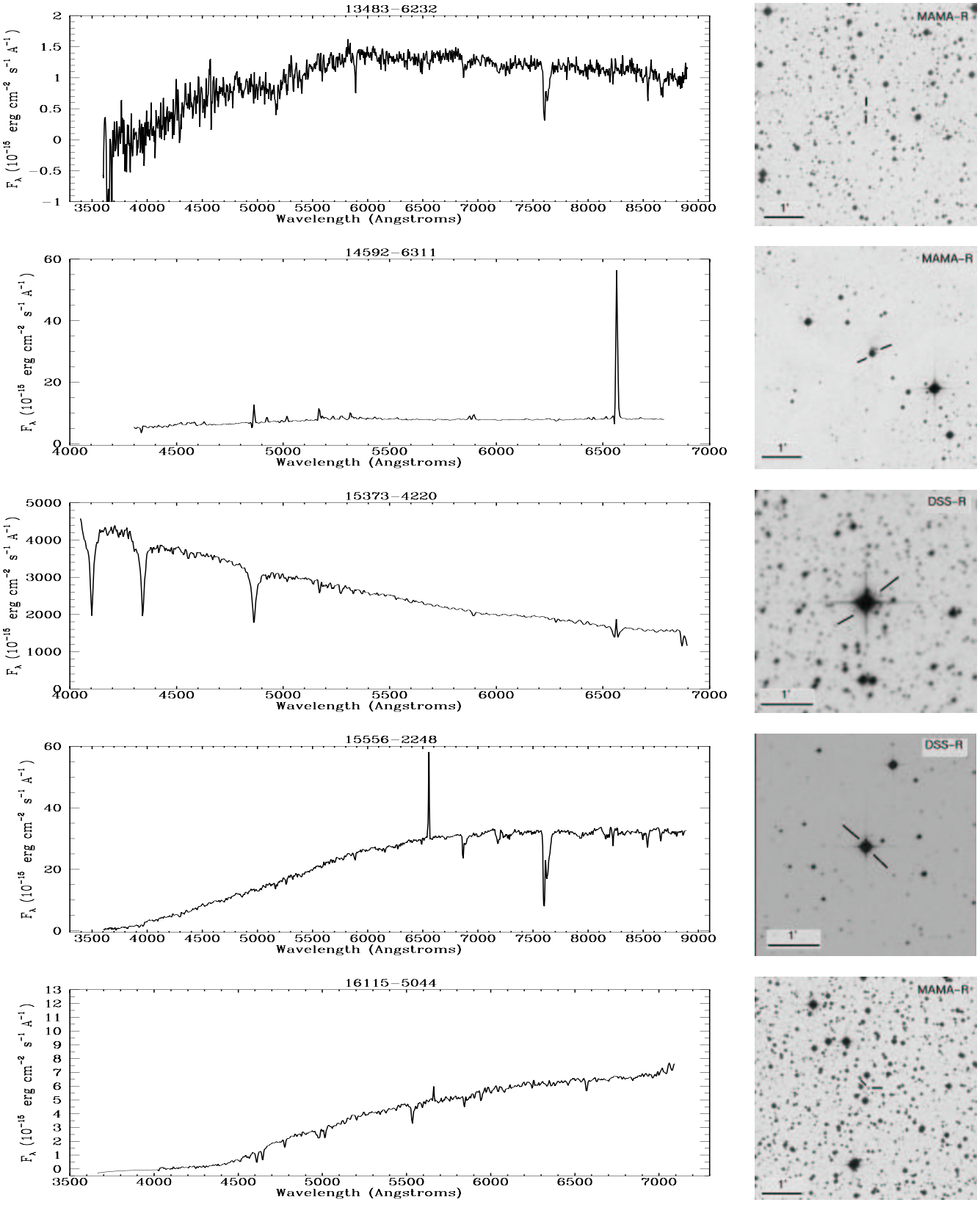

Fig. D.1. Spectra of the objects classified as young stars in the sample together with their corresponding identification charts (continued).

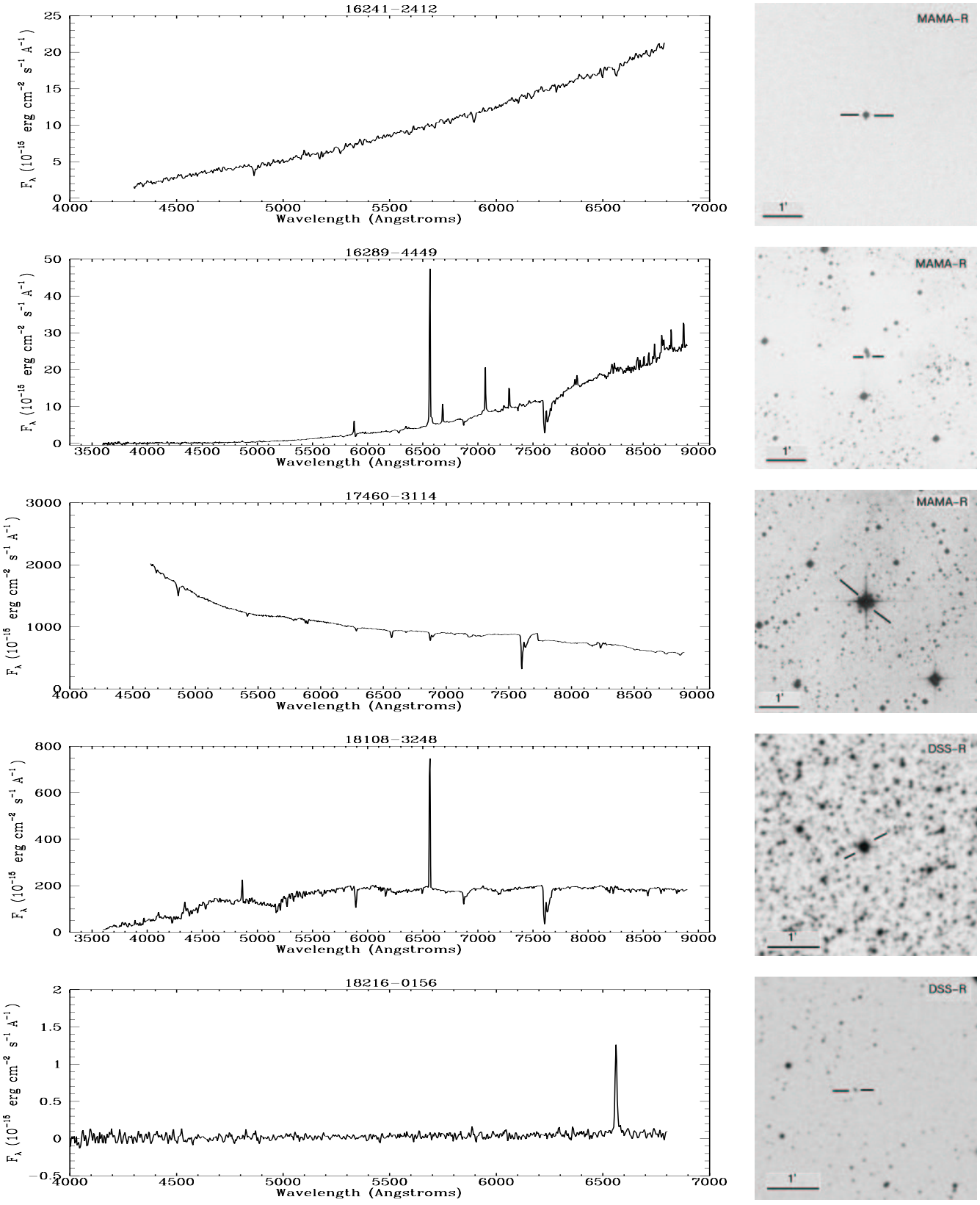

Fig. D.1. Spectra of the objects classified as young stars in the sample together with their corresponding identification charts (continued).

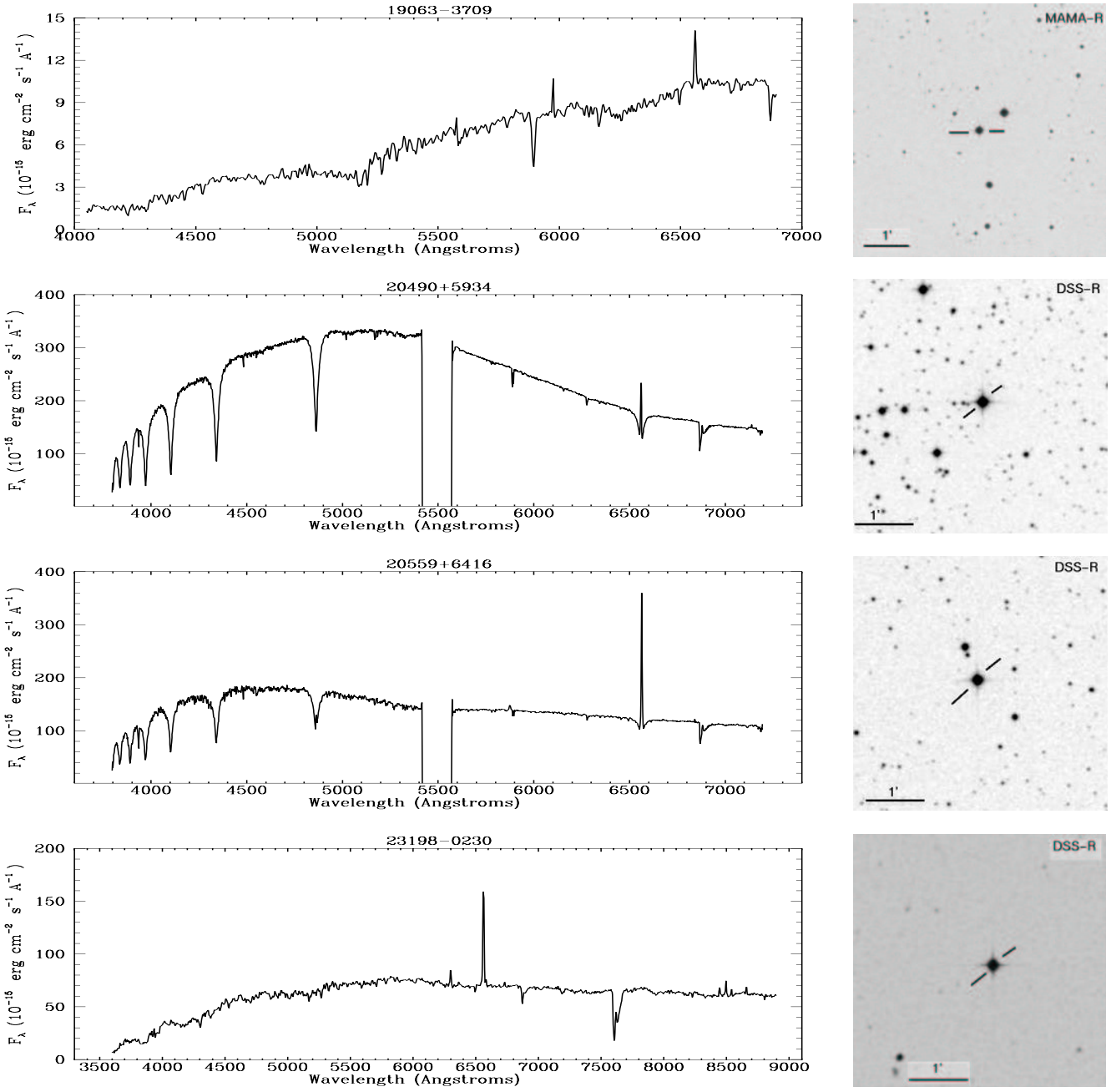

Fig. D.1. Spectra of the objects classified as young stars in the sample together with their corresponding identification charts (continued).

Appendix E: Atlas of galaxies

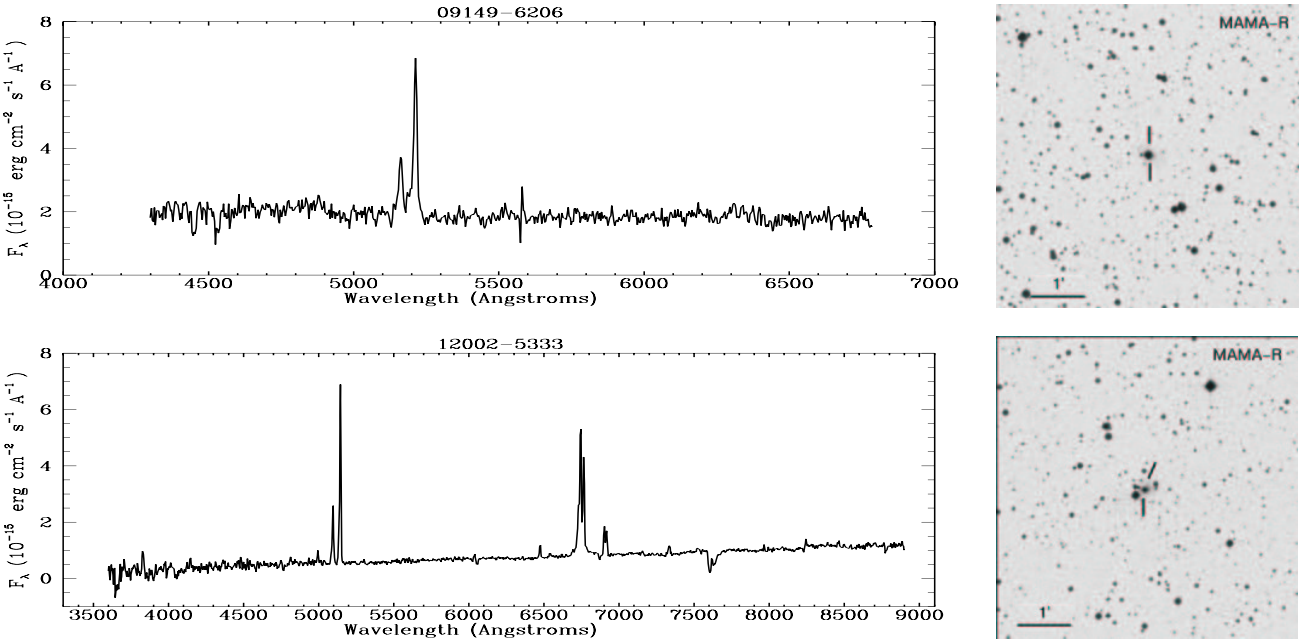

Fig. E.1. Spectra of the sources classified as galaxies in the sample together with their corresponding identification charts.

Appendix F: Atlas of peculiar sources

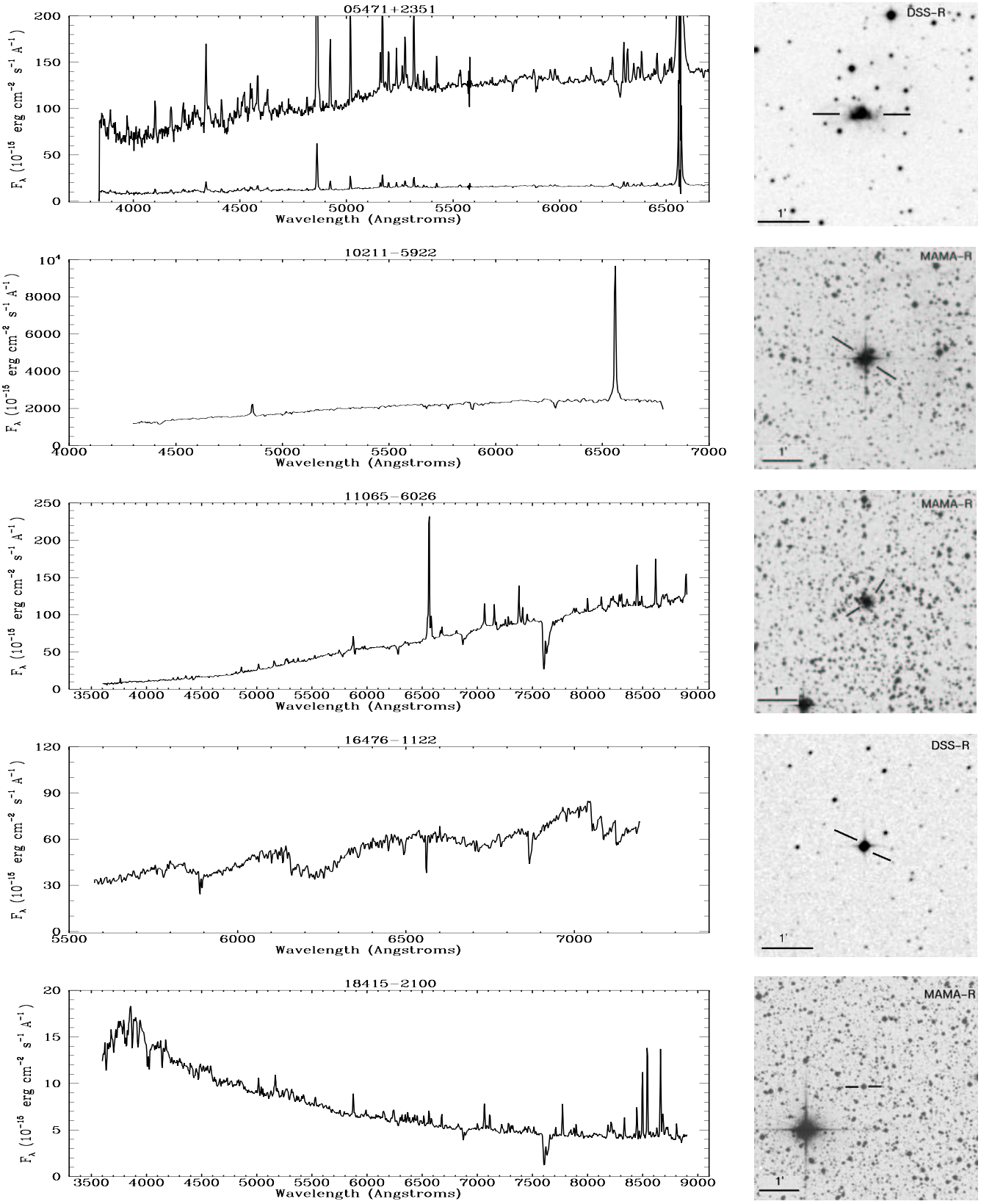

Fig. F.1. Spectra of the peculiar sources in the sample together with their corresponding identification charts.